ORNL/TM-7394

ornl

OAK RIDGE NATIONAL LABORATORY

UNION CARBIDE

# Time-Dependent Properties of Welds in Type 316 Stainless Steel Formed-and-Welded Pipes

J. W. McEnerney
V. K. Sikka



METALS and CERAMICS
ENERGY
RESEARCH
DEVELOPMENT
OAK RIDGE NATIONAL LABORATORY



OPERATED BY
UNION CARBIDE CORPORATION
FOR THE UNITED STATES
DEPARTMENT OF ENERGY

Printed in the United States of America. Available from
the Department of Energy
Technical Information Center
P.O. Box 62, Oak Ridge, Tennessee 37830
Printed Copy A05 ; Microfiche A01

ORNL/TM-7394
Distribution
Categories
UC-79h, -k, -r

Contract No. W-7405-eng-26

METALS AND CERAMICS DIVISION

# TIME-DEPENDENT PROPERTIES OF WELDS IN TYPE 316 STAINLESS STEEL FORMED-AND-WELDED PIPES

J. W. McEnerney and V. K. Sikka

Date Published: September 1980



OAK RIDGE NATIONAL LABORATORY
Oak Ridge, Tennessee 37830
operated by
UNION CARBIDE CORPORATION
for the
U.S. DEPARTMENT OF ENERGY

CONTENTS

# TIME-DEPENDENT PROPERTIES OF WELDS IN TYPE 316 STAINLESS STAINLESS STEEL FORMED-AND-WELDED PIPES*

J. W. McEnerney and V. K. Sikka

## ABSTRACT

Creep-rupture, fatigue, and creep-fatigue tests were performed on solution-annealed seam welds from five type 316 stainless steel formed-and-welded pipes. Test specimens were oriented in both longitudinal and transverse directions with respect to the axial seam welds. All tests were performed in air. Creep-rupture tests were performed at 538 and 649°C and had maximum rupture lives of approximately 7000 h; fatigue tests were performed at 593°C for total strain ranges of 0.5 and 2.0%; and creep-fatigue tests were performed at 593°C with total strain ranges of 1 and 2% and a tensile hold time of 0.1 h.

The results of the creep-rupture tests showed considerable variation among our welds. The submerged-arc (SA) and gas tungsten-arc (GTA) welds with type 16-8-2 filler metal had the shortest rupture lives and fell below the American Society of Mechanical Engineers (ASME) Code Case N-47 minimum expected values. Two GTA welds and one SA weld with type 16-8-2 filler metal had minimum creep rates ($\dot{e}_m$) that were 1 to 2 orders of magnitude greater than rates for an autogenous GTA weld and a GTA-SA weld with type 316 filler metal. The predicted isochronous stress-strain behavior was comparable with that for minimum creep rate (i.e., the three welds with high $\dot{e}_m$ exceeded the ASME Code Case N-47 isochronous stress-strain curves). The predicted stresses to the onset of tertiary creep for all welds were in excess of the code case allowable stresses. The welds experienced alternating regions of high and low ductility similar to those for wrought material. However, the SA weld with type 16-8-2 filler metal appeared to have consistently lower ductility than the wrought material.

The results of the fatigue and creep-fatigue tests demonstrated that the welds behaved similarily to wrought material. Both the fatigue and creep-fatigue (by linear damage summation) failures exceeded the Code Case N-47 minimum design requirements. However, the safety margins encountered for creep fatigue were lower than expected.

Based upon the potential variation in weld metal properties, we recommend that elevated-temperature qualification testing be employed to ensure that welds meet minimum required properties. With additional evaluation the use of such qualification tests may make it unnecessary to arbitarily penalize welds with the one-half allowable strain requirement.

---

*Work performed under DOE/RRT AF 15 10 15, Task OR-1.4, Fabrication Technology.

## INTRODUCTION

Formed-and-welded pipe is being considered for fast breeder reactor (FBR) sodium coolant piping applications. The time-independent properties of five formed-and-welded pipes were characterized in a previous report.[1] The purpose of this report is to characterize the creep-rupture, fatigue, and creep-fatigue properties of the five pipes.

## DESCRIPTION OF THE PIPES

Five formed-and-welded pipes were procured in accordance with modified ASME Code[2] material specifications. The plate used to form the pipes was manufactured in accordance with SA-240, type 316 (ref. 3), while the pipes were manufactured in accordance with SA-358 (ref. 4) and SA-312 (ref. 5). The pipes were manufactured and certified in accordance with the requirements of ASME Code, Sect. III, Div. 1, Class 1 (ref. 6) or 2 (ref. 7). Each of the pipe sections was 1.83 m long, with a 12.77-mm-thick wall and a 0.91-m OD prototypic of the Clinch River Breeder Reactor Plant (CRBRP). The pipes contained a longitudinal seam weld. Table 1 summarizes the identifications, material specifications, code classes, welding processes, filler metals, final heat treatments, and hydrostatic test pressures for the pipes. Tables 2 and 3 provide the chemical compositions and ferrite content, respectively, of the pipes. Further information describing the pipes is available in the earlier report.[1]

## CREEP-RUPTURE PROPERTIES

Creep-rupture tests were performed at 538 and 649°C in air on weld specimens that were oriented in transverse and longitudinal directions with respect to the seam weld. The longitudinal specimens are all weld metal, while the transverse specimens are a composite of base metal, heat-affected zone (HAZ) and weld metal. However, because of the geometry of the weld cross section, some of the longitudinal specimens contain some base metal. Figure 1 shows the creep-rupture test specimen

Table 1. Fabrication Information for Formed-and-Welded 1.83-m-long by 0.91-m-OD by 12.70-mm-wall Pipes of Type 316 Stainless Steel

| Identification | ASME Code, Sect. II, Material Specifications | | ASME Code, Sect. III, Class | Welding Process[a] | Filler Metal Type | Final Heat Treatment[b] | | Hydrostatic Test Pressure (MPa) |
|---|---|---|---|---|---|---|---|---|
| | Plate | Pipe | | | | Temperature (°C) | Time (h) | |
| E-13 | SA-240 | SA-358 | 1 | GTA with both hot and cold wire additions | 16-8-2 | 1060 | 0.5 | 2.76 |
| F-14 | SA-240 | SA-358 | 1 | GTA with cold wire additions | 16-8-2 | 1066 | 0.2[c] | 3.10 |
| G-15 | SA-240 | Sa-358 | 1 | GTA with cold wire additions and SA | 316 | 1093 | 0.5 | |
| G-16 | SA-240 | SA-312 | 2 | Autogenous GTA | None | 1038–1066 | 0.5 | |
| H-22 | SA-240 | SA-358 | 1 | SA | 16-8-2 | 1066 | 0.8 | 3.45 |

[a]GTA = gas tungsten-arc; SA = submerged-arc.

[b]Followed by water quench.

[c]Minimum.

Table 2. Chemical Analyses of Formed-And-Welded Pipes

| Pipe | Location | Content, wt % | | | | | | | | | | | | | | | |
|---|---|---|---|---|---|---|---|---|---|---|---|---|---|---|---|---|---|
| | | C | Mn | P | S | Si | Ni | Cr | Mo | V | Nb | Ti | Co | Cu | Al | B | N |
| **Vendor Analysis** | | | | | | | | | | | | | | | | | |
| E-13 | Plate | 0.074 | 1.78 | 0.020 | 0.012 | 0.91 | 11.48 | 17.18 | 2.01 | | | | | | | | |
| | Weld | 0.060 | 1.66 | 0.012 | 0.012 | 0.49 | 10.79 | 16.43 | 2.00 | | | | | | | | |
| F-14 | Plate | 0.043 | 1.68 | 0.031 | 0.008 | 0.61 | 11.10 | 17.55 | 2.08 | | | | | | | | |
| | Weld | 0.040 | 1.68 | 0.027 | 0.010 | 0.48 | 11.31 | 17.94 | 2.18 | | | | | | | | |
| G-15 | Plate | 0.055 | 1.63 | 0.025 | 0.024 | 0.45 | 12.10 | 16.40 | 2.15 | | | | | | | | |
| | Weld | 0.055 | 1.58 | 0.026 | 0.025 | 0.46 | 12.20 | 16.40 | 2.20 | | | | | | | | |
| G-16 | Plate | 0.058 | 1.72 | 0.025 | 0.024 | 0.46 | 12.20 | 16.70 | 2.32 | | | | | | | | |
| | Weld | 0.051 | 1.65 | 0.025 | 0.024 | 0.42 | 12.20 | 16.30 | 2.17 | | | | | | | | |
| H-22 | Plate | 0.053 | 1.82 | 0.020 | 0.012 | 0.50 | 13.30 | 16.65 | 2.28 | | | | | | | | |
| | Weld | 0.060 | 1.65 | 0.024 | 0.019 | 0.55 | 10.06 | 15.33 | 2.04 | | | | | | | | |
| **Overcheck Analysis[a]** | | | | | | | | | | | | | | | | | |
| E-13 | Plate | 0.066 | 1.63 | 0.032 | 0.009 | 0.58 | 11.29 | 16.09 | 2.85 | 0.06 | <0.01 | 0.01 | 0.17 | 0.22 | 0.01 | 0.001 | 0.039 |
| | Weld | 0.053 | 1.57 | 0.014 | 0.014 | 0.49 | 9.42 | 16.18 | 1.95 | 0.04 | <0.01 | 0.01 | 0.06 | 0.13 | <0.01 | 0.001 | 0.041 |
| F-14 | Plate | 0.048 | 1.67 | 0.022 | 0.009 | 0.52 | 11.18 | 17.85 | 2.00 | 0.08 | <0.01 | 0.01 | 0.21 | 0.19 | <0.01 | 0.001 | 0.056 |
| | Weld | 0.026 | 1.57 | 0.020 | 0.009 | 0.51 | 11.62 | 17.88 | 2.08 | 0.08 | <0.01 | 0.01 | 0.18 | 0.17 | <0.01 | 0.001 | 0.037 |
| G-15 | Plate | 0.064 | 1.57 | 0.029 | 0.026 | 0.47 | 12.63 | 16.39 | 2.19 | 0.05 | 0.01 | 0.03 | 0.22 | 0.26 | <0.01 | 0.003 | 0.074 |
| | Weld | 0.051 | 1.50 | 0.026 | 0.021 | 0.53 | 12.68 | 16.19 | 2.17 | 0.05 | 0.01 | 0.02 | 0.23 | 0.27 | <0.01 | 0.002 | 0.059 |
| G-16 | Plate | 0.064 | 1.46 | 0.027 | 0.025 | 0.52 | 12.67 | 16.20 | 2.15 | 0.05 | 0.01 | 0.02 | 0.22 | 0.26 | <0.01 | 0.003 | 0.083 |
| | Weld | 0.055 | 1.46 | 0.027 | 0.023 | 0.49 | 12.67 | 16.33 | 2.15 | 0.05 | 0.01 | 0.02 | 0.22 | 0.27 | <0.01 | 0.002 | 0.062 |
| H-22 | Plate | 0.057 | 1.84 | 0.030 | 0.018 | 0.60 | 13.17 | 16.37 | 2.21 | 0.07 | <0.01 | 0.01 | 0.08 | 0.45 | <0.01 | 0.002 | 0.076 |
| | Weld | 0.055 | 1.72 | 0.025 | 0.021 | 0.53 | 9.83 | 15.14 | 2.06 | 0.04 | <0.01 | 0.01 | 0.08 | 0.21 | <0.01 | 0.002 | 0.044 |

[a]Spectrographic chemical analysis performed by Combustion Engineering, Chattanooga, Tenn. Weld metal was analyzed in region where dilution effects were minimized.

Table 3. Ferrite Content of Formed-And-Welded Pipes

| Pipe | Location | Ferrite Number | | | Measured Ferrite[d] (Area %) |
|---|---|---|---|---|---|
| | | Calculated Vendor[a] | Calculated Overcheck[b] | Measured[c] | |
| E-13 | Outside | 0 | 2.2 | 0.1–0.2 | 1.6 |
| | Center | 0 | 2.2 | 0.1–0.3 | 1.3 |
| | Inside | 0 | 2.2 | 0.2–0.4 | 2.4 |
| F-14 | Outside | 4.5 | 6.0 | 3.2–4.8 | 7.2 |
| | Center | 4.5 | 6.0 | 2.4–2.8 | 5.8 |
| | Inside | 4.5 | 6.0 | 0.6–1.2 | 1.8 |
| G-15 | All | 0 | 0 | 0 | 0 |
| G-16 | All | 0 | 0 | 0 | 0 |
| H-22 | All | 0 | 0 | 0 | 0 |

[a]Calculated from Delong Diagram, using vendor chemical analysis shown in Table 2 and assuming 0.06% N.

[b]Calculated from Delong diagram, using overcheck chemical analysis shown in Table 2.

[c]Magnetic permeability measurements made with Twin City Testing Corporation Ferritescope, type FE8e2, model B, with 1 probe type KF. Calibration was performed in accordance with AWS A4.2-74, using Teledyne McKay weld metal secondary standards. Measurements were made on five specimens sectioned at 0.3-m intervals along the weld.

[d]Quantitative television microscope analysis was made on one specimen per pipe, which was etched with 15 g $K_3Fe(CN)_6$, 15 g KOH, 100 mL $H_2O$ at 98°C to identify the ferrite phase. The area percentage of ferrite was averaged for six 0.150-$mm^2$ areas at the outside, center, and inside of the weld.

design and the location of the specimen relative to the blanks containing the weld. The temperature of the specimen reduced section was held within ±2°C of the nominal test temperature. Strains during loading and testing were measured from an averaging extensometer mounted on the shoulders of the specimen. The stresses were selected to produce rupture times in the range 100 to 1000 h.

The creep-rupture data for the welds in the five pipes are summarized in Table 4. The times and corresponding strains to several important

# Table 4. Summary of Creep-Rupture Data for Formed-and-Welded Pipe

| Test | Specimen | Orientation[a] | Test Temperature (°C) | Stress (MPa) | Strain, % | | | | | | Time, h | | | | Minimum Creep Rate, $\dot{e}_m$ (%/h) | Reduction in Area (%) |
|---|---|---|---|---|---|---|---|---|---|---|---|---|---|---|---|---|
| | | | | | Loading ($e_1$) | Transient ($e_{pc}$) | Primary ($e_1$) | Secondary ($e_2$) | 0.2% Offset ($e_3$) | Fracture ($e_f$) | Primary ($t_1$) | Secondary ($t_2$) | 0.2% Offset ($t_3$) | Rupture ($t_r$) | | |
| | | | | | | | | Pipe E-13 | | | | | | | | |
| 19951 | 13 | L | 538 | 310 | 9.54 | 0.20 | 0.45 | 2.35 | 2.50 | 16.03 | 165.0 | 1400.0 | 1470.0 | 1750.9 | 0.0016 | 15.56 |
| 19952 | 14 | T | 538 | 310 | 8.43 | 0.20 | 0.30 | 1.00 | 1.20 | 14.40 | 180.0 | 1200.0 | 1410.0 | 1619.1 | 0.00068 | 32.64 |
| 19611 | 4 | L | 538 | 379 | 19.46 | 0.00 | 0.00 | 1.50 | 2.15 | 34.04 | 0.0 | 67.5 | 91.2 | 209.4 | 0.022 | 42.90 |
| 19612 | 5 | T | 538 | 379 | 17.93 | 0.23 | 0.43 | 1.30 | 1.68 | 21.72 | 26.5 | 150.0 | 174.5 | 209.4 | 0.0072 | 24.98 |
| 19615 | 31 | L | 649 | 152 | 0.28 | 0.19 | 0.25 | 2.00 | 2.50 | 42.78 | 7.5 | 175.0 | 210.0 | 854.4 | 0.0103 | 70.07 |
| 19953 | 32 | T | 649 | 152 | 0.62 | 0.60 | 1.20 | 4.80 | 5.20 | 21.60 | 120.0 | 760.0 | 820.0 | 1368.9 | 0.0054 | 56.81 |
| 19613 | 22 | L | 649 | 207 | 2.45 | 0.25 | 0.50 | 7.50 | 9.75 | 46.27 | 1.0 | 21.5 | 27.5 | 65.7 | 0.34 | 57.32 |
| 19614 | 23 | T | 649 | 207 | 2.33 | 0.75 | 1.38 | 11.88 | 12.88 | 26.64 | 5.0 | 82.0 | 87.0 | 107.1 | 0.1355 | 54.07 |
| | | | | | | | | Pipe F-14 | | | | | | | | |
| 19618 | 13 | L | 538 | 310 | 9.88 | 0.65 | 1.40 | 3.30 | 3.90 | 28.18 | 85.0 | 300.0 | 355.0 | 649.7 | 0.0087 | 46.16 |
| 19954 | 14 | T | 538 | 310 | 9.81 | 0.20 | 0.30 | 1.50 | 1.90 | 24.0 | 60.0 | 580.0 | 680.0 | 1164.7 | 0.0022 | 47.95 |
| 19616 | 4 | L | 538 | 379 | | | | | | Failed During Loading | | | | | | |
| 19617 | 5 | T | 538 | 379 | 23.68 | 0.00 | 0.00 | 0.20 | 0.50 | 35.05 | 0.0 | 8.7 | 13.0 | 42.6 | 0.0266 | 64.11 |
| 19955 | 31 | L | 649 | 152 | 1.17 | 0.50 | 1.00 | 8.00 | 9.50 | 62.40 | 10.0 | 170.0 | 200.0 | 618.6 | 0.0425 | 74.78 |
| 19956 | 32 | T | 649 | 152 | 0.38 | 0.40 | 0.80 | 4.20 | 5.00 | 23.20 | 25.0 | 240.0 | 275.0 | 502.5 | 0.0160 | 75.08 |
| 19619 | 22 | L | 649 | 207 | 4.16 | 0.50 | 2.00 | 15.00 | 16.00 | 50.74 | 1.0 | 9.8 | 10.3 | 15.9 | 1.4750 | 70.98 |
| 19620 | 23 | T | 649 | 207 | 4.02 | 0.00 | 0.00 | 5.40 | 6.20 | 23.04 | 0.0 | 12.4 | 13.8 | 24.1 | 0.436 | 61.40 |
| | | | | | | | | Pipe G-15 | | | | | | | | |
| 19959 | 13 | L | 538 | 310 | 8.08 | 0.15 | 0.18 | 0.37 | 0.63 | 15.18 | 180.0 | 1740.0 | 2030.0 | 2091.9 | 0.00013 | 19.52 |
| 19960 | 14 | T | 538 | 310 | 11.43 | 0.11 | 0.12 | 0.22 | 0.42 | 15.20 | 110.0 | 1500.0 | 1580.0 | 1602.3 | 0.00007 | 28.15 |
| 19957 | 4 | L | 538 | 379 | 22.42 | 0.45 | 0.55 | 1.00 | 1.25 | 29.60 | 75.0 | 485.0 | 525.0 | 539.8 | 0.0012 | 23.90 |
| 19958 | 5 | T | 538 | 379 | 21.68 | 0.25 | 0.30 | 0.50 | 0.55 | 27.20 | 55.0 | 345.0 | 355.0 | 444.9 | 0.00075 | 33.75 |
| 20602 | 31 | L | 649 | 152 | 0.43 | 1.10 | 1.25 | 1.75 | 2.12 | 25.61 | 550.0 | 4100.0 | 4600.0 | 6990.7 | 0.00017 | 64.82 |
| 20603 | 32 | T | 649 | 152 | 0.42 | 0.94 | 1.06 | 1.37 | 1.62 | 20.80 | 1050.0 | 3500.0 | 4200.0 | 6329.1 | 0.00013 | 48.03 |
| 19961 | 22 | L | 649 | 207 | 1.52 | 0.40 | 0.74 | 2.30 | 2.87 | 4.80 | 28.0 | 148.0 | 177.0 | 189.2 | 0.0128 | 10.74 |
| 19962 | 23 | T | 649 | 207 | 3.38 | 0.50 | 1.10 | 2.70 | 3.05 | 10.40 | 25.0 | 93.0 | 101.0 | 117.5 | 0.0233 | 16.02 |
| | | | | | | | | Pipe G-16 | | | | | | | | |
| 20239 | 13 | L | 538 | 310 | 14.88 | 0.15 | 0.19 | 0.35 | 0.60 | 20.00 | 150.0 | 1180.0 | 1470.0 | 1572.5 | 0.00018 | 27.12 |
| 20262 | 14 | T | 538 | 310 | 10.70 | 0.10 | 0.11 | 0.20 | 0.40 | 16.0 | 170.0 | 1680.0 | 1800.0 | 1875.1 | 0.00005 | 27.51 |
| 19963 | 4 | L | 538 | 379 | 26.88 | 0.80 | 0.90 | 1.3 | 1.60 | 33.60 | 56.0 | 280.0 | 332.0 | 374.8 | 0.00187 | 34.70 |
| 19964 | 5 | T | 538 | 379 | 21.25 | 0.33 | 0.35 | 0.60 | 0.82 | 26.40 | 70.0 | 380.0 | 455.0 | 456.7 | 0.00068 | 35.62 |
| 20604 | 31 | L | 649 | 152 | 0.58 | 1.50 | 1.63 | 2.25 | 2.50 | 25.60 | 1000.0 | 3750.0 | 4000.0 | 6263.9 | 0.0002 | 54.48 |
| 20605 | 32 | T | 649 | 152 | 1.18 | 1.10 | 1.30 | 1.85 | 2.20 | 18.40 | 1000.0 | 3450.0 | 4050.0 | 5700.9 | 0.00022 | 51.36 |
| 19965 | 22 | L | 649 | 207 | 4.42 | 0.60 | 1.00 | 4.50 | 4.90 | 18.40 | 8.0 | 73.0 | 76.5 | 89.8 | 0.054 | 22.54 |
| 19966 | 23 | T | 649 | 207 | 4.77 | 0.40 | 0.78 | 2.58 | 2.85 | 11.20 | 12.5 | 71.0 | 73.0 | 73.3 | 0.0305 | 28.98 |
| | | | | | | | | Pipe H-22 | | | | | | | | |
| 20263 | 15 | L | 538 | 310 | 14.43 | 0.15 | 0.30 | 0.98 | 1.30 | 20.00 | 60.0 | 325.0 | 380.0 | 464.0 | 0.0025 | 20.89 |
| 19969 | 12 | T | 538 | 310 | 10.82 | 0.20 | 0.25 | 0.65 | 0.88 | 17.18 | 85.0 | 600.0 | 630.0 | 660.2 | 0.00073 | 17.36 |
| 19968 | 11 | L | 538 | 379 | 19.72 | 0.80 | 1.50 | 3.30 | 3.95 | 29.60 | 125.0 | 438.0 | 512.5 | 565.8 | 0.00575 | 33.48 |
| 19967 | 5 | T | 538 | 379 | 17.41 | 0.64 | 1.00 | 1.56 | 1.94 | 20.75 | 44.0 | 114.0 | 136.0 | 152.6 | 0.0081 | 24.70 |
| 20240 | 33 | L | 649 | 152 | 0.80 | 0.15 | 0.30 | 4.00 | 5.00 | 14.40 | 5.0 | 151.3 | 181.3 | 247.9 | 0.0254 | 28.70 |
| 19971 | 21 | T | 649 | 152 | 0.65 | 0.15 | 0.40 | 1.60 | 2.38 | 9.95 | 30.0 | 165.0 | 235.0 | 418.1 | 0.00865 | 36.33 |
| 20241 | 24 | L | 649 | 207 | 4.24 | 0.10 | 0.30 | 6.75 | 7.60 | 16.87 | 3.0 | 3.6 | 10.4 | 12.7 | 0.695 | 23.86 |
| 19970 | 14 | T | 649 | 207 | 3.35 | 0.30 | 0.65 | 4.10 | 4.55 | 10.33 | 1.8 | 17.8 | 19.0 | 20.6 | 0.215 | 30.67 |

[a] L = Longitudinal; T = Transverse

events during each test were obtained by visual estimates from strain-time curves. These included the end of first-stage creep ($t_1$ and $e_1$), the end of second-stage creep or the onset of tertiary creep by departure from linearity ($t_2$ and $e_2$), and a 0.2% offset from second-stage creep ($t_3$ and $e_3$). The minimum creep rate ($\dot{e}_m$) was determined from the slope of the strain-time curve during second-stage creep. Figure 2 pictorially defines the creep quantities that were examined.

## Time to Rupture and Minimum Creep Rate

The ASME Code Case N-47 expected minimum stress-to-rupture values[8] (Table 1—14.6B) for type 316 stainless steel and a recently developed heat-centered model[9] for type 316 stainless steel have been used to characterize the rupture life of our welds. The heat-centered model[9] is of the form

$$\log t_r = c_h + a_1\sigma + a_2 \log \sigma + a_3/T \ , \qquad (1)$$

where

$t_r$ = time to rupture, h;
$c_h$ = heat constant;
$a_1$, $a_2$, $a_3$ = least squares regression constants;
$\sigma$ = stress, MPa;
$T$ = temperature, K.

Data from tests of wrought type 316 stainless steel at Oak Ridge National Laboratory (ORNL), from other sources within the United States, from the United Kingdom Atomic Energy Authority (UKAEA), and from the British Steelmaker's Creep Committee (BSCC) were used to develop the constants for Eq. (1). These constants are listed below:

| Constant | Value |
|---|---|
| $c_{h(avg)}$ | −11.87 |
| $a_1$ | −0.01312 |
| $a_2$ | −2.552 |
| $a_3$ | 20,880 |

Note that the heat constant, $c_h$, is an average value that represents all the heats of material in the population of 1269 tests. Individual heat constants can be used to describe various heats of material. The use of Eq. (1) with the average heat constant enables prediction of the average rupture life for wrought type 316 stainless steel.

Figure 3 shows a comparison of stress vs rupture life for our welds at test temperatures of 538 and 649°C. This figure also shows the ASME Code Case N-47 minimum and the predicted wrought material average, using the heat-centered model. Figure 3 shows that the welds in pipes E-13, G-15, and G-16 were close to the predicted average for wrought material. However, the welds in pipes F-14 and H-22 fell below the average and in some cases fell below the ASME minimum. The lower rupture life for F-14 is related to low carbon plus nitrogen content, as previously reported.[1] However, the lower rupture life for H-22 is related to tne welding process that was used. The weld in this pipe was made by the SA process. It has been reported[10] that for high-stress tests on type 16-8-2 weld metal, the welds made by the shielded metal-arc (SMA) process were the strongest, followed by the GTA and SA processes. This trend is followed when comparing the tests for pipes E-13 (GTA) vs H-22 (SA). However, the tests on pipe F-14 (GTA) had similar rupture lives as those for H-22. This situation highlights the importance of heat-to-heat variation, which in this case appears to have negated the expected[10] difference between the processes. It is also reported[10] that for longer term, low-stress tests, differences in properties of welds made by various processes may gradually disappear. This is attributed to the promotion of equilibrium microstructures.

Figure 4 provides a convenient method for comparing the rupture lives of longitudinal vs transverse specimens. Nine points lie on each side of the line for equal rupture life, and one falls on the line. Although a few of the points on the longitudinal side may show a greater difference, the rupture life between the two orientations does not appear to significantly vary.

The ASME Code Case N-47 does not provide requirements for the minimum creep rate of structural materials. However, a recently developed[9] heat-centered model can again be used to predict the average minimum creep rate of wrought type 316 stainless steel. The heat-centered model is of the form

$$\log \dot{e}_m = c_h + a_1\sigma + a_2 \log \sigma - a_3/T \ , \qquad (2)$$

where

$\dot{e}_m$ = minimum creep rate, %/h;
$c_h$ = heat constant;
$a_1$, $a_2$, $a_3$ = least squares regression constants;
$\sigma$ = stress, MPa;
$T$ = temperature, K.

Data from ORNL and UKAEA tests were fit to Eq. (2) with the constants shown below:

| Constant | Value |
|---|---|
| $c_{h(\text{avg})}$ | 13.314 |
| $a_1$ | 0.0097 |
| $a_2$ | 4.5097 |
| $a_3$ | −24,890 |

Figure 5 shows a comparison of stress vs minimum creep rate for the welds in our pipes. This figure also includes the predicted wrought material average, using the heat-centered model. Figure 5 shows that the welds from G-15 and G-16 had lower or equal $\dot{e}_m$ values at all temperatures compared with the average values for the wrought material. The welds from E-13, F-14, and H-22 had equal or greater $\dot{e}_m$ values at all temperatures compared with those of the wrought material. It is interesting that the three welds containing type 16-8-2 filler metal (E-13, F-14, H-22) had the greatest $\dot{e}_m$ values at all temperatures and stress conditions. The type 16-8-2 filler metal deposited by the GTA process (E-13) had lower $\dot{e}_m$ values

than those deposited by the SA process (H-22). As previously discussed, pipe F-14 (GTA process) was considered to be weaker from compositional differences. The weld with type 316 filler metal (G-15) and the autogenous weld (G-16) had $\dot{e}_m$ values about 1 to 2 orders of magnitude lower than the three with type 16-8-2 filler metal.

Figure 6 shows that the $\dot{e}_m$ values for the longitudinal specimens were greater than those for the transverse specimens. Since the longitudinal specimens will generally be all weld metal, this indicates that the weld metal creeps at a greater rate than the composite of weld metal, HAZ and base metal in the transverse specimens.

A previous report[11] has described the use of models containing an ultimate tensile strength (UTS) term to predict the time to rupture and the minimum creep rate of our welds. These models were of the form

$$\log t_r = 5.138 - 2.181 \log \sigma(13{,}768/T) - 3771/TS_u \ , \tag{3}$$

and

$$\log \dot{e}_m = 3.534 + 2.0734 \log \sigma - 45.064S_u/T + 0.01836S_u \log \sigma \ , \tag{4}$$

where

$t_r$ = time to rupture, h;

$\sigma$ = stress, MPa;

$T$ = temperature, K;

$S_u$ = ultimate tensile strength, MPa, at temperature of interest determined at a strain rate of $8.33 \times 10^{-5}$/s;

$\dot{e}_m$ = minimum creep rate, %/h.

The model for $t_r$ [Eq. (3)] agreed well with our experimental data. However, the model for $\dot{e}_m$ [Eq. (4)] predicted values that were more than an order of magnitude higher than our experimental values for two of the five welds (G-15 and G-16). This inaccuracy was attributed to the occurrence of flat-top creep curves. Equation 3 provides the ability to predict $t_r$ with only data from a tensile test. As reported,[11] this

predicting capability enables the establishment of a qualification test procedure to assure that ASME Code Case N-47 minimum time-to-rupture requirements are met.

The heat-centered model can also be used to predict $t_r$ and $\dot{e}_m$ for different welds. Equations (1) and (2) can be solved for the heat constant, $C_h$, by using experimental values from creep-rupture tests. Table 5 shows the calculated individual weld heat constants for the $t_r$ and $\dot{e}_m$ models. respectively. Three $C_h$ values were calculated for each weld to represent longitudinal specimens, transverse specimens, and all specimens. Figures 7 through 11 show comparisons of predicted $t_r$ and $\dot{e}_m$ values with experimental data. The predicted values used the all-specimen $C_h$ constants. An examination of these figures indicates that the experimental data fall at or close to the predicted values. The $C_h$ constants in Table 5 provide the same relative characterization of the welds, as previously discussed. Table 5 shows that pipes F-14 and H-22 have the lowest $C_h$ values, which result in lower predicted $t_r$. In addition, longitudinal and transverse $C_h$ values do not differ greatly. Table 5 also shows that pipes G-15 and G-16 have the lowest $C_h$ values, which result in lower predicted $\dot{e}_m$. It can also be said that the longitudinal $C_h$ values are higher than the transverse ones, indicating a higher predicted $\dot{e}_m$ for the longitudinal direction. An examination of Figs. 7 through 11(c) and (d) indicates that separate predictions would more adequately describe the transverse and longitudinal data. It is important to note that the heat-centered model was able to predict the $\dot{e}_m$ values for all welds, whereas the previously described UTS model[11] did not agree with the experimental data for G-15 and G-16.

## Isochronous Stress-Strain Curves

We have previously[1] shown that the total true tensile elastic-plastic stress-strain behavior (up to 5% strain) of our welds can be analytically described. The plastic behavior was described by

$$\sigma - \sigma_{PL} = [CPe_p/(1 - Pe_p)] + He_p \ , \qquad (5)$$

Table 5. Time-to-Rupture[a] and Minimum Creep Rate[b] Model Heat Constants, $c_h$, for the Welds in the Formed-and-Welded Pipe

| Pipe | Time-to-Rupture Constants[c] | | | Minimum Creep Rate Constants[c] | | |
|---|---|---|---|---|---|---|
| | All Specimens | Longitudinal Specimens | Transverse Specimens | All Specimens | Longitudinal Specimens | Transverse Specimens |
| E-13 | −12.028 (0.127) | −12.076 (0.146) | −11.981 (0.100) | 13.582 (0.275) | 13.775 (0.196) | 13.390 (0.199) |
| F-14 | −12.494 (0.200) | −12.540 (0.264) | −12.460 (0.173) | 14.142 (0.347) | 14.459 (0.213) | 13.904 (0.185) |
| G-15 | −11.667 (0.331) | −11.611 (0.331) | −11.724 (0.379) | 12.343 (0.371) | 12.385 (0.329) | 12.302 (0.457) |
| G-16 | −11.770 (0.368) | −11.774 (0.396) | −11.766 (0.399) | 12.491 (0.484) | 12.642 (0.528) | 12.341 (0.456) |
| H-22 | −12.422 (0.477) | −12.425 (0.667) | −12.420 (0.294) | 13.682 (0.435) | 13.853 (0.533) | 13.512 (0.282) |

[a] $\log t_r = c_h - 0.01312\sigma - 2.522 \log\sigma + 20880/T$, where $T$ = temperature, K.

[b] $\log \dot{e}_m = c_h + 0.0097\sigma + 4.5097 \log\sigma - 24890/T$.

[c] Numbers in parentheses are standard deviations.

where

$\sigma$ = stress, MPa;

$\sigma_{PL}$ = proportional limit, MPa;

$C$ = constant (measure of strength level);

$P$ = constant (describes shape of stress-strain curve before steady-state hardening, generally $P = 500C$);

$e_p$ = true plastic strain;

$H$ = constant (steady-state hardening rate, $d\sigma/d\sigma$).

The elastic strain can be determined by using the relationship between stress and the elastic modulus. A model has recently been developed by Booker[12] where creep strain is described by

$$e_c = [Cpt/(1 + pt)] + \dot{e}_m t \quad , \tag{6}$$

where

$e_c$ = creep-strain, %;

$C$ = parameter limiting value of transient primary creep, %;

$p$ = parameter relating the sharpness of the curvature of the primary creep region, 1/h;

$t$ = time, h;

$\dot{e}_m$ = minimum creep rate, %/h, from Eq. (2).

The parameters $C$ and $p$ are described by

$$p = 1.94\dot{e}_m^{0.73} \quad , \tag{7}$$

and

$$C = 1.16\dot{e}_m^{0.07} \quad , \tag{8}$$

Since $\dot{e}_m$ values were generally greater for longitudinally oriented specimens, we have limited our analysis to these specimens to provide a conservative characterization of the weldment. By using the $\dot{e}_m$

longitudinal specimen heat constants, $c_h$ (Table 5), and Eqs. (6) through (8), the creep strain-time behavior for each of our longitudinal creep-rupture tests was predicted. Figures 12 through 16 show comparisons of predicted creep strain with our experimental data. The predicted values were shown to the time of onset of tertiary creep for each test. An examination of these figures indicates that the use of the predicted values will generally produce greater than actual strains [Figs. 12(a), (b), and (c); 13(a) and (b); 14(a); 15(a); and 16(a) and (b)]. Some of the predicted values were approximately equal to and/or greater than the actual strain [Figs. 14(a), (c), and (d) and 15(c)]. Figure 16(c) showed accurate predictions to about 1.5% before becoming nonconservative. In addition, of the five remaining nonconservative predictions, two appear to be related to insufficient data [Figs. 12(d) and 13(c)].

Isochronous stress-strain curves can be produced by using the previously verified[1] model for tensile elastic-plastic total true strain and Booker's[12] model for creep strain. Based upon our analysis of longitudinal tests (which were shown to have higher $\dot{e}_m$ values) and our generally conservative predictions of creep strain, we expect that our isochronous stress-strain curves will conservatively characterize the weldments from our pipes. Figures 17 through 21 show the isochronous stress-strain curves for the welds in each of the pipes. These figures used times and the range of strains as shown in the ASME Code Case N-47 (Figs. T-1800-B-5 and T-1800-B-9). The curves for the welds at 538°C exhibit a compressed spacing between the isochronous lines. This behavior is especially apparent for the welds from pipes G-15 and G-16 [Figs. 19(a) and 20(a)]. The compressed behavior is a result of the previously reported[11] flat-top nature of the creep curve for weld metal as shown in Fig. 22.

A convenient method for comparing the ASME Code Case N-47 isochronous stress-strain curves with those for our welds is to construct a table of predicted stresses to produce a given strain. Because Code Case N-47 limits the strain accumulation in a weld to one-half that for the surrounding base metal, we have predicted stresses to produce strains of 0.5 and 1%. The value of 1% strain corresponds with the Code Case N-47 maximum accumulated inelastic strain averaged through the thickness.

Table 6 provides a comparison of the predicted stresses to produce 0.5 and 1% strains. The stress values of welds that are less than those for Code Case N-47 are underlined. It is important to note that welds E-13, F-14, and H-22 had lower predicted stresses than the code case for both 0.5 and 1% strains. The results of this comparison show the same general trends as previously discussed. The welds in G-15 and G-16 had stress values that were generally equal to or greater than the code values. This is to be expected since these welds had $\dot{e}_m$ values that were lower than the average for wrought material, as shown in Fig. 5. The lower stress values for the welds from E-13, F-14, and H-22 also correspond with the results shown in Fig. 5. This correlation with minimum creep rate data is expected since the creep-strain Eqs. (6 through 8) have $\dot{e}_m$ terms. The weld from F-14 had the most stress values that were lower than the code values. This again corresponds with the previous characterization of the F-14 weld being weaker because of composition variation.

## Time to Onset of Tertiary Creep

The time to onset of tertiary creep is an important instability that should be considered for design purposes. Previous work[9,13] has shown that time-to-rupture ($t_r$) and time-to-onset of tertiary ($t_2$) data for wrought type 316 stainless steel can be fit to a model of the form

$$t_2 = 0.526 t_r^{1.004} , \tag{9}$$

where

$t_2$ = time to onset of tertiary creep, h;

$t_r$ = time to rupture, h.

Figure 23 shows a comparison of time to onset of tertiary creep with time to rupture. The values predicted by Eq. (9) are also shown as a solid line on this figure. The experimental data closely follow the predicted values. The data appear to scatter or deviate more from the predicted values for shorter times.

Table 6. Comparison of Predicted Stresses with Code Case N-47 Stress for 0.5 and 1% Total Strains

| Temperature (°C) | Time (h) | Predicted Stress, MPa, for Indicated Strains[a] | | | | | | | | | | | |
|---|---|---|---|---|---|---|---|---|---|---|---|---|---|
| | | ASME Code Case N-47 Stress, MPa, for Indicated Strains | | E-13 | | F-14 | | G-15 | | G-16 | | H-22 | |
| | | 0.5% | 1% | 0.5% | 1% | 0.5% | 1% | 0.5% | 1% | 0.5% | 1% | 0.5% | 1% |
| 538 | $10^3$ | 152 | 168 | 184 | 197 | 168 | 181 | 182 | 196 | 152 | 162 | 153 | 163 |
| 538 | $10^4$ | 141 | 156 | 158 | 188 | 134 | 168 | 178 | 192 | 150 | 160 | 146 | 158 |
| 538 | $10^5$ | 124 | 140 | 122 | 161 | 101 | 133 | 170 | 185 | 144 | 155 | 130 | 149 |
| 649 | $10^3$ | 79 | 92 | 70 | 92 | 55 | 72 | 113 | 143 | 104 | 131 | 70 | 91 |
| 649 | $10^4$ | 61 | 71 | 48 | 66 | 37 | 50 | 81 | 107 | 74 | 98 | 47 | 64 |
| 649 | $10^5$ | 45 | 52 | 33 | 45 | 24 | 34 | 58 | 78 | 52 | 71 | 32 | 44 |

[a]The stress values of welds that are less than those for ASME Code Case N-47 are underlined.

Equation (9) can be used to describe $t_2$ as a function of stress. This can be done by using Eq. (1) to determine $t_r$ in Eq. (9). Figures 24 through 28 show comparisons of predicted $t_2$ with experimental data from longitudinally oriented weld specimens. The predicted values show good agreement with the experimental data except for H-22 at 538°C [Fig. 28(a)]. However, it appears that one data point must be incorrect. When using these figures it is important to realize that predicted values extend 3 to 4 orders of magnitude beyond the experimental data. A convenient way to determine if any of the welds would reach their predicted $t_2$ instability within code case design limits is to construct a table of predicted stresses for the onset of tertiary creep for various times. Table 7 provides a comparison of these predicted $t_2$ values with the Code Case N-47 stresses for 0.5 and 1% strains. It can be seen that in all cases the strain-limited code case stresses were lower than the predicted stresses for onset of tertiary creep in the weld.

## Creep Ductility

The effect of variables such as temperature, stress, grain size, and chemical composition on creep ductility have been discussed in a previous report.[14] Figure 29 shows a schematic indicating that variations in these variables can produce alternating regions of high and low ductility. Because of those variations, evaluating creep ductility results can be difficult unless sufficient data exist to define the alternating ductility regions. The scatter generally associated with ductility data is a further complication. Since we have only a limited amount of data for each weld, it is difficult to clearly define the various ductility regions.

Figures 30 and 31 show comparisons of reduction in area (RA) and elongation at fracture, respectively, with time to rupture. At 538°C both RA and elongation appear to be passing through a region of low ductility (region II of Fig. 29). At 649°C the data are scattered too much to enable an overall characterization. However, the appearance of scattering may result from the individual welds being in different ductility regions.

Table 7. Comparison of Predicted Stresses for Time to Onset of Tertiary Creep with Code Case N-47 Stresses for 0.5 and 1% Total Strains

| Temperature (°C) | Time (h) | ASME Code Case N-47 Stress, MPa, for Indicated Strains | | Predicted Stress, MPa, for Time to Onset of Tertiary Creep | | | | |
|---|---|---|---|---|---|---|---|---|
| | | 0.5% | 1% | E-13 | F-14 | G-15 | G-16 | H-22 |
| 538 | $10^3$ | 152 | 168 | 310 | 282 | 340 | 330 | 290 |
| 538 | $10^4$ | 141 | 156 | 251 | 227 | 280 | 270 | 242 |
| 538 | $10^5$ | 124 | 140 | 198 | 172 | 222 | 212 | 178 |
| 649 | $10^3$ | 79 | 92 | 140 | 119 | 163 | 155 | 122 |
| 649 | $10^4$ | 61 | 71 | 96 | 78 | 115 | 108 | 81 |
| 649 | $10^5$ | 45 | 52 | 60 | 46 | 76 | 69 | 58 |

For elongation at 649°C and to some extent at 538°C, the longitudinal specimens have greater ductility than the transverse. This indicates that the weld metal is more ductile than the weld metal-HAZ-base metal composite. This trend is not present in the RA data because these ductility values cannot represent the entire composite.

To evaluate the cyclic variations in ductility, we have compared RA minimum creep rate or tensile test strain rate. Figures 32 through 36 show this comparison with the trend curve for the ORNL reference heat of wrought type 316. These figures indicate that the welds pass through alternating ductility regions similar to those for wrought material. The weld regions appear to be shifted in some cases [Fig. 32(a)] and to have lower minimums in other cases [Figs. 34(b) and 35(b)]. The SA weld from pipe H-22 (Fig. 36) appears to be the only one that can be characterized as consistently falling below the wrought material trend. When examining these data it is important to remember the amount of potential variation; furthermore, we are only comparing the welds to one heat of wrought material.

## Characterization of Microstructure

Longitudinal creep-rupture specimens tested at 538°C and 310 MPa have been examined to characterize the microstructure. Figure 37 shows photomicrographs at or near the rupture for specimens from each pipe. As you may recall from Table 3, the welds from G-15, G-16, and H-22 contained no ferrite, while E-13 had a ferrite number (FN) of 0.1 to 0.4 and F-14 had a FN of 0.6 to 4.8. The effect of the varying ferrite content can clearly be seen in Fig. 37. The welds that did not contain ferrite [Fig. 37(c), (d), and (e)] had extensive intergranular tearing. Both initiation and propagation of tears occurred along the grain boundaries. In addition, the grain size in these welds was coarser than that for the weld with 0.6 to 4.8 FN [F-14, Fig. 37(b)]. Two fracture initiation processes appear to be occurring in E-13 [Fig. 37(a)]. Intergranular tearing is present in regions with coarse grain size, while tearing of partially transformed ferrite islands occurs in finer grained ferrite-containing regions. The propagation of cracks appears to be both trans- and intragranular. The

fracture process in F-14 [Fig. 37(b)] consists of crack initiation at partially transformed ferrite islands followed by transgranular linkage. Figure 38 provides a more detailed view of crack initiation at a ferrite island in F-14. Our characterization of grain boundary processes dominating in fully austenitic material and changing to matrix deformation with increasing amounts of ferrite agrees with other reported[15] observations.

## FATIGUE TESTING

Fully reversed push-pull strain-controlled fatigue tests were performed in air at 593°C and were conducted in a closed-loop electrohydraulic test machine. Uniform gage length specimens of the configuration shown in Fig. 39 were used. Specimen removal from the welds was the same as shown in Fig. 1. Strain was controlled by the use of an axial extensometer. Both continuous cycling and cycling with a tensile hold time of 0.1 h were used. The triangular waveforms and resultant hysteresis loops are shown in Fig. 40. All tests were performed at a ramp strain rate of $4 \times 10^{-3}$/s. Specimens were induction heated in air with the temperature being monitored and controlled by thermocouples spot welded to the specimen outside the gage area. The temperature over the uniform gage section of the specimen was uniform within ±2°C.

Table 8 summarizes the test data. The elastic ($\Delta\varepsilon_e$) and plastic ($\Delta\varepsilon_p$) strain range, the tensile ($\sigma_t$) and compressive ($\sigma_c$) stress amplitude, and the relaxation stress ($\sigma_{t_n}$) values for each test were measured from a hysteresis loop near the half life ($N_f/2$ or $N_h/2$). The continuous cycles to failure ($N_f$) and cycles to failure with a hold time ($N_h$) were defined as the points at which the tensile load dropped by 50%. This was determined from a continuous strip chart recording of load vs time.

### Continuous Cycling Tests

The Manson-Coffin[16] power-law equations can be used to describe the relationships between cycles to failure and the elastic and plastic strain

Table 8. Summary of Data for Strain-Controlled, Low-Cycle Fatigue Testing[a] of Formed-and-Welded Pipe in Air at 593°C

| Specimen | Orientation[b] | Total Strain Range, $\Delta\varepsilon_t$ (%) | Tensile Hold Time, $t_h$ (h) | Values in Stabilized Region[c] | | | | | | | Cycles to Failure[d] | |
|---|---|---|---|---|---|---|---|---|---|---|---|---|
| | | | | Strain Range, % | | Stress Amplitude, MPa | | | Tensile Relaxation Stress, MPa | | Continuous ($N_f$) | With Hold Time ($N_f$) |
| | | | | Elastic ($\Delta\varepsilon_e$) | Plastic ($\Delta\varepsilon_p$) | Total ($\Delta\sigma$) | Tensile ($\sigma_t$) | Compressive ($\sigma_c$) | $\sigma_{t_r}$ | At $0.1t_h$ $\sigma_{0.1}$ | | |
| **Pipe E-13** | | | | | | | | | | | | |
| 8 | L | 0.500 | | 0.330 | 0.170 | 449.5 | 222.0 | 227.5 | | | 6840 | |
| 9 | T | 0.500 | | 0.325 | 0.175 | 460.6 | 224.1 | 236.5 | | | 9595 | |
| 17 | L | 2.000 | | 0.670 | 1.330 | 686.7 | 340.6 | 346.1 | | | 450 | |
| 18 | T | 2.000 | | 0.560 | 1.440 | 732.8 | 357.8 | 375.0 | | | 367 | |
| 26 | L | 0.500 | 0.1 | Equipment Malfunction | | | | | | | | |
| 27 | T | 1.000 | 0.1 | 0.420 | 0.580 | 591.5 | 290.2 | 301.3 | 259.0 | 264.7 | | 651 |
| 35 | L | 2.000 | 0.1 | 0.550 | 1.450 | 639.8 | 317.8 | 322.0 | 276.1 | 288.6 | | 350 |
| 36 | T | 2.000 | 0.1 | 0.500 | 1.500 | 724.9 | 358.1 | 366.8 | 293.1 | 305.8 | | 131 |
| **Pipe F-14** | | | | | | | | | | | | |
| 8 | L | 0.500 | | 0.315 | 0.185 | 346.1 | 177.9 | 168.2 | | | 15,105 | |
| 9 | T | 0.500 | | 0.300 | 0.200 | 383.3 | 191.0 | 192.3 | | | 7,776 | |
| 17 | L | 2.000 | | 0.530 | 1.470 | 672.2 | 328.2 | 344.0 | | | 392 | |
| 18 | T | 2.000 | | Specimen Broke from Machine Malfunction | | | | | | | | |
| 26 | L | 1.000 | 0.1 | 0.440 | 0.560 | 454.3 | 216.5 | 237.8 | 204.0 | 208.3 | | 1338 |
| 27 | T | 1.000 | 0.1 | Invalid Test | | | | | | | | |
| 35 | L | 2.000 | 0.1 | 0.560 | 1.440 | 592.9 | 291.6 | 301.3 | 248.2 | 260.8 | | 208 |
| 36 | T | 2.000 | 0.1 | 0.530 | 1.470 | 603.9 | 304.7 | 299.2 | 267.2 | 279.8 | | 320 |
| **Pipe G-15** | | | | | | | | | | | | |
| 8 | L | 0.500 | | 0.355 | 0.145 | 408.1 | 209.6 | 198.5 | | | 18,965 | |
| 9 | T | 0.500 | | 0.300 | 0.200 | 470.2 | 235.8 | 234.4 | | | 6,250 | |
| 17 | L | 2.000 | | 0.540 | 1.460 | 862.4 | 422.6 | 439.8 | | | 182 | |
| 18 | T | 2.030 | | 0.600 | 1.430 | 827.9 | 388.1 | 439.8 | | | 212 | |
| 26 | L | 1.000 | 0.1 | 0.480 | 0.520 | 686.0 | 338.5 | 347.5 | 294.7 | 300.4 | | 317 |
| 27 | T | 1.000 | 0.1 | 0.444 | 0.556 | 659.1 | 324.7 | 334.4 | 279.6 | 289.5 | | 274 |
| 35 | L | 2.000 | 0.1 | 0.480 | 1.520 | 685.3 | 341.3 | 344.0 | 294.7 | 310.2 | | 96 |
| 36 | T | 2.000 | 0.1 | 0.550 | 1.450 | 741.1 | 366.8 | 374.3 | 305.0 | 319.4 | | 91 |
| **Pipe G-16** | | | | | | | | | | | | |
| 8 | L | 0.500 | | 0.365 | 0.135 | 461.9 | 231.6 | 230.3 | | | 7,502 | |
| 9 | T | 0.500 | | 0.300 | 0.200 | 470.2 | 235.8 | 234.4 | | | 17,942 | |
| 17 | L | 2.000 | | 0.520 | 1.480 | 790.8 | 392.3 | 398.5 | | | 224 | |
| 18 | T | 2.020 | | 0.600 | 1.420 | 785.2 | 381.9 | 403.3 | | | 374 | |
| 26 | L | 1.000 | 0.1 | 0.487 | 0.513 | 628.3 | 309.8 | 318.5 | 276.7 | 283.9 | | 234 |
| 27 | T | 1.000 | 0.1 | 0.494 | 0.506 | 650.7 | 302.6 | 348.1 | 274.7 | 283.1 | | 357 |
| 35 | L | 1.980 | 0.1 | 0.625 | 1.350 | 683.2 | 339.2 | 344.0 | 309.4 | 317.8 | | 177 |
| 36 | T | 1.980 | 0.1 | 0.610 | 1.370 | 708.7 | 351.6 | 357.1 | 307.5 | 318.9 | | 133 |
| **Pipe H-22** | | | | | | | | | | | | |
| 8 | L | 0.500 | | 0.338 | 0.162 | 362.0 | 191.7 | 170.3 | | | 8744 | |
| 9 | T | 0.500 | | 0.325 | 0.175 | 424.7 | 209.6 | 215.1 | | | 7281 | |
| 17 | L | 2.000 | | 0.600 | 1.400 | 794.9 | 388.8 | 406.1 | | | 322 | |
| 18 | T | 2.000 | | 0.538 | 1.462 | 696.3 | 347.5 | 348.8 | | | 245 | |
| 26 | L | 1.000 | 0.1 | 0.494 | 0.506 | 492.9 | 239.2 | 253.7 | 219.4 | 223.7 | | 830 |
| 27 | T | 1.000 | 0.1 | 0.380 | 0.620 | 527.4 | 266.1 | 261.3 | 236.5 | 245.1 | | 398 |
| 35 | L | 2.000 | 0.1 | 0.563 | 1.437 | 599.1 | 299.9 | 299.2 | 265.8 | 278.6 | | 70 |
| 36 | T | 2.000 | 0.1 | 0.600 | 1.400 | 629.4 | 309.5 | 319.9 | 265.8 | 278.6 | | 121 |

[a] Test conducted at strain rate of $4 \times 10^{-3}$/s on uniform-gage specimens, using an axial extensometer to control strain.

[b] L = longitudinal; T = transverse.

[c] The values for the stabilized region were generally near $N_f/2$ or $N_h/2$.

[d] The point at which $\sigma_t$ decreases by 50%.

ranges for continuous cycling fatigue behavior. These equations are of the forms

$$\Delta\varepsilon_e = AN_f^{-\alpha} , \tag{10}$$

$$\Delta\varepsilon_p = BN_f^{-\beta} , \tag{11}$$

and

$$\Delta\varepsilon_t = \Delta\varepsilon_e + \Delta\varepsilon_p = AN_f^{-\alpha} + BN_f^{-\beta} , \tag{12}$$

where

$\Delta\varepsilon_e$ = elastic strain range;
$\Delta\varepsilon_p$ = plastic strain range;
$\Delta\varepsilon_t$ = total strain range;
$N_f$ = cycles to failure;
$A$, $\alpha$, $B$, $\beta$ = constants.

Wrought material data from a recent survey[17] of type 316 stainless steel fatigue testing were fit by linear regression analysis to Eqs. (10) and (11). The constants that resulted from fitting the data from 19 fatigue tests to the power-law equations are as follows: for elastic strain [Eq. (10)] $A$ = 1.343, $\alpha$ = 0.151, and $r^2$ = 0.916 and for plastic strain [Eq. (11)] $B$ = 34.754, $\beta$ = 0.519, and $r^2$ = 0.980, where $r^2$ = the coefficient of determination.

Figure 41 provides a comparison of total strain range vs cycles to failure for the welds in our pipes. Values predicted by the previously described power-law model for wrought material are shown for comparison. In addition, the ASME Code Case N-47 (Fig. T-1420-1B) inelastic analysis design line for 593 to 649°C is included[8]. Figure 41 shows that the data for our welds consistently fall slightly below the values predicted for wrought material. However, in all cases the weld data were considerably above the Code Case N-47 design line. The various welds do not appear to differ consistently. Figure 42 shows a comparison of longitudinal vs transverse cycles to failure. The differences between longitudinal and

transverse cycles to failure for all welds are not consistent. However, the weld in G-16 shows the transverse direction to have a greater life, while H-22 shows the longitudinal direction to be slightly greater.

The data for each weld were fit by linear regression analysis to the Manson-Coffin power-law relationships [Eqs. (10) and (11)]. We did this to enable estimation of individual weld $N_f$ values for linear damage summation (LDS) analysis of creep-fatigue data to be presented in a later section. Table 9 summarizes the constants that resulted from fitting the data. Figure 43 shows how the values predicted by the resulting power-law equations compare with the actual data. Although the data are limited, the predicted values agree reasonably well with the available data. The data for weld G-16 [Fig. 43(d)] deviate the most. This results from the previously discussed differences between the longitudinal and transverse directions.

Figures 44 through 48 compare tensile stress amplitude $\sigma_t$ vs percentage cyclic life for continuous cycle fatigue tests on the welds from each pipe. These figures conveniently make relative comparisons of strain hardening, stress amplitude, crack initiation, and crack propagation characteristics among the various welds. The tensile stress amplitude values were used instead of the total stress values because the compressive component would misrepresent crack extension. Except for the 2.0% strain range tests for the welds in G-15 and G-16 (type 316 filler metal and autogenous, respectively), the remaining welds strain hardened and reached a steady or nearly steady stress amplitude condition within 5 to 10% of the cyclic life. Whereas, G-15 and G-16 did not reach a steady $\sigma_t$ until 20 to 30% of cyclic life. The welds with the lowest stress amplitude (F-14 and H-22) were the same ones that had the lowest creep-rupture lives and UTS values. Both the percentage of cyclic life at which crack initiation occurs and the rate of crack propagation varied somewhat. These differences predominated between longitudinal and transverse specimens tested at a $\Delta\varepsilon_t$ of 0.5%. However, the variation showed no clear trend. A recent study[18] of the effect of fatigue specimen geometry indicated that surface flaws present during low strain range tests have more influence on uniform-gage specimens. Some of the variation with initiation might be caused by this effect.

Table 9. Summary of Constants[a] Resulting from Fitting Data to Power-Low Relationships Between Cycles to Failure and Elastic and Plastic Strain Ranges

| Pipe | Elastic Strain | | | Plastic Strain | | |
|---|---|---|---|---|---|---|
| | $A$ | $\alpha$ | $r^2$ | $B$ | $\beta$ | $r^2$ |
| E-13 | 2.051 | 0.202 | 0.932 | 86.696 | 0.690 | 0.991 |
| F-14 | 1.334 | 0.157 | 0.940 | 50.582 | 0.598 | 0.981 |
| G-15 | 1.089 | 0.127 | 0.825 | 22.439 | 0.523 | 0.992 |
| G-16 | 1.230 | 0.140 | 0.915 | 32.063 | 0.557 | 0.910 |
| H-22 | 1.393 | 0.159 | 0.949 | 53.703 | 0.641 | 0.997 |

[a]The equation for elastic strain is $\Delta\varepsilon_e = AN_f^{-\alpha}$, and the one for plastic strain is $\Delta\varepsilon_p = BN_f^{-\beta}$, where $N_f$ = cycles to failure. $r^2$ = coefficient of determination.

Figures 49 through 53 show photomicrographs of secondary cracks in longitudinally oriented continuous cycle fatigue specimens tested at 593°C and 2.0% total strain range. The welds in pipes E-13 (Fig. 49) and H-22 (Fig. 53) contained only a few secondary cracks. However, these cracks had propagated extensively. The welds from pipes F-14, G-15, and G-16 (Figs. 50, 51, and 52) contained a larger number of secondary cracks that had not propagated much. In general, the secondary cracks for all pipes propagated transgranularly with no observable damage ahead of the crack tip. Figure 50 shows that ferrite is not involved in the crack propagation process. However, it is important to note that the ferrite has not transformed and therefore may behave differently if it were transformed. Our observations of transgranular crack propagation for continuous cycle fatigue tests are consistent with results reported[19] for type 16-8-2 weld metal deposited by the SA process.

## Cycling with a Tensile Hold Period

Figure 54 shows a comparison of total strain range vs cycles to failure for fatigue tests with a tensile hold period of 0.1 h. In addition to the data from our welds, this figure also includes wrought

type 316 data from a recent compilation.[17] The data from our welds fall within the scatter of the wrought material data. It is important to note that the wrought material data represent only two heats, with one heat (65808) predominating. Therefore, although our weld data compare with values available for wrought material, a larger number of heats is needed to make the comparison more meaningful. Figure 54 does not show any clear trends among the various welds. Figure 55 compares longitudinal vs transverse cycles to failure. Although five out of eight points indicate that the longitudinal specimens have a greater $N_h$, the reversal of the trend for two welds and the generally small differences make it difficult to determine if one direction is favored.

The ASME Code Case N-47 uses the LDS approach to design for creep fatigue in welds. This approach defines creep-fatigue damage $D$, as the sum of creep, $D_c$, and fatigue, $D_f$, damage components given by

$$D = D_c + D_f \ . \tag{13}$$

Failure occurs when $D$ reaches a critical value. The creep and fatigue damage components are given by

$$D_c = \sum_i t/t_{r_i} \ , \tag{14}$$

and

$$D_f = \sum_j n/N_{f_j} \ , \tag{15}$$

where

$t$ = time,

$t_r$ = time to rupture,

$n$ = number of cycles,

$N_f$ = continuous cycles to failure.

The creep damage, $D_c$, is the summation of the different time fractions of rupture life that occur during stress relaxation in the hold period. Campbell[20] outlined an approach for analyzing $D_c$ using type 304 stainless steel creep-fatigue data. Booker[21] recently used this technique to examine 2 1/4 Cr-1 Mo data. The approach involves numerical integration of the hold period relaxation curve to calculate creep damage per cycle. Depending upon whether test results are to be compared with actual data or with Code Case N-47 requirements, the integration would be performed by using $t_r$ or $T_d$ given by

$$D_c(1) = \int_0^{t_h} dt/t_r \text{ or } \int_0^{t_h} dt/T_d \ , \tag{16}$$

where

$D_c(1)$ = creep damage per cycle,

$t_h$ = hold time,

$t_r$ = time to rupture for mateiral of interest,

$T_d$ = Code Case N-47 allowable time for stress values in Fig. I-14.6B that were divided by the reduction factor from Table T-1411-1.

To perform the numerical integration, a relationship between rupture life, $t_r$ or $T_d$, and time must be established. By using Eq. (1) with the all-specimen heat constant for each of our welds (listed in Table 5), $t_r$ can be defined in terms of stress (since temperature is known for each test, it is assumed constant). Expected minimum stress-rupture values[8] from Code Case N-47, Table I-14.6B, for 593°C were fit to a polynomial to provide a continous function for integration. Stress as a function of time during our relaxation periods can be described by the Gittus[22] equation given by

$$\ln (\sigma_t/\sigma) = ct^m \ , \tag{17}$$

where

$\sigma_t$ = peak tensile stress,

$\sigma$ = stress at time $t$,

$c$, $m$ = constants.

The constants $c$ and $m$ can be determined from

$$m = \ln [\ln (\sigma_t/\sigma_{0.1})/\ln (\sigma_t/\sigma_{t_r})]/\ln (0.1t_h/t_h) , \quad (18)$$

and

$$c = \ln (\sigma_t/\sigma_{t_r})/t_h^m , \quad (19)$$

where

$\sigma_t$ = peak tensile stress,

$\sigma_{0.1}$ = stress at time $0.1t_h$,

$\sigma t_r$ = relaxed stress at end of hold period,

$t_h$ = hold period.

The values of $\sigma_t$, $\sigma_{0.1}$, and $\sigma_{t_r}$ were measured from the relaxation curves for each of our tests and can be found in Table 8. Once the creep damage per cycle, $D_c(1)$, is determined by using the above approach, the creep damage component, $D_c$, can be determined from

$$D_c = N_h D_c(1) , \quad (20)$$

where $N_h$ = cycles to failure with hold time. The fatigue damage component, $D_f$, would be determined by using either $N$ or $N_d$, depending upon whether data or Code Case N-47 requirements, respectively, are used for comparison. The value of $D_f$ would then be given by

$$D_F = N_h/N_f \text{ or } N_h/N_d , \quad (21)$$

where

$N_h$ = cycles to failure with hold time for material and conditions of interest,

$N_f$ = continuous cycles to failure for material and conditions of interest,

$N_d$ = number of Code Case N-47 design allowable cycles from Fig. T-1420-1.

The results of LDS analysis by using values derived from data ($t_r$ and $N_f$) and Code Case N-47 limits ($T_d$ and $N_d$) are presented in Table 10. Note that when $N_f$ data were not available, values predicted by Eq. (12), with constants shown in Table 10, were used. Figure 56 shows our LDS data, using $t_r$ and $N_f$ plotted on a damage diagram that includes Campbell's[20] average and minimum trend curves for a heat of type 304 stainless steel. Campbell had defined $N_f$ and $N_d$ as the number of cycles to 5% drop in load; since we have used a 50% drop, comparison of our LDS data with Campbell's may be affected for tests with long crack extention times. An examination of Fig. 56 shows that over 80% of our data falls below the average trend curve. However, all our data are above the minimum trend curve. Campbell's average trend curve was used as the Code Case N-47 creep-fatigue damage envelope for types 304 and 316 stainless steel shown in Fig. T-1420-2. A safety factor is introduced into this figure by using the $t_d$ and $N_d$ values [from Eq. (16) and (21), respectively] to perform the LDS analysis. Figure 57 shows our data for the LDS analysis, using $T_d$ and $N_d$. It is evident that all our tests showed failures that exceeded the code case limits. However, our data varied considerably for the margin of safety, which ranged from about 5 to 80, using a 45° line through the cusp of the code case damage envelope to determine the multiple of $D_F$ = 0.6. The safety margins were lower than expected. This can be explained by examining Fig. 56. As previously discussed, this figure shows that over 80% of our tests failed below Campbell's average trend curve. Since Code Case N-47 uses this curve and applies separate safety factors through stress-rupture and fatigue design curves, it would be consistent for our data to show a reduced safety margin.

Figures 58 through 61 show photomicrographs of secondary cracks in longitudinally oriented fatigue specimens tested with a 2.0% total strain range and a tensile hold period of 0.1 h. It was previously discussed that longitudinal specimens might contain some areas of base metal within the gage length. This occurred for two specimens, F-14 and G-16 (Fig. 60), within the current group we were examining. No secondary cracks were observed on the weld metal edge of the specimen from F-14. In addition, no damage was observable in the weld metal away from the edge. Secondary

Table 10. Creep-Fatigue Linear Damage Summation Data[a]

| Specimen | Using $t_r$ and $N_f$ | | | | Using $T_d$ and $N_d$ | | | |
|---|---|---|---|---|---|---|---|---|
| | Creep Damage per Cycle,[b] $D_c(1)$ | Creep Damage,[c] $D_c$ | Fatigue Damage,[d] $D_F$ | Critical Damage,[e] $D$ | Creep Damage per Cycle,[b] $D_c(1)$ | Creep Damage,[c] $D_c$ | Fatigue Damage,[d] $D_F$ | Critical Damage,[e] $D$ |
| E-13-27 | $2.968 \times 10^4$ | 0.193 | 0.407[f] | 0.600 | $1.981 \times 10^{-2}$ | 12.896 | 16.275 | 29.171 |
| E-13-35 | 8.336 | 0.292 | 0.667 | 0.959 | 2.397 | 8.390 | 17.500 | 25.890 |
| E-13-36 | 13.040 | 0.171 | 0.338 | 0.509 | 3.122 | 4.090 | 6.550 | 10.640 |
| F-14-26 | 1.088 | 0.146 | 0.743[f] | 0.889 | 1.696 | 22.692 | 33.450 | 56.142 |
| F-14-35 | 8.027 | 0.167 | 0.447 | 0.614 | 1.899 | 3.950 | 10.400 | 14.350 |
| F-14-36 | 14.250 | 0.456 | 0.688 | 1.144 | 2.176 | 6.963 | 16.000 | 22.963 |
| G-15-26 | 5.158 | 0.164 | 0.264[f] | 0.428 | 3.013 | 9.551 | 7.925 | 17.476 |
| G-15-27 | 4.029 | 0.110 | 0.228[f] | 0.338 | 2.463 | 6.749 | 6.850 | 13.599 |
| G-15-35 | 6.279 | 0.060 | 0.527 | 0.587 | 3.317 | 3.184 | 4.800 | 7.984 |
| G-15-36 | 11.820 | 0.108 | 0.429 | 0.537 | 4.093 | 3.725 | 4.550 | 8.275 |
| G-16-26 | 3.826 | 0.090 | 0.156[f] | 0.246 | 2.337 | 5.469 | 5.850 | 11.319 |
| G-16-27 | 3.557 | 0.127 | 0.238[f] | 0.365 | 2.300 | 8.211 | 8.925 | 17.136 |
| G-16-35 | 13.940 | 0.247 | 0.290 | 1.037 | 4.220 | 7.469 | 8.850 | 16.319 |
| G-16-36 | 13.490 | 0.179 | 0.356 | 0.535 | 4.182 | 5.562 | 6.650 | 12.212 |
| H-22-26 | 1.596 | 0.132 | 0.638[f] | 0.770 | 1.724 | 14.309 | 20.750 | 35.059 |
| H-22-27 | 3.486 | 0.139 | 0.306[f] | 0.445 | 1.797 | 7.152 | 9.950 | 17.102 |
| H-22-35 | 12.500 | 0.088 | 0.207 | 0.295 | 2.150 | 1.505 | 1.750 | 3.255 |
| H-22-36 | 12.340 | 0.149 | 0.494 | 0.643 | 2.150 | 2.602 | 3.025 | 5.627 |

[a] $t_r$ = time to rupture; $N_f$ = continuous cycles to failure; $T_d$ = Code Case N-47 allowable time for stress values in Fig. I-14.6 B that were divided by the reduction factor from Table T-1411-1; $N_d$ = number of Code Case N-47 design allowable cycles from Fig. T-1420-1.

[b] $D_c(1) = \int_0^{t_h} dt/t_r$, where $t_h$ = hold time.

[c] $D_c = N_h D_c(1)$, where $N_h$ = cycles to failure with hold time.

[d] $D_f = N_h/N_f$.

[e] $D = D_c + D_F$.

[f] Used predicted $N_f$ to calculate value.

cracks were present in the base metal and propagated intergranularly. Cracking appeared to initiate on the base metal side and propagate across to the weld metal. The specimen from G-16 [Fig. 60(a)] had approximately 0.65 mm of base metal at one edge. It can be seen that cracks propagated intergranularly through the base metal. Propagation of the cracks into the weld metal depended upon intersection with a weld metal grain boundary. Some base metal cracks were not able to propagate into the weld metal. In addition to crack propagation from the base metal, cracks were initiating independently in the weld metal along grain boundaries. The specimens that contained all weld metal, E-13, G-15, and H-22 (Figs. 58, 59, and 61) contained secondary cracks that initiated either transgranularly [Fig. 59(b)] or intergranularly [Fig. 61(b)] and then propagated intergranularly. The initiation process depended upon grain orientation. The grain orientation for H-22 [Fig. 61(b)] was perpendicular to the stress direction and therefore provided favorable conditions for intergranular initiation. Figure 61(a) also shows the presence of oxide formation along the secondary crack. Damage at ferrite islands away from the specimen edge can be seen in Fig. 58(b). However, propagation of secondary cracks does not appear to be dependent upon damaged ferrite.

Our characterization of both matrix and intergranular cracking, with the latter predominating, corresponds with previously reported[19] observations for type 16-8-2 weld metal deposited by the SA process. In addition, our observations for F-14 (no secondary cracks in weld metal) and G-16 [Fig. 60(b)] support the reported[19] higher resistance of weld metal to interphase cracking.

## DISCUSSION

The ASME Code Case N-47 considers time-dependent material properties and guards against time-dependent rupture modes such as creep-rupture, fatigue, creep fatigue, and gross distortion from ratchetting. The design of components is based upon the control of both load and deformation. The control of these design parameters must then be translated into material property requirements.

The material properties needed to meet design load controls are primarily assured through a knowledge of the material's creep-rupture behavior. The relationship between load and time to rupture, $t_r$, is used to construct models that will ensure the proper safety margins. Our analysis has shown that our welds had $t_r$ values that ranged from slightly below the Code Case N-47 minimum to above the average for wrought material (Fig. 3). The variation of weld metal time-to-rupture values has been previously reported.[10,11,15,23–25] The variation between welds results from variables such as welding process [SMA, GTA, gas metal-arc (GMA), SA], filler metal and flux composition, arc atmosphere composition, dilution (function of base metal composition), heat input (function of amperage, voltage, travel speed, and process characteristics), and heat treatment (all our welds were solution annealed, whereas most austenitic stainless steel welds are used as welded). The $t_r$ values for welds have generally been reported[10,23–25] to be within the scatter for wrought material. In addition, it is also reported[10] that some differences in weld metal properties will probably be reduced after long service periods as a result of microstructures reaching equilibrium conditions.

The most prudent approach for ensuring that welds meet the design requirements for $t_r$ would be to require procedure qualification tests for high-temperature service. A method that utilizes elevated-temperature UTS has already been reported.[11] However, short-term creep-rupture tests could also be used to verify that minimum property requirements have been met. Based upon our tests of solution-annealed longitudinal seam welds and the results[10,23–25] of tests on as-deposited and heat-treated welds, it is apparent that welds can be produced that have equal or greater $t_r$ values than wrought material. Therefore, with proper qualification testing it should be possible to ensure that welds will meet load-controlled design requirements.

Strain-controlled design requirements would be associated with material properties that are determined by tensile, creep-rupture, and fatigue behavior. Although creep-fatigue behavior is also an important consideration for strain control, we will treat it separately, as does Code Case N-47. Strain-controlled design requirements limit both the

total accumulated strain during life and the magnitude and number of strain reversals resulting from fatigue. The code case utilizes a knowledge of isochronous stress-strain behavior to limit total accumulated strain. The isochronous stress-strain curves are determined from both tensile elastic-plastic and creep-strain behavior. For normal service life, minimum creep rate, $\dot{e}_m$, becomes the most important material property to describe accumulated strain. However, Code Case N-47 does not provide limits for $\dot{e}_m$. We have shown that the $\dot{e}_m$ values for our welds fall above and below the average for wrought material (Fig. 5). The autogenous weld and the one with type 316 filler metal showed $\dot{e}_m$ values that were 1 to 2 orders of magnitude lower than values for type 16-8-2 deposited by the GTA or SA processes. A range of $\dot{e}_m$ values for as-deposited and heat-treated welds, that fall above and below trend curves for wrought material have been reported.[24] The variability of weld metal $\dot{e}_m$ values again highlights the desirability of performing a qualification test. However, since Code Case N-47 does not provide requirements, minimum values based upon wrought material properties would need to be established. The previously reported[11] method that used UTS to predict $\dot{e}_m$ was not able to predict the behavior of flat-top creep curves. However, the recently[9] developed heat-centered models for $t_r$ and $\dot{e}_m$ would provide a convenient method for establishing minimum requirments to be used for creep-rupture qualification testing.

In addition to limiting the total accumulated strain, the code case seeks to avoid instabilities in welds that could lead to sudden failure. To do this, the total inelastic strains accumulated in the weld are not allowed to exceed one-half the strain values permitted for the base material. This one-half allowable strain is used to guard against limited ductility in the weld metal and high strain concentrations (both metallurgical and geometric) in the HAZ. We have already shown (Table 7) that our welds would not reach the tertiary creep instability for the code case allowable stresses for total accumulated strains of 0.5 and 1.0%. Ductility has been reported[14] to pass through alternating high and low regions resulting from variations in temperature, stress, grain size, chemical composition, and material condition (Fig. 29). Because our data was

limited, it was hard to characterize the alternating regions. However, Figs. 32 through 36 show that, except for the SA weld (pipe H-22), the weld ductility was generally comparable with the trend curve for the ORNL reference heat of wrought type 316 stainless steel. Large variations in weld ductility data have been reported[10,24] by other investigators and have been acknowledged[24] as comparable with the scatter for wrought material data. However, the similarity in alternation of weld metal and wrought material ductility is not discernable until corrected for strain rate effects, as shown in Figs. 32 through 36.

The use of qualification test data to meet minimum ductility requirements would be difficult because of the inherent scatter. However, at the same time it appears that the one-half allowable strain imposed upon the weld metal is not justified for all welds based upon low ductility criteria. For our welds, metallurgical and geometric strain concentrations in the HAZ may not apply since our solution annealing has eliminated most effects except for some grain growth.

Table 6 has shown that three or our five welds have greater predicted strains for given stresses as compared to the code case for both full and one-half allowable strain. However, it should be recalled that our predictions are generally conservative. Other work has shown[25] that GTA-deposited type 16-8-2 welds have isochronous stress-strain behavior that is comparable to wrought material. It therefore appears that high-temperature qualification of welding procedures is a more sound approach than the one-half allowable strain rule.

The fatigue aspect of design control of strain was addressed in Fig. 41. This figure shows that our welds fall just below the average for wrought material but well above the code case inelastic design line. In addition, other work[19] has shown that SA-deposited type 16-8-2 weld metal had greater resistance to fatigue loading than a heat of wrought material.

It is hard to relate the code case LDS approach for analysis of creep fatigue directly to material properties. However, our data (Fig. 52) and those of Raske[19] indicate that the weld cycles to failure, $N_h$, fall within the scatter for the available wrought material data. Figure 57 shows that our creep-fatigue failures occur in excess of the code case creep-fatigue damage envelope. However, the design safety margin may be somewhat reduced.

Based upon the foregoing discussion, it is reasonable to expect that welds can be made that can have adequate properties to meet base metal design requirements. However, it also appears that elevated-temperature qualification testing should be performed to assure that minimum requirements are met. With the use of this qualification testing, it might then be justifiable to drop the one-half allowable strain penalty for welds.

## CONCLUSIONS

The following conclusions can be made based upon the results of creep-rupture, fatigue, and creep-fatigue tests on the welds from our five formed-and-welded pipes.

1. Time-to-rupture values varied from below the ASME Code Case N-47 minimum to above the the average for wrought material. The SA weld and a GTA weld with low carbon and nitrogen had the lowest values.

2. Minimum creep rate values were above and below the average for wrought material. The longitudinally oriented specimens had greater creep rates than those with a transverse orientation. The values for the autogenous weld and for the one with type 316 filler metal were 1 to 2 orders of magnitude lower than the values for the three welds with type 16-8-2 filler (two GTA, one SA).

3. Conservative predictions of our weld isochronous stress-strain behavior resulted in predicted strains for three welds in excess of the ASME Code Case N-47 requirements. These were the same welds that experienced higher minimum creep rates.

4. We predicted the time to onset of tertiary creep for our welds to occur well in excess of the stress limits for ASME Code Case N-47.

5. Our welds experience the same type of alternating ductility regions found in wrought material. Except for the SA-deposited type 16-8-2 weld, the ductility appeared to be comparable with the wrought material.

6. The fatigue cycles to failure, $N_f$, values of our welds were slightly lower than values for wrought material but were well in excess of the ASME Code Case N-47 inelastic design line.

7. The creep-fatigue cycles to failure, $N_h$, values of our welds were comparable with those for the available wrought material.

8. Although our creep-fatigue failures were in excess of the ASME Code Case N-47 creep-fagtigue damage envelope, our safety margins were lower than expected.

9. Based upon the variation in time-dependent weld properties that we have seen in our data and in data from others, it appears justifiable to require elevated-temperature qualification testing of weld procedures rather than arbitrarily penalizing all welds.

## ACKNOWELDGMENTS

We would like to acknowledge Vulcan Testing, Inc., for performing the creep-rupture tests; Metcut Research Associates, Inc., for performing the fatigue and creep-fatigue tests; R. Baldwin and S. E. Hanzelka for processing data; C. W. Houck for performing metallographic examinations; M. K. Booker for discussions concerning analysis of data; K. C. Liu and P. L. Rittenhouse for reviewing this report; B. G. Ashdown for editing the manuscript; and K. A. Witherspoon for final preparation of the report for publication.

## REFERENCES

1. J. W. McEnerney and V. K. Sikka, *Characterization of Time-Dependent Properties of Formed and Welded Pipe for Breeder Reactor Applications*, ORNL/TM-6609 (April 1979).
2. *ASME Boiler and Pressure Vessel Code*, American Society of Mechanical Engineers, New York, 1977.
3. "Specification for Chromium and Chromium-Nickel Stainless Steel Plate, Sheet, and Strip for Fusion-Welded Unified Pressure Vessels," SA-240, in *ASME Boiler and Pressure Vessel Code, Sect. II, Material Specifications, Part A — Ferrous*, American Society of Mechanical Engineers, New York, 1975 summer addenda.

4. "Specification for Electric-Fusion-Welded Austenitic Chromium-Nickel Alloy Steel Pipe for High-Temperature Service," in *ASME Boiler and Pressure Vessel Code, Sect. II, Material Specifications Part A — Ferrous*, American Society of Mechanical Engineers, New York, 1974–1975 summer addenda.
5. "Specification for Seamless and Welded Austenitic Stainless Steel Pipe," SA-312, in *ASME Boiler and Pressure Vessel Code, Sect. III*, American Society of Mechanical Engineers, New York, 1974–1975 summer addenda.
6. *ASME Boiler and Pressure Vessel Code, Sect. III, Div. 1, Nuclear Power Plant Components, Subsect. NB — Class 1 Components*, American Society of Mechanical Engineers, New York, 1974–1975 summer addenda.
7. *ASME Boiler and Pressure Vessel Code, Sect. III, Div. 1, Nuclear Power Plant Components, Subsect. NC — Class 2 Components*, American Society of Mechanical Engineers, New York, 1974–1975 summer addenda.
8. *ASME Boiler and Pressure Vessel, Code Cases, Nuclear Components, N-47*, American Society of Mechanical Engineers, New York, 1977.
9. M. K. Booker, B.L.P. Booker, and C. R. Brinkman, *A Comparative Analysis of British and American Tensile and Creep Data for Type 316 Stainless Steel*, ORNL-5632 (April 1980).
10. R. L. Klueh and D. P. Edmonds, *Effects of Different Fluxes on Elevated-Temperature Strength of 16-8-2 Submerged-Arc Welds*, ORNL-5594 (February 1980).
11. V. K. Sikka and J. W. McEnerney, *Use of Ultimate Tensile Strength to Estimate the Creep-Rupture Behavior of Austenitic Weld Metals and Castings*, ORNL/TM-6781 (May 1979).
12. M. K. Booker, *Analysis of the Creep Strain-Time Behavior of Type 316 Stainless Steel*, ORNL/BRP-80-7 (report in press).
13. V. K. Sikka, H. E. McCoy, M. K. Booker, and C. R. Brinkman, "Heat-to-Heat Variation in Creep Properties of Types 304 and 316 Stainless Steels," *J. Pressure Vessel Technol.* 97(4): 243–51 (November 1975).

14. J. W. McEnerney and V. K. Sikka, *Characterization of Three Developmental Centrifugally Cast-and-Worked Austenitic Stainless Steel Pipes, Part II — Mechanical Properties Evaluation*, ORNL/TM-7238 (June 1980).

15. R. G. Thomas, "The Effect of δ-Ferrite on the Creep Rupture Properties of Austenitic Weld Metals," *Weld. J. (Miami)* 57(3): 81-s—86-s (March 1978).

16. S. S. Manson, "'Fatigue' A Complex Subject — Some Simple Approximations," *Exp. Mech.* 5(7): 193—226 (July 1965).

17. D. R. Dierchs, *A Compilation of United States and British Elevated-Temperature, Strain-Controlled Fatigue Data on Type 316 Stainless Steel*, ANL/MSD-78-4 (March 1978).

18. J. P. Strizak and C. R. Brinkman, *Influence of Melting Practice and Heat Treatment on the Continuous Cycling Fatigue and Subcritical Crack Growth Properties of 2 1/4 Cr-1 Mo Steel*, ORNL/TM-6782 (May 1979).

19. D. T. Raske, *Cyclic-Deformation Resistance of Weld-Deposited Type 16-8-2 Stainless Steel at 593°C*, ANL-77-72 (August 1977).

20. R. D. Campbell, "Creep/Fatigue Interaction Correlation for 304 Stainless Steel Subjected to Strain-Controlled Cycling with Hold Times at Peak Strains," *J. Eng. Ind.* 93: 887—92 (November 1971).

21. M. K. Booker, *Construction of Creep-Fatigue Elastic-Analysis Curves and Interim Analysis of Long-Term Creep-Fatigue Data for 2 1/4 Cr-1 Mo Steel*, ORNL/TM-6324 (July 1978).

22. J. H. Gittus, "Implications of Some Data on Relaxation Creep in Nimonic 80A," *Philos. Mag.* 9: 749 (1964).

23. R. T. King, N. C. Cole, and R. G. Berggren, "Properties and Structure of 16-8-2 Stainless Steel Weld Metals," *ASME Publication*, 75-PVP-45, American Society of Mechanical Engineers, New York, 1975.

24. A. L. Ward, *Austenitic Stainless Steel Weld Materials, A Data Compilation and Review*, HEDL-TME 74-75 (May 1974).

25. A. L. Ward and L. D. Blackburn, "Creep and Rupture Behavior of Weld-Deposited Type 16-8-2 Stainless Steel at 593°C," *J. Eng. Mater. Technol.* 99: 159—67 (April 1977).

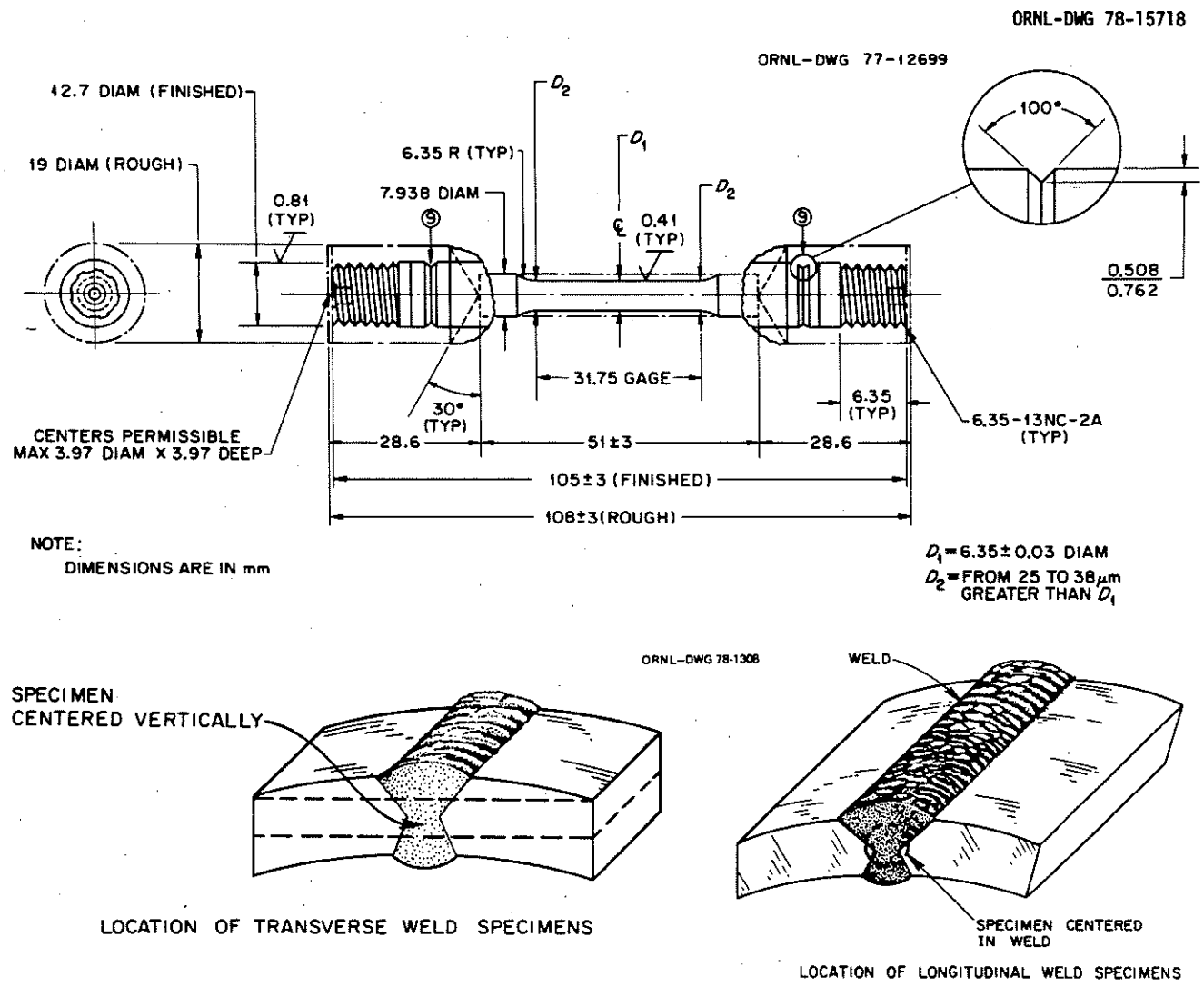


Fig. 1. Creep-Rupture Test Specimen Design and Its Location and Removal from Blanks Containing Welds.

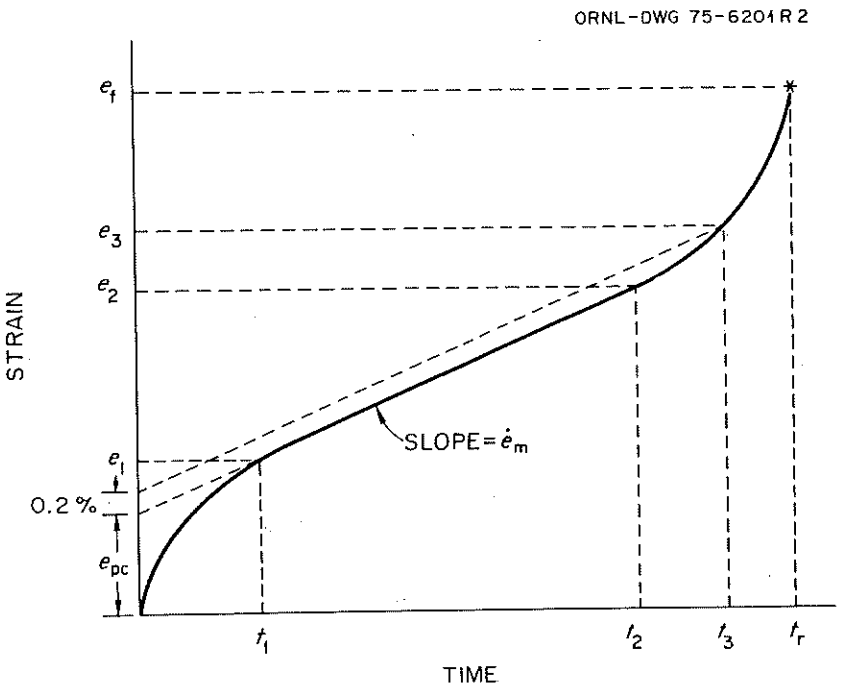


Fig. 2. Definitions of Creep Quantities Examined.

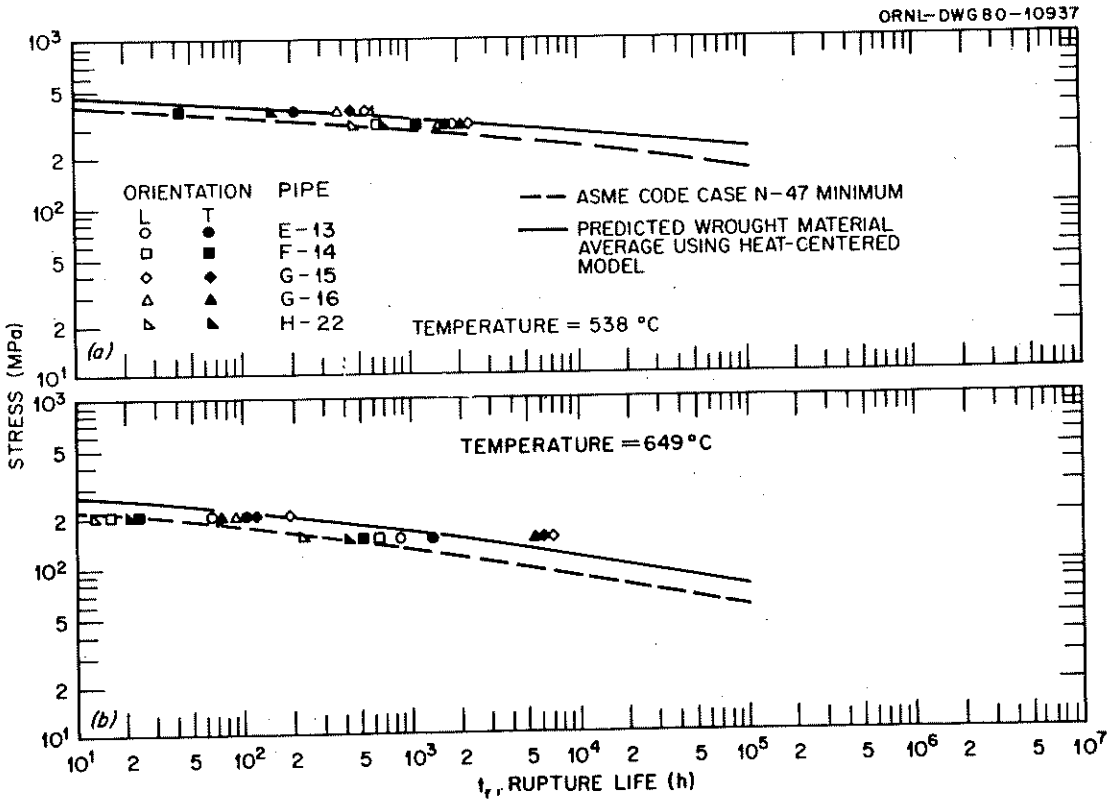


Fig. 3. Comparison of Stress vs Rupture Life for Specimens Tested at (a) 538°C and (b) 649°C.

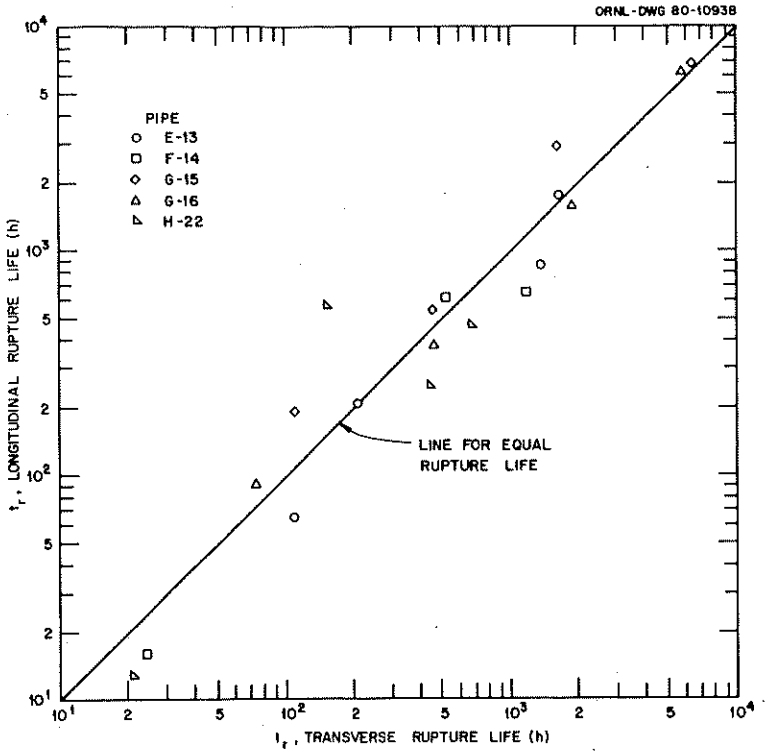


Fig. 4. Comparison of Rupture Life for Transverse vs Longitudinal Specimens.

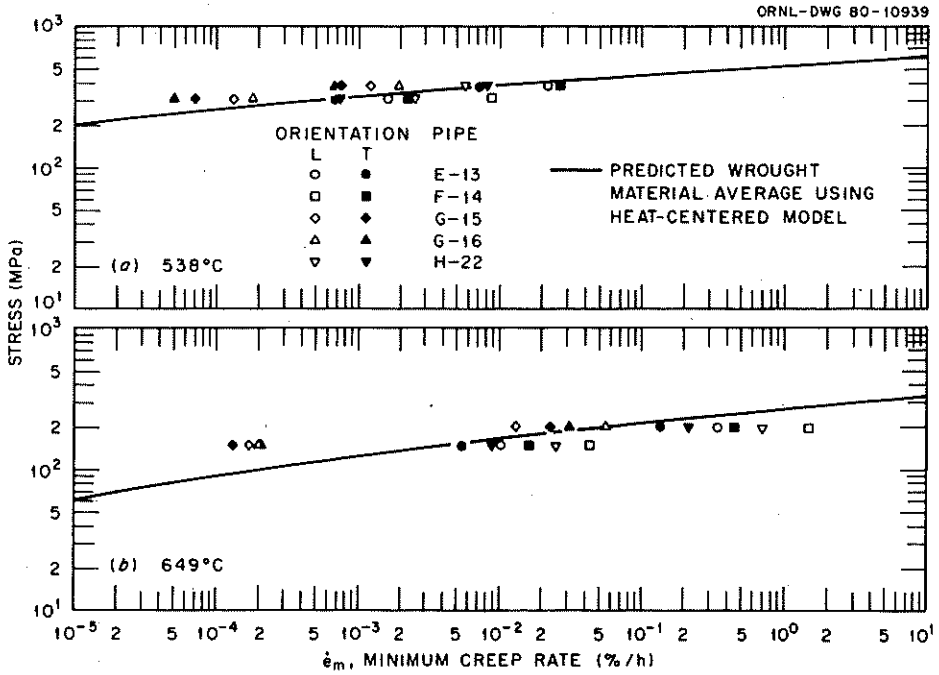


Fig. 5. Comparison of Stress vs Minimum Creep Rate for Specimens Tested at (a) 538°C and (b) 649°C.

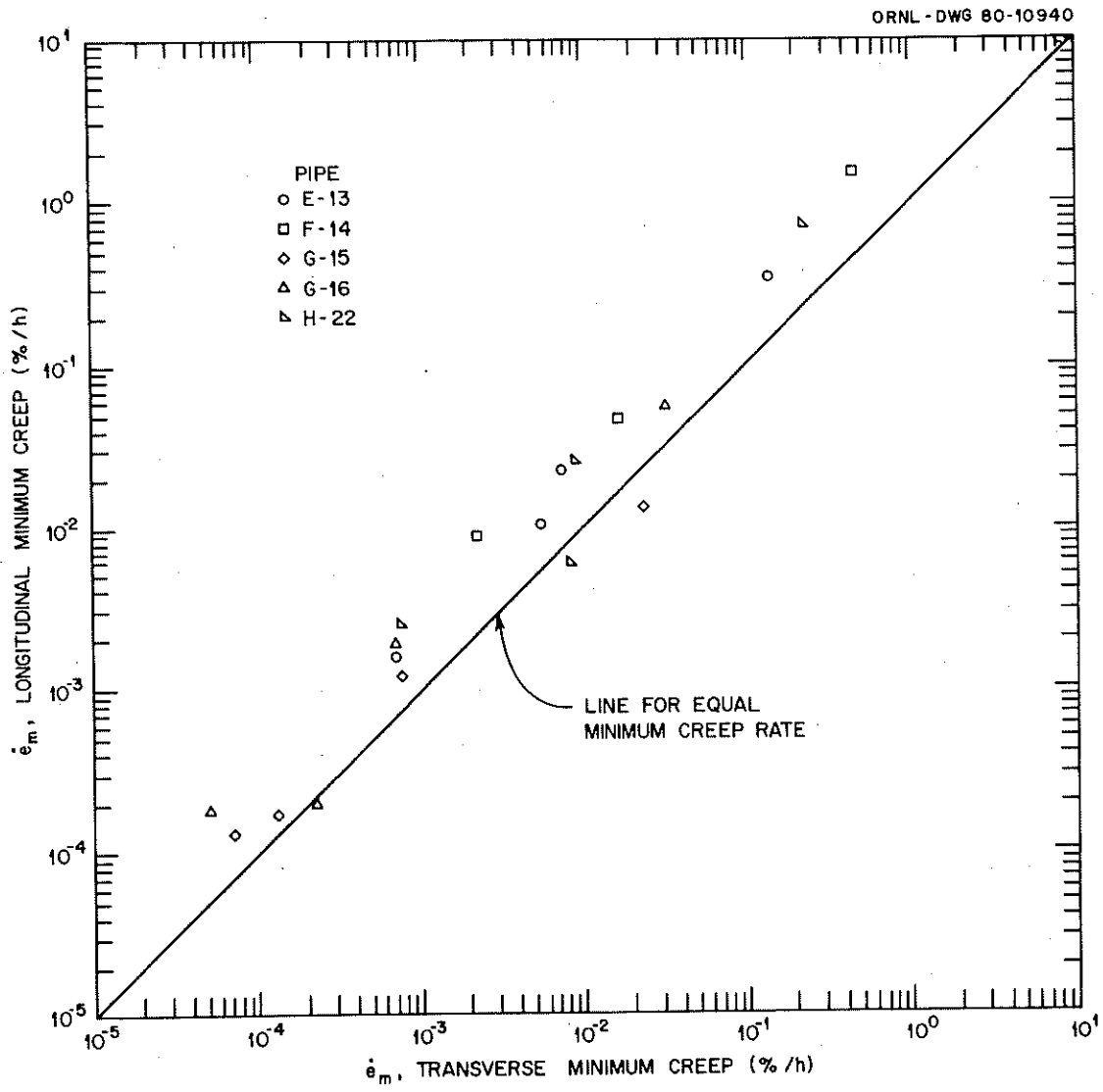


Fig. 6. Comparison of Minimum Creep Rates for Longitudinal vs Transverse Specimens.

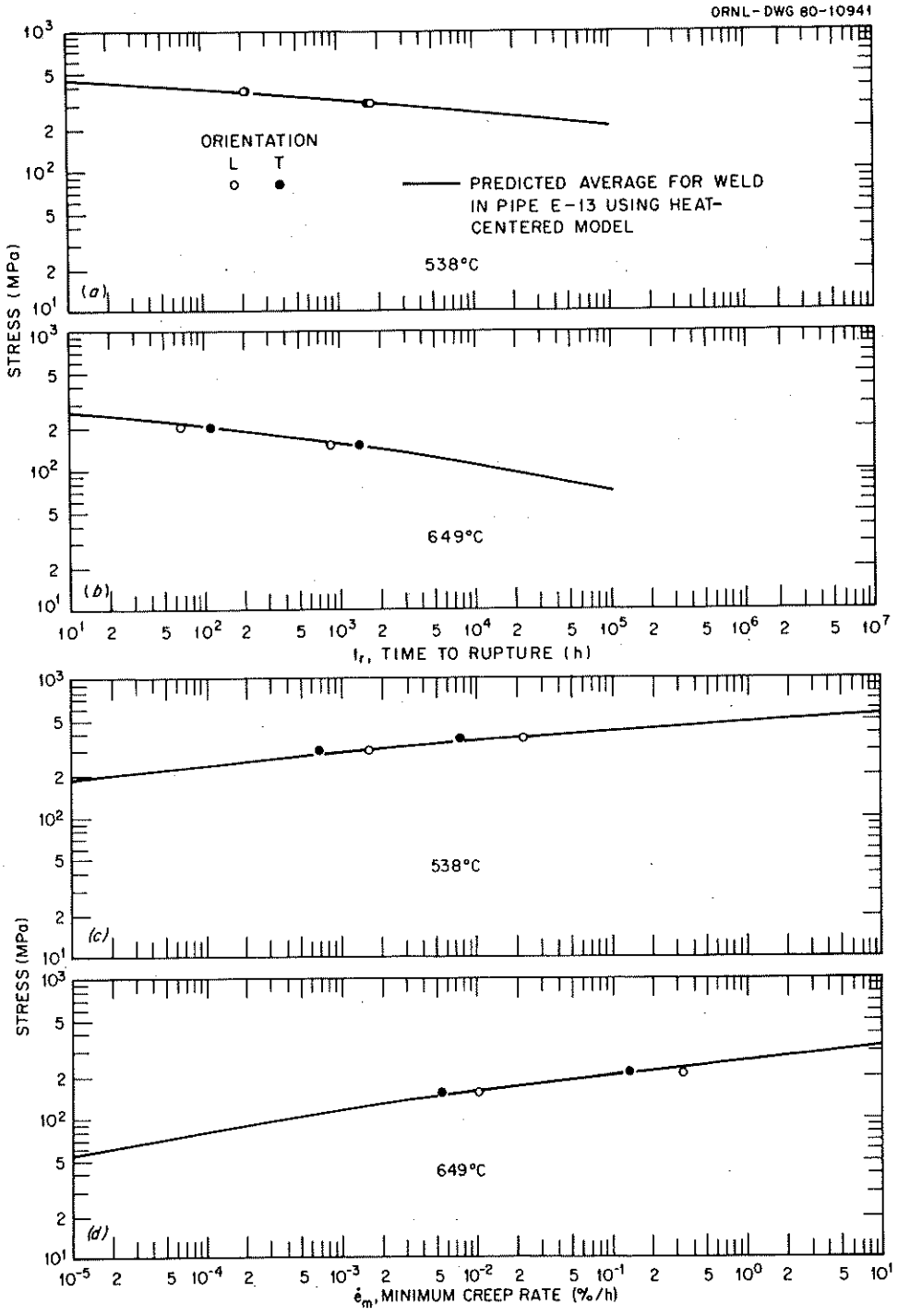


Fig. 7. Comparison of Predicted Time to Rupture ($t_r$) and Minimum Creep Rate ($\dot{e}_m$) with Experimental Data for the Welds in Pipe E-13. (a) $t_r$ at 538°C. (b) $t_r$ at 649°C. (c) $\dot{e}_m$ at 538°C. (d) $\dot{e}_m$ at 649°C.

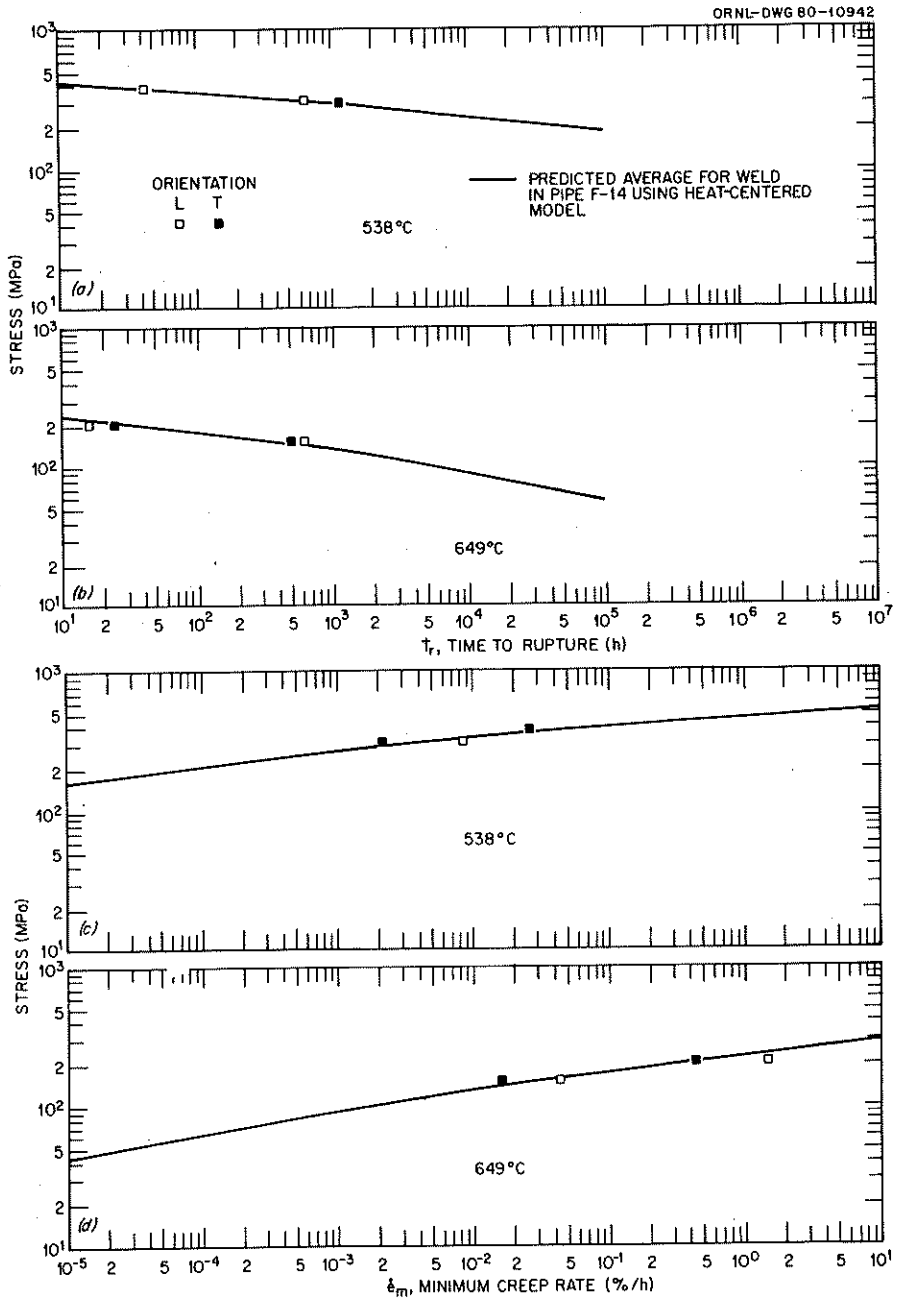


Fig. 8. Comparison of Predicted Time to Rupture ($t_r$) and Minimum Creep Rate ($\dot{\varepsilon}_m$) with Experimental Data for the Welds in Pipe F-14. (a) $t_r$ at 538°C. (b) $t_r$ at 649°C. (c) $\dot{\varepsilon}_m$ at 538°C. (d) $\dot{\varepsilon}_m$ at 649°C.

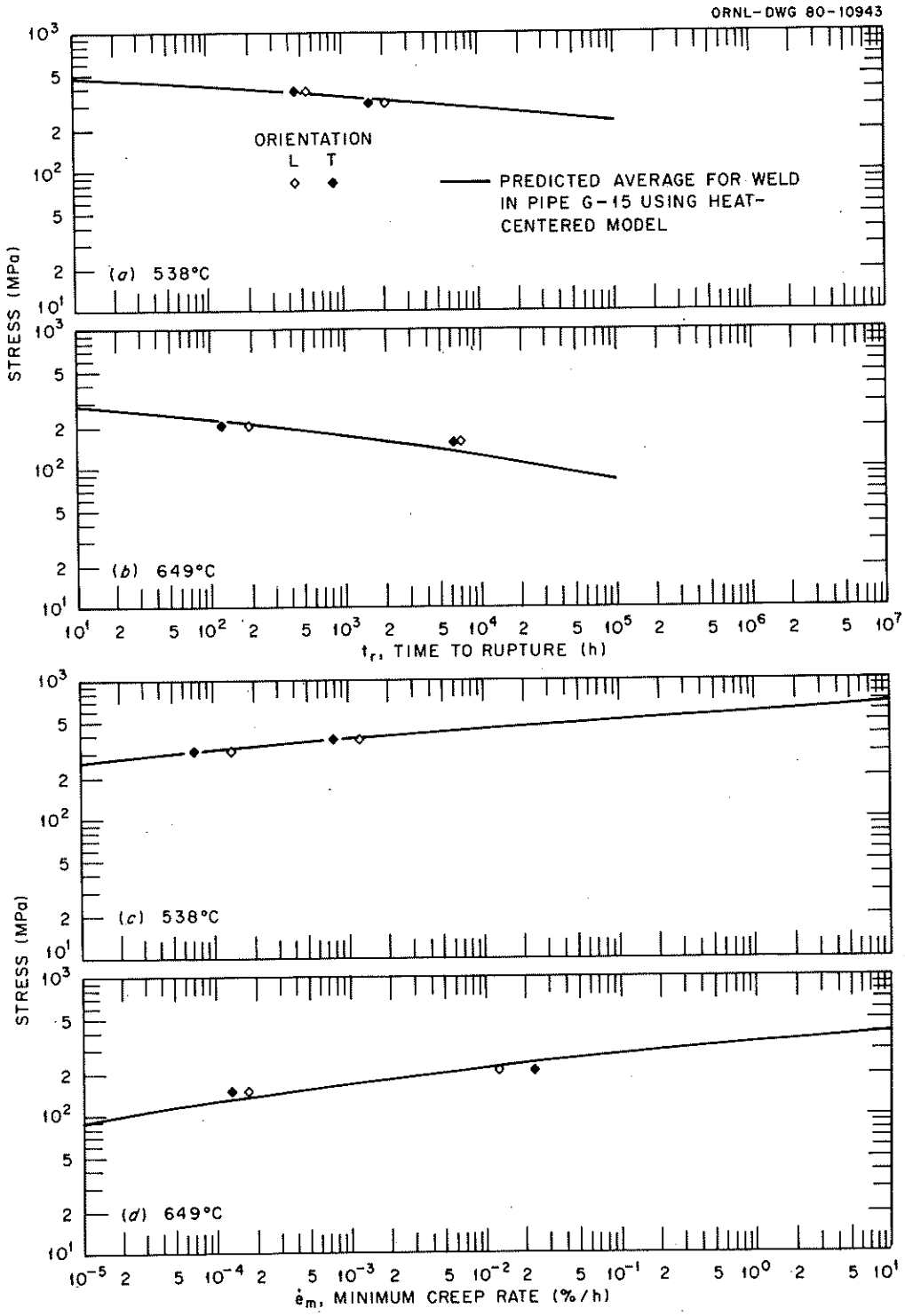


Fig. 9. Comparison of Predicted Time to Rupture ($t_r$) and Minimum Creep Rate ($\dot{e}_m$) with Experimental Data for the Welds in Pipe G-15. (a) $t_r$ at 538°C. (b) $t_r$ at 649°C. (c) $\dot{e}_m$ at 538°C. (d) $\dot{e}_m$ at 649°C.

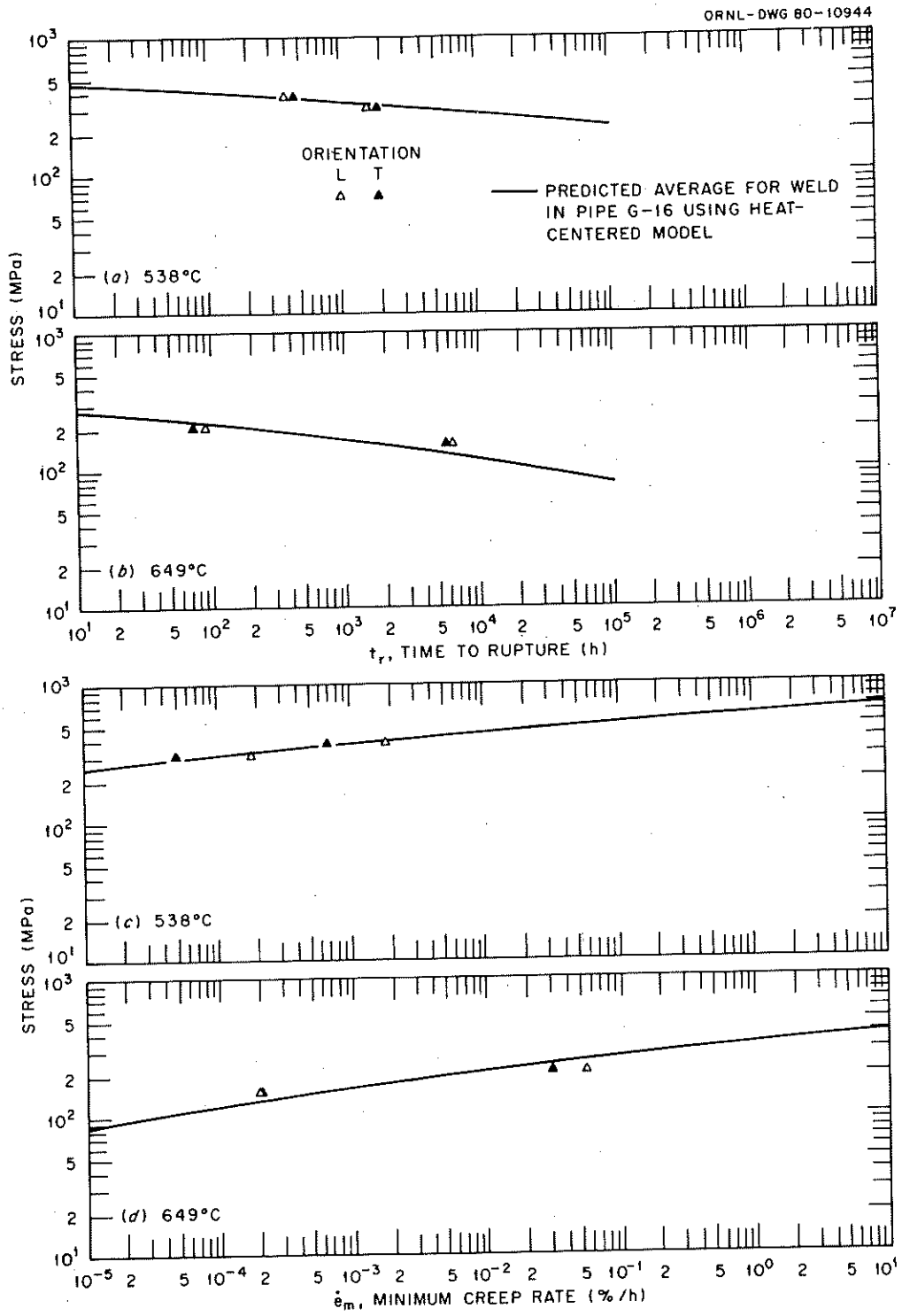


Fig. 10. Comparison of Predicted Time to Rupture ($t_r$) and Minimum Creep Rate ($\dot{e}_m$) with Experimental Data for the Welds in Pipe G-16. (a) $t_r$ at 538°C. (b) $t_r$ at 649°C. (c) $\dot{e}_m$ at 538°C. (d) $\dot{e}_m$ at 649°C.

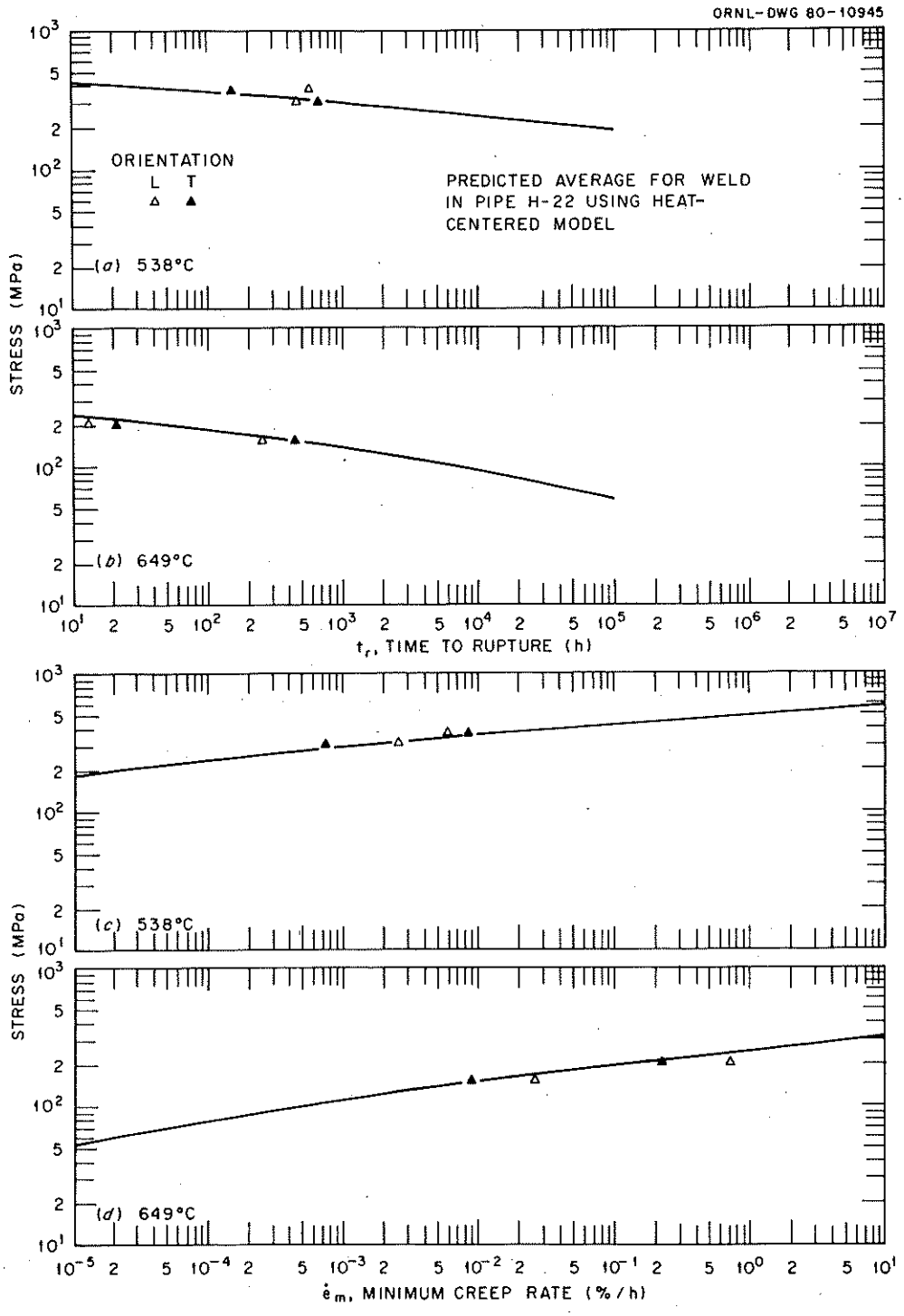


Fig. 11. Comparison of Predicted Time to Rupture ($t_r$) and Minimum Creep Rate ($\dot{e}_m$) with Experimental Data for the Welds in Pipe H-22. (a) $t_r$ at 538°C. (b) $t_r$ at 649°C. (c) $\dot{e}_m$ at 538°C. (d) $\dot{e}_m$ at 649°C.

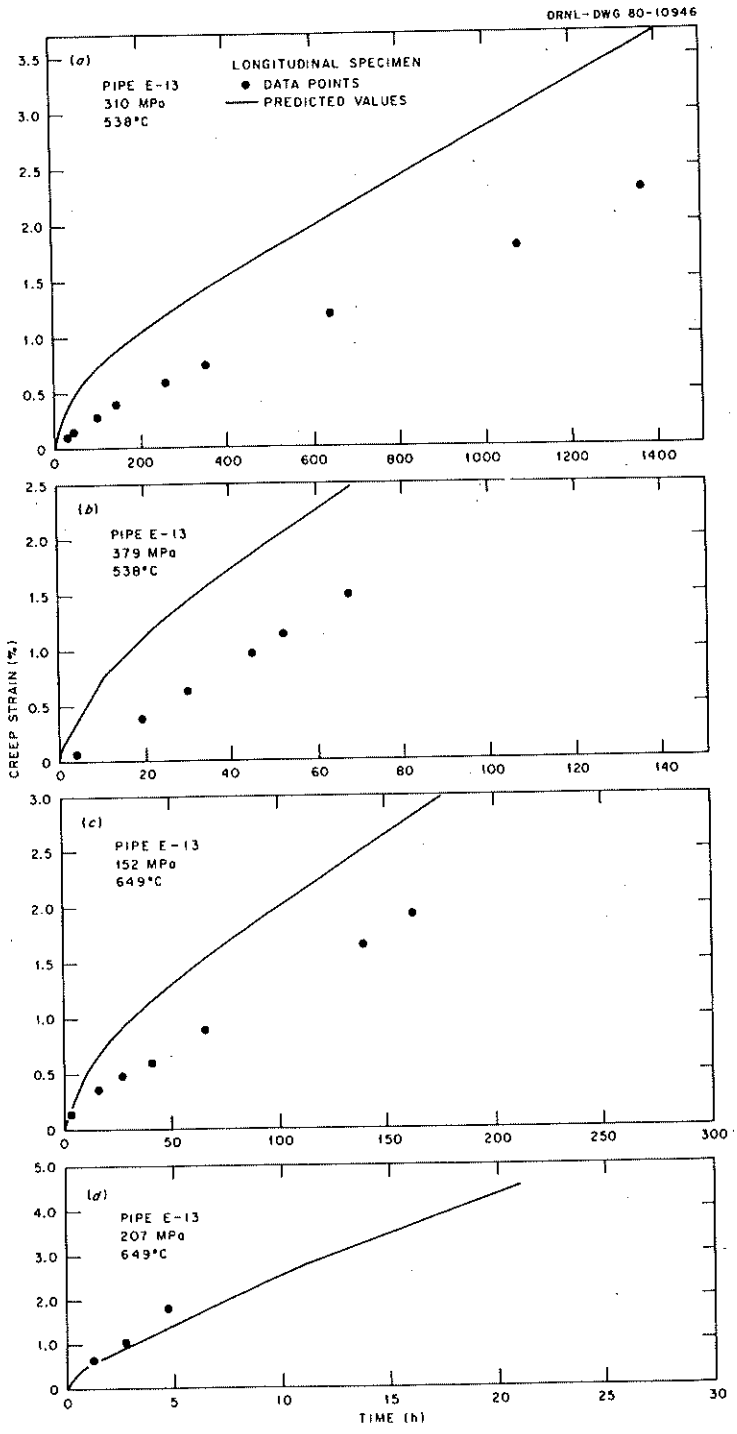


Fig. 12. Comparison of Predicted Creep Strain with Experimental Data for Longitudinally Oriented Weld Metal from Pipe E-13. (a) 310 MPa, 538°C. (b) 379 MPa, 538°C. (c) 152 MPa, 649°C. (d) 207 MPa, 649°C.

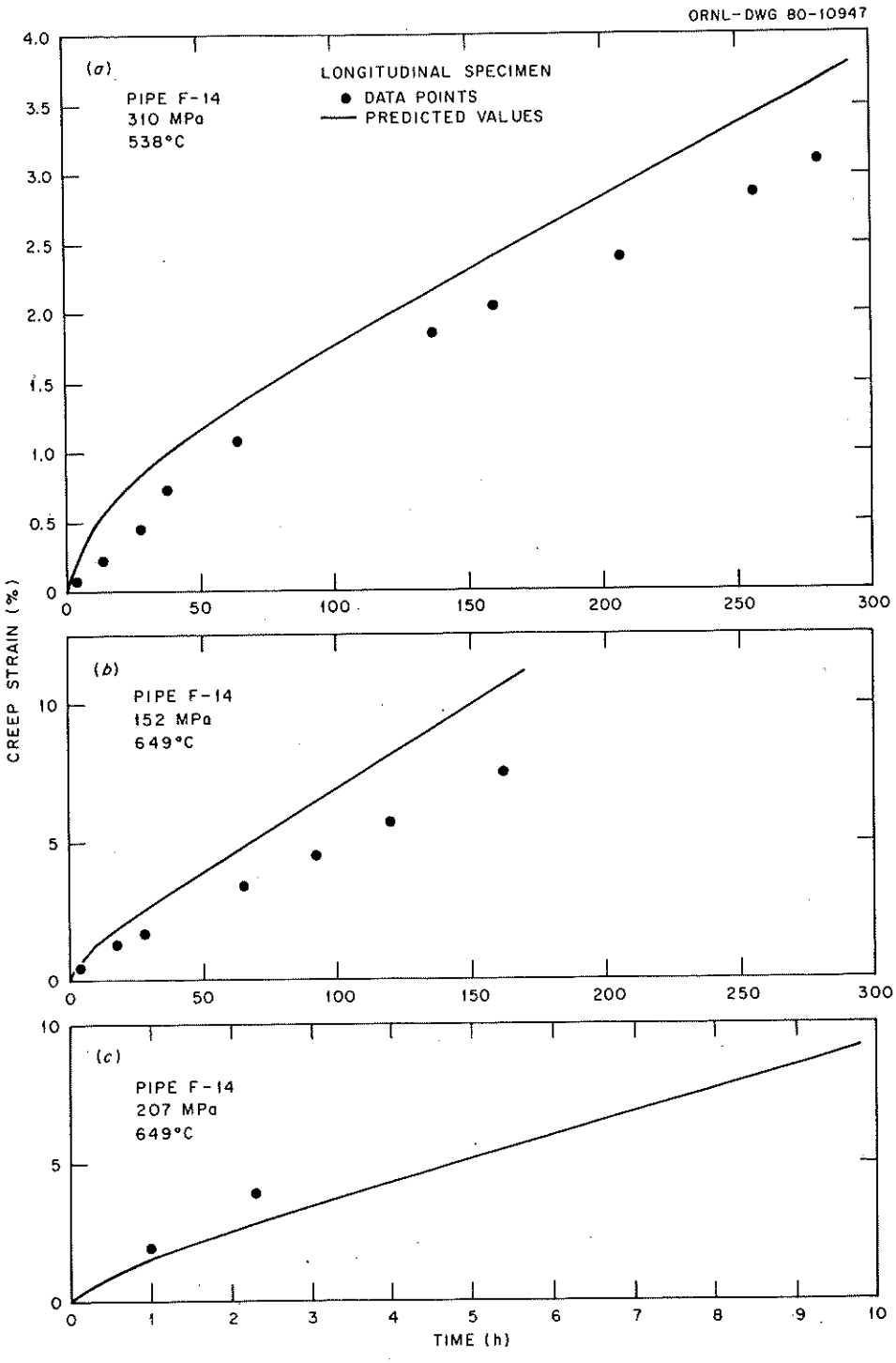


Fig. 13. Comparison of Predicted Creep Strain with Experimental Data for Longitudinally Oriented Weld Metal from Pipe F-14. (a) 310 MPa, 538°C. (b) 152 MPa, 649°C. (c) 207 MPa, 649°C.

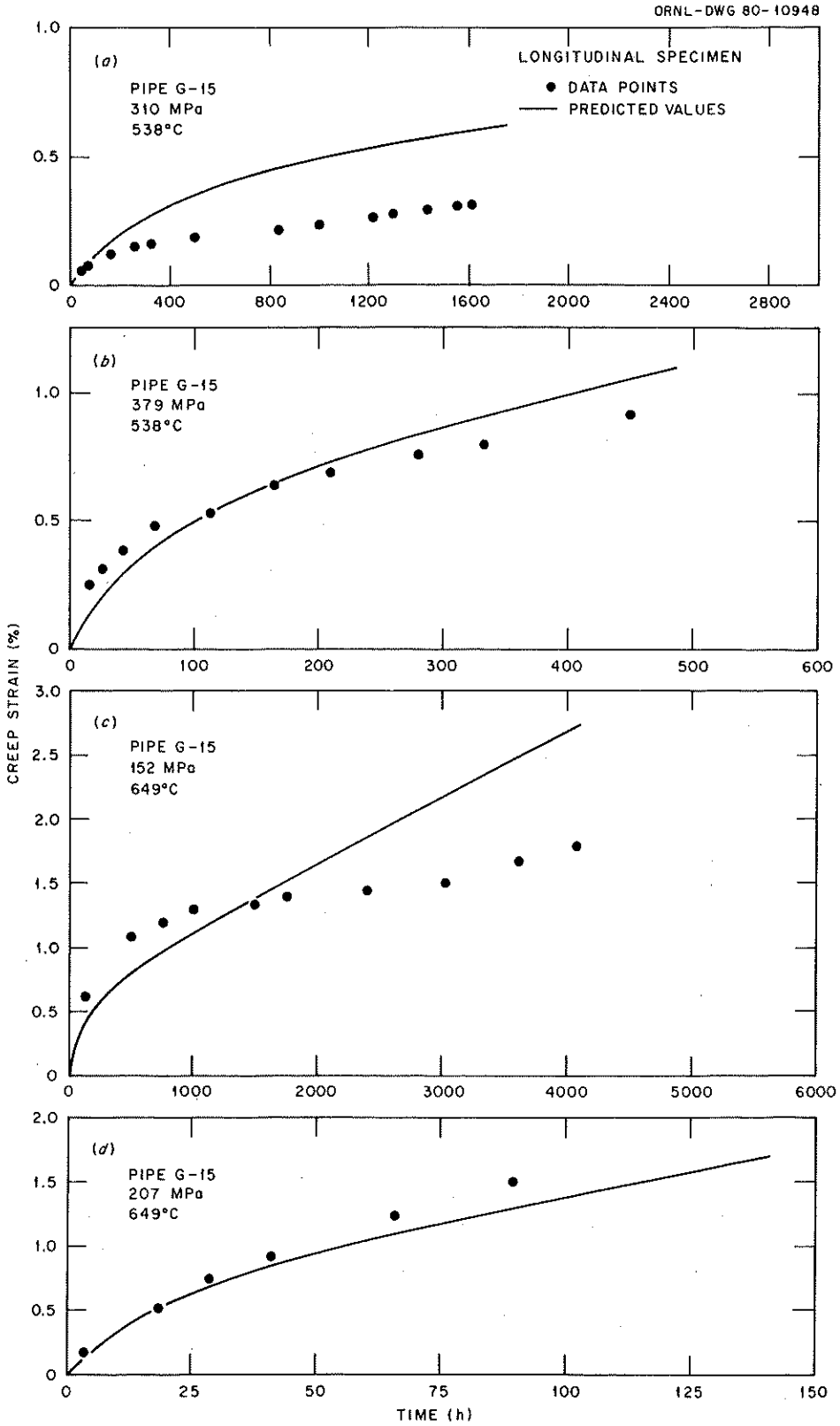


Fig. 14. Comparison of Predicted Creep Strain with Experimental Data for Longitudinally Oriented Weld Metal from Pipe G-15. (a) 310 MPa, 538°C. (b) 379 MPa, 538°C. (c) 152 MPa, 649°C. (d) 207 MPa, 649°C.

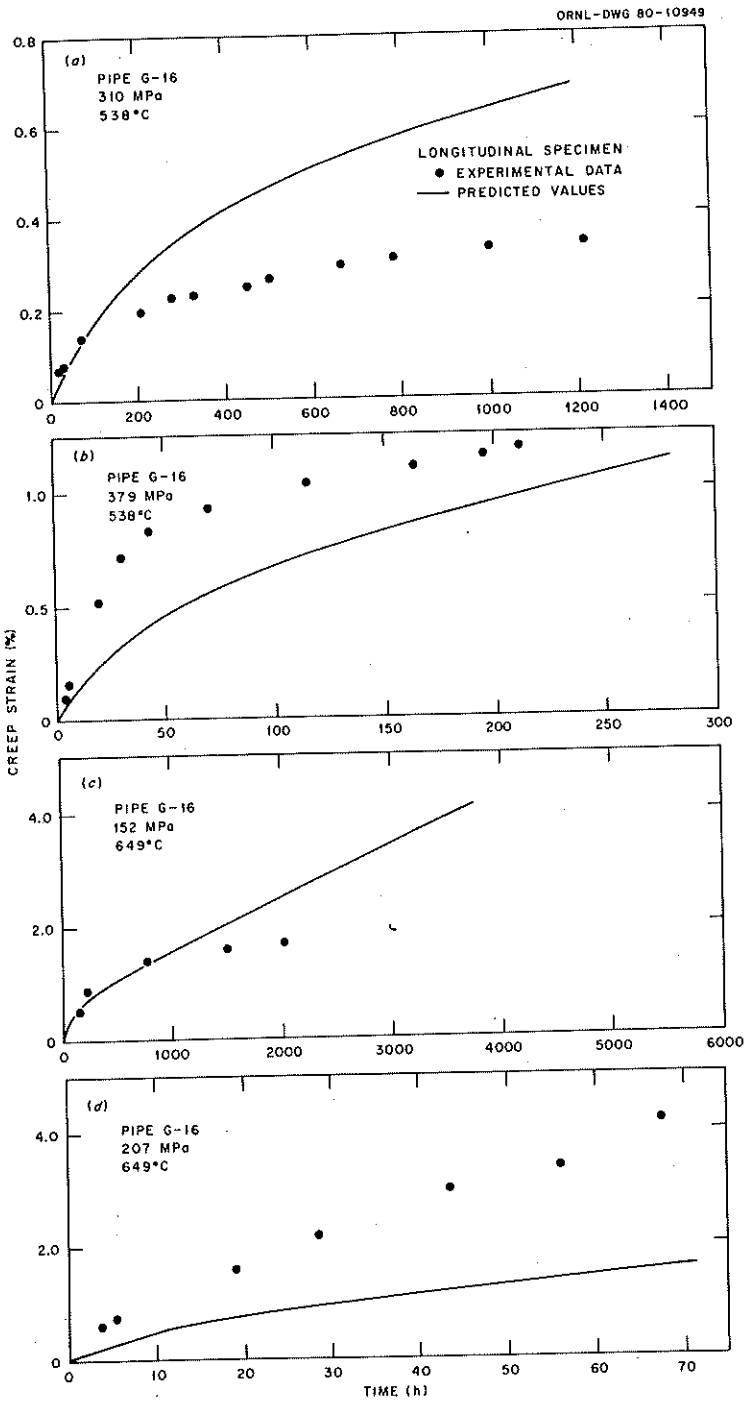


Fig. 15. Comparison of Predicted Creep Strain with Experimental Data for Longitudinally Oriented Weld Metal from Pipe G-16. (a) 310 MPa, 538°C. (b) 379 MPa, 538°C. (c) 152 MPa, 649°C. (d) 207 MPa, 649°C.

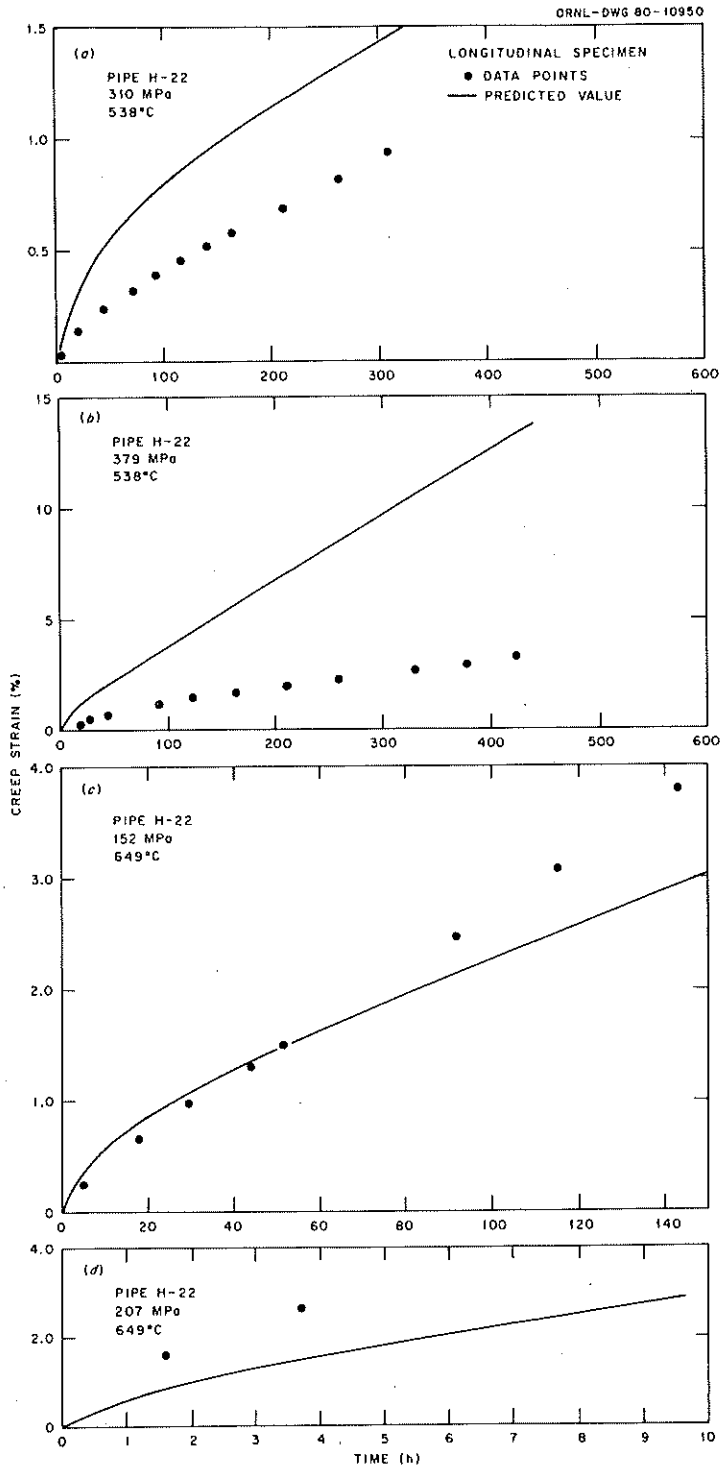


Fig. 16. Comparison of Predicted Creep Strain with Experimental Data for Longitudinally Oriented Weld Metal from Pipe H-22. (a) 310 MPa, 538°C. (b) 379 MPa, 538°C. (c) 152 MPa, 649°C. (d) 207 MPa, 649°C.

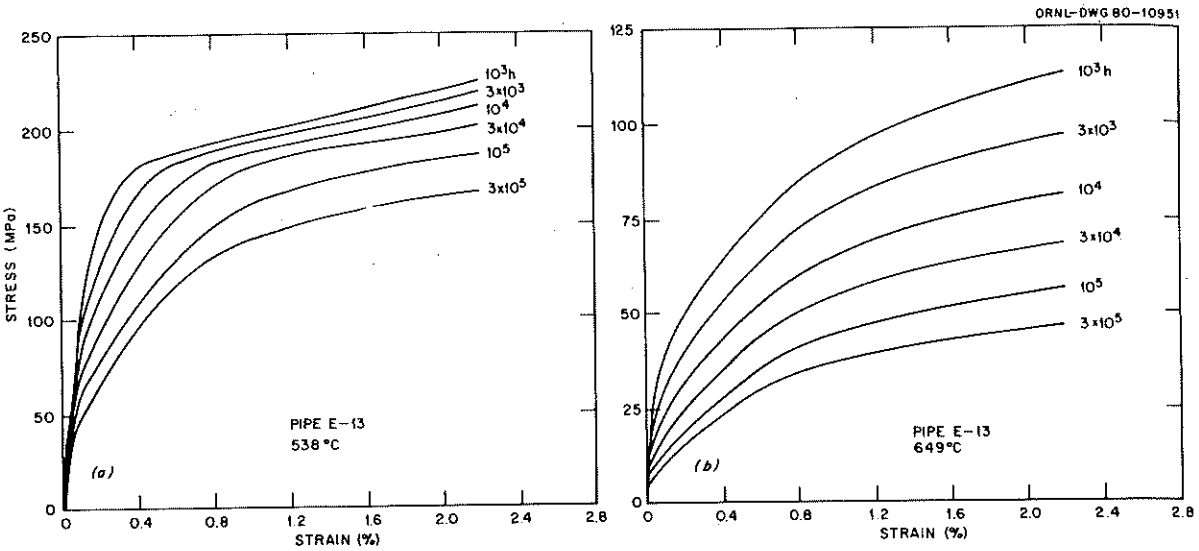


Fig. 17. Isochronous Stress-Strain Curves for Longitudinally Oriented Weld Metal from Pipe E-13. (a) 538°C. (b) 649°C.

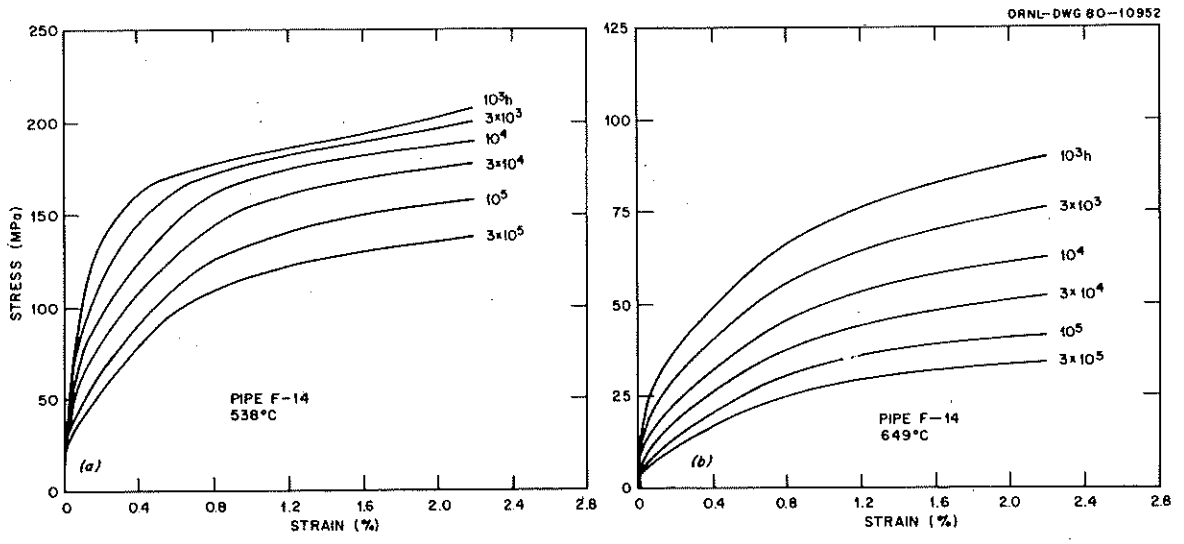


Fig. 18. Isochronous Stress-Strain Curves for Longitudinally Oriented Weld Metal from Pipe F-14. (a) 538°C. (b) 649°C.

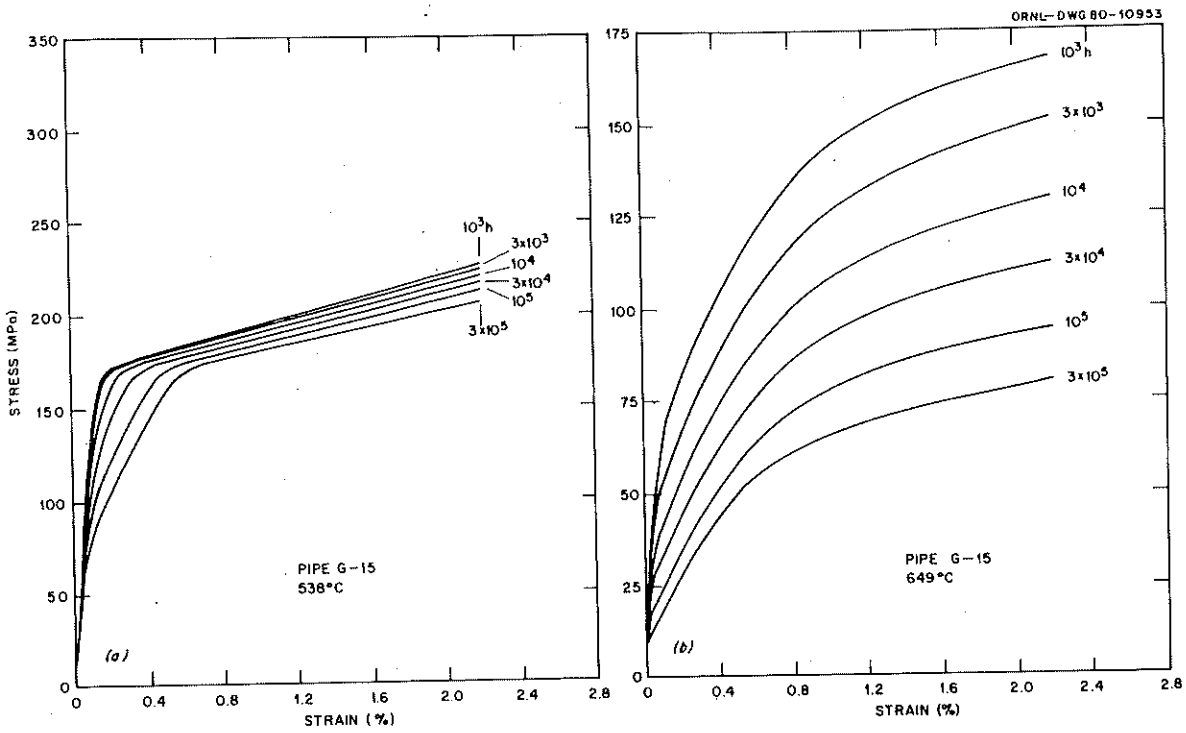


Fig. 19. Isochronous Stress-Strain Curves for Longitudinally Oriented Weld Metal from Pipe G-15. (a) 538°C. (b) 649°C.

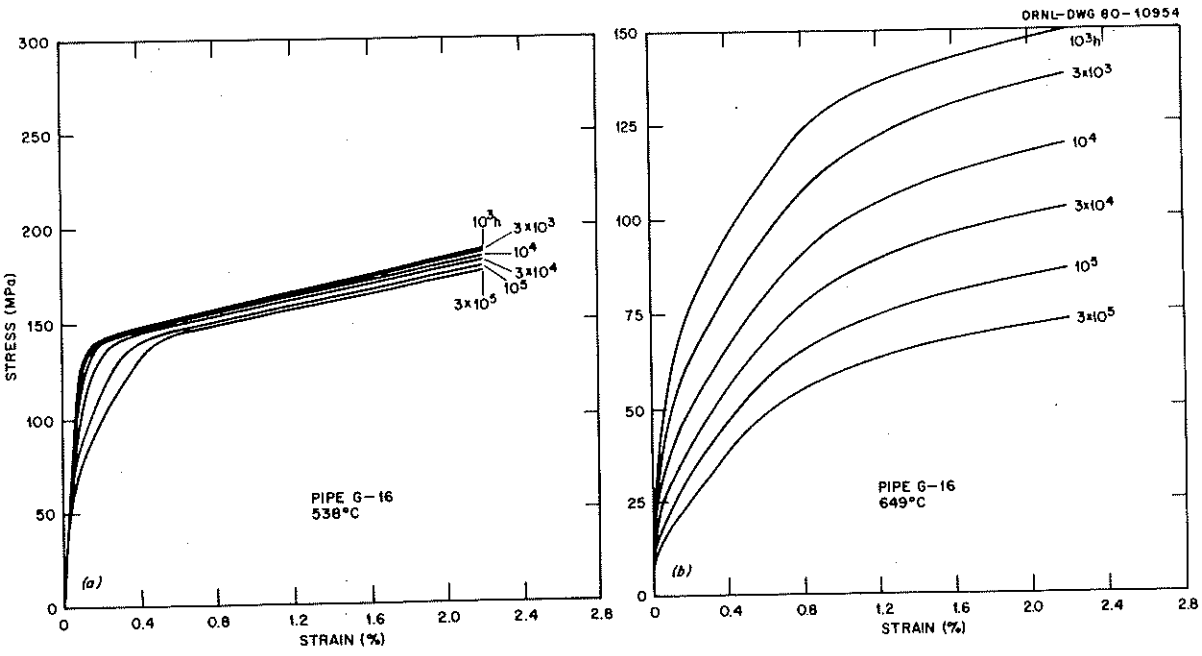


Fig. 20. Isochronous Stress-Strain Curves for Longitudinally Oriented Weld Metal from Pipe G-16. (a) 538°C. (b) 649°C.

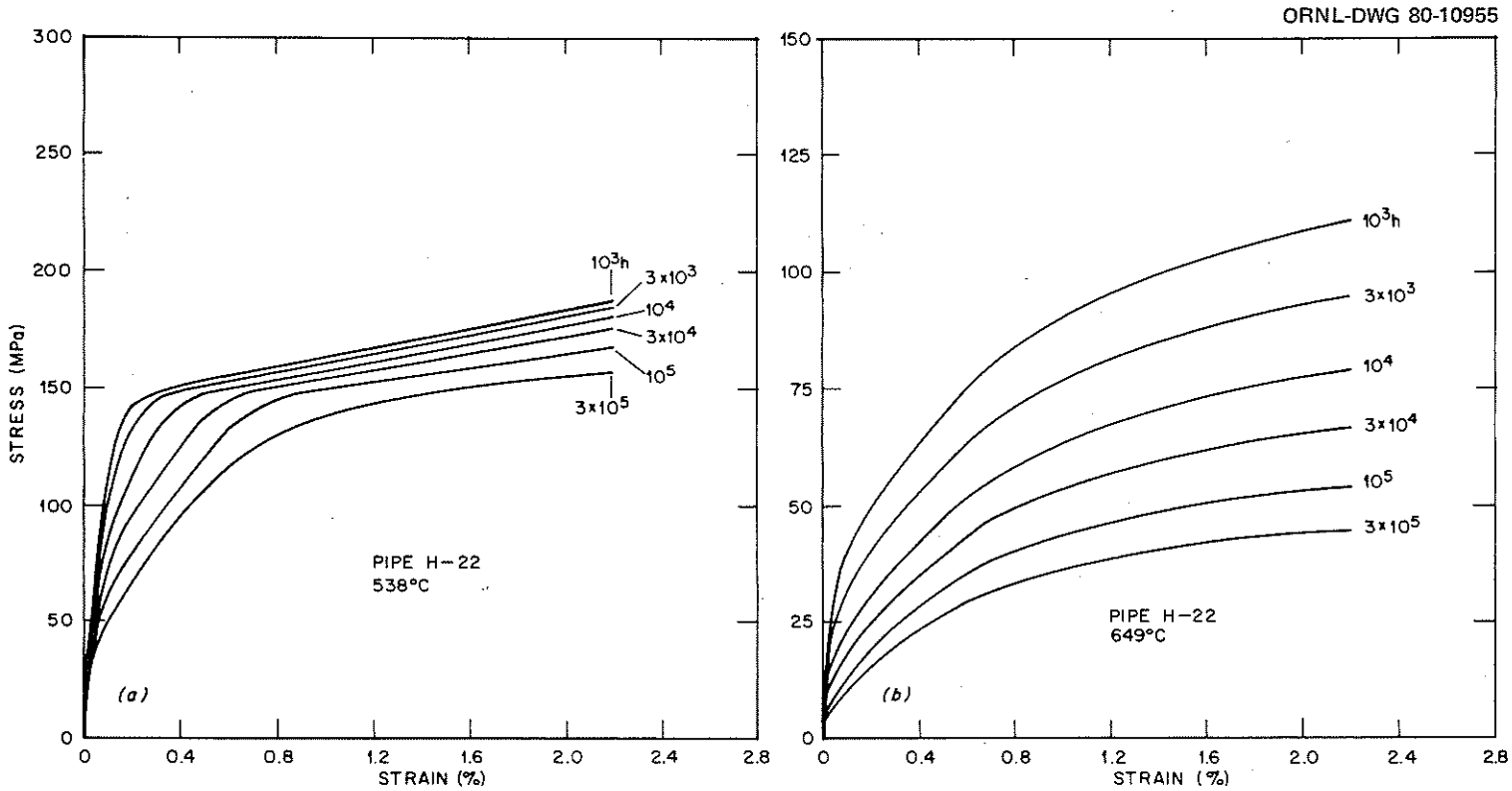


Fig. 21. Isochronous Stress-Strain Curves for Longitudinally Oriented Weld Metal from Pipe H-22. (a) 538°C. (b) 649°C.

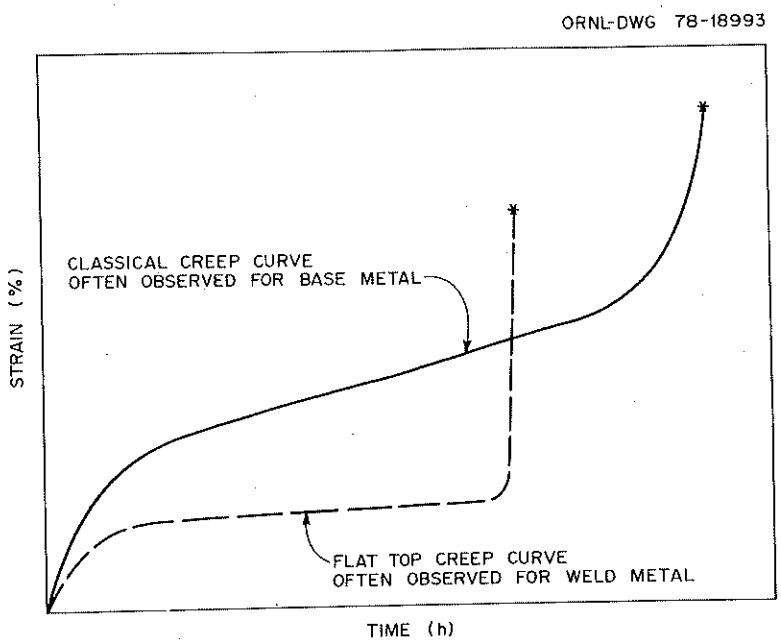


Fig. 22. Schematic Showing Classical Creep Curve Often Observed for Base Metal and Flat-Top Creep Curve Often Observed for Weld Metal Specimens.

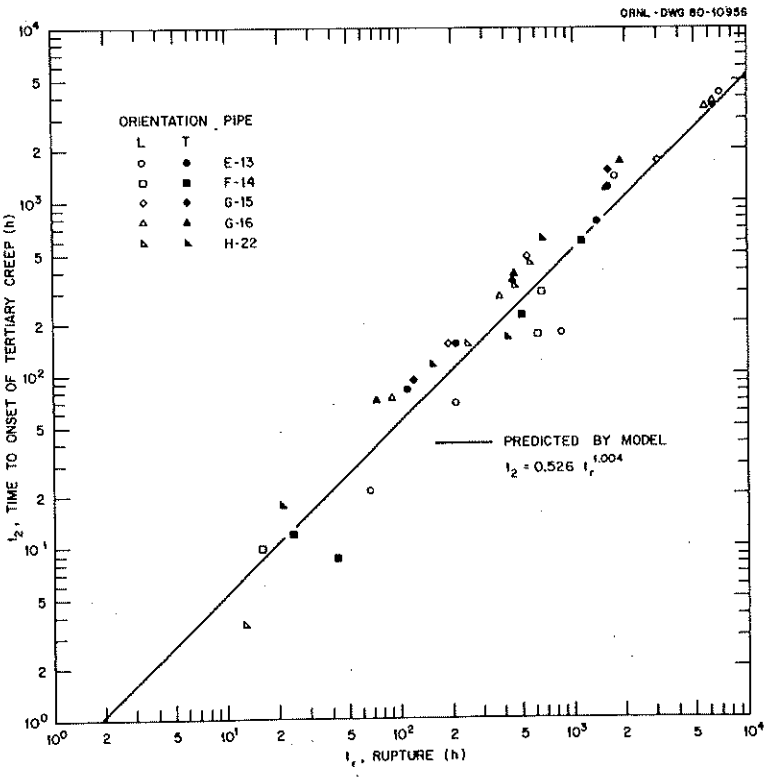


Fig. 23. Comparison of Time to Onset of Tertiary Creep with Time to Rupture for All Pipe Weld Specimens.

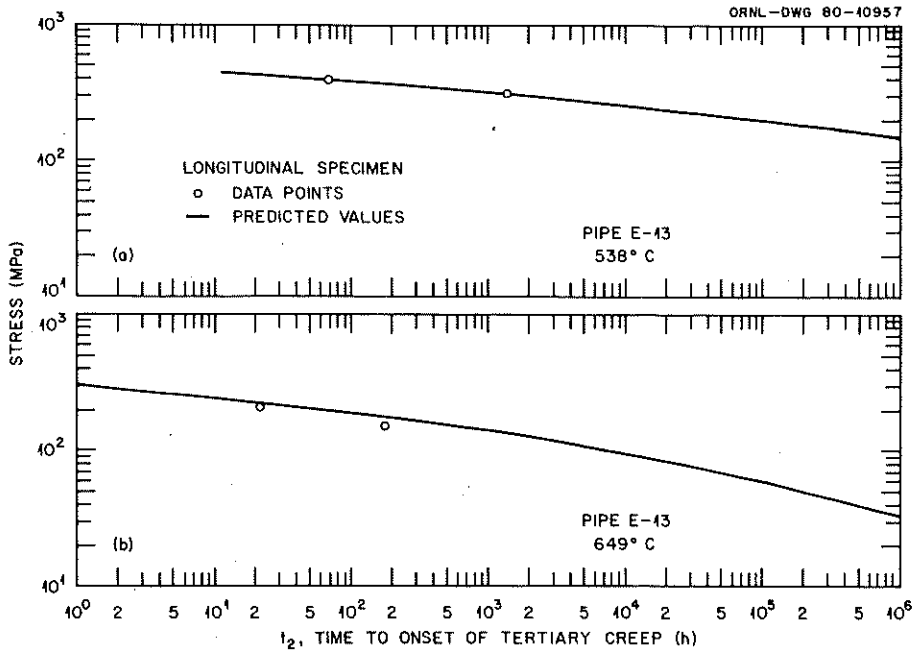


Fig. 24. Comparison of Predicted Time to Onset of Tertiary Creep with Experimental Data for the Welds in Pipe E-13. (a) 538°C. (b) 649°C.

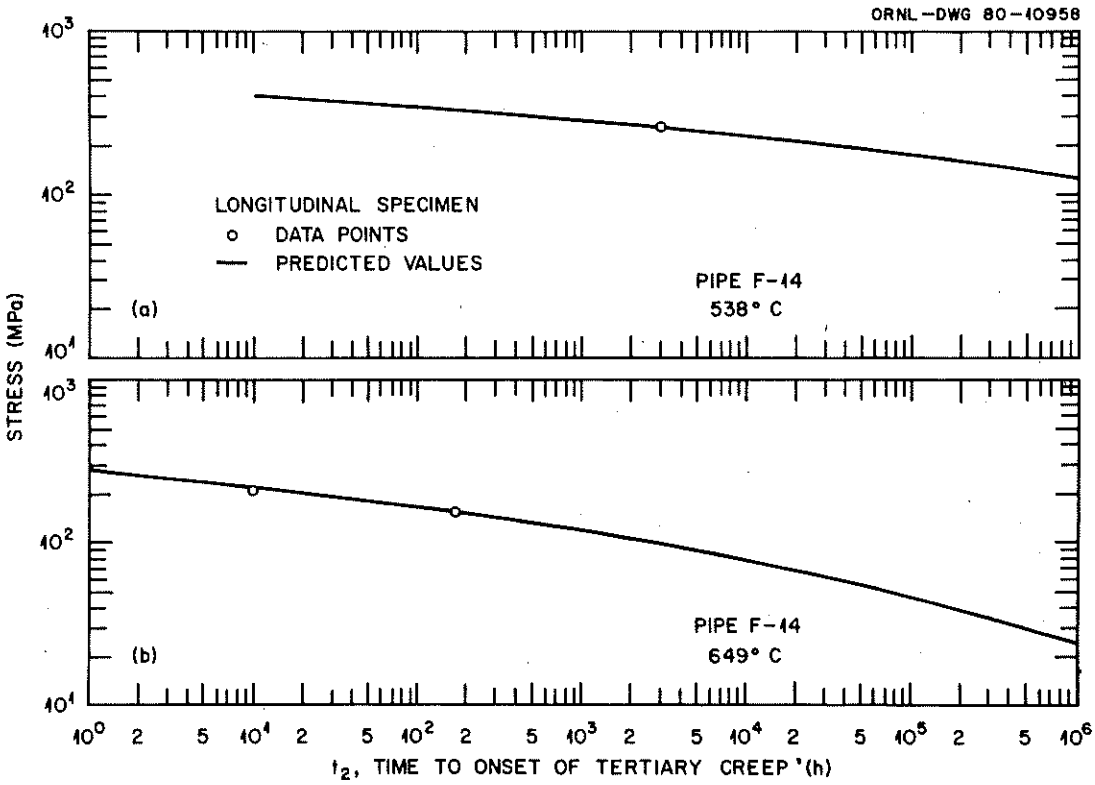


Fig. 25. Comparison of Predicted Time to Onset of Tertiary Creep with Experimental Data for the Welds in Pipe F-14. (a) 538°C. (b) 649°C.

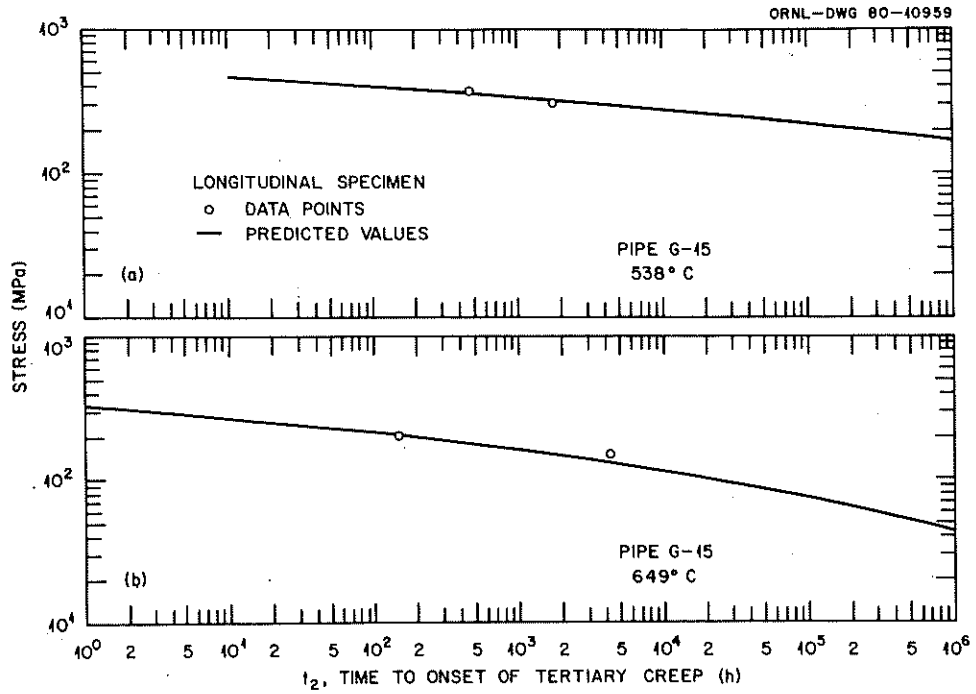


Fig. 26. Comparison of Predicted Time to Onset of Tertiary Creep with Experimental Data for the Welds in Pipe G-15. (a) 538°C. (b) 649°C.

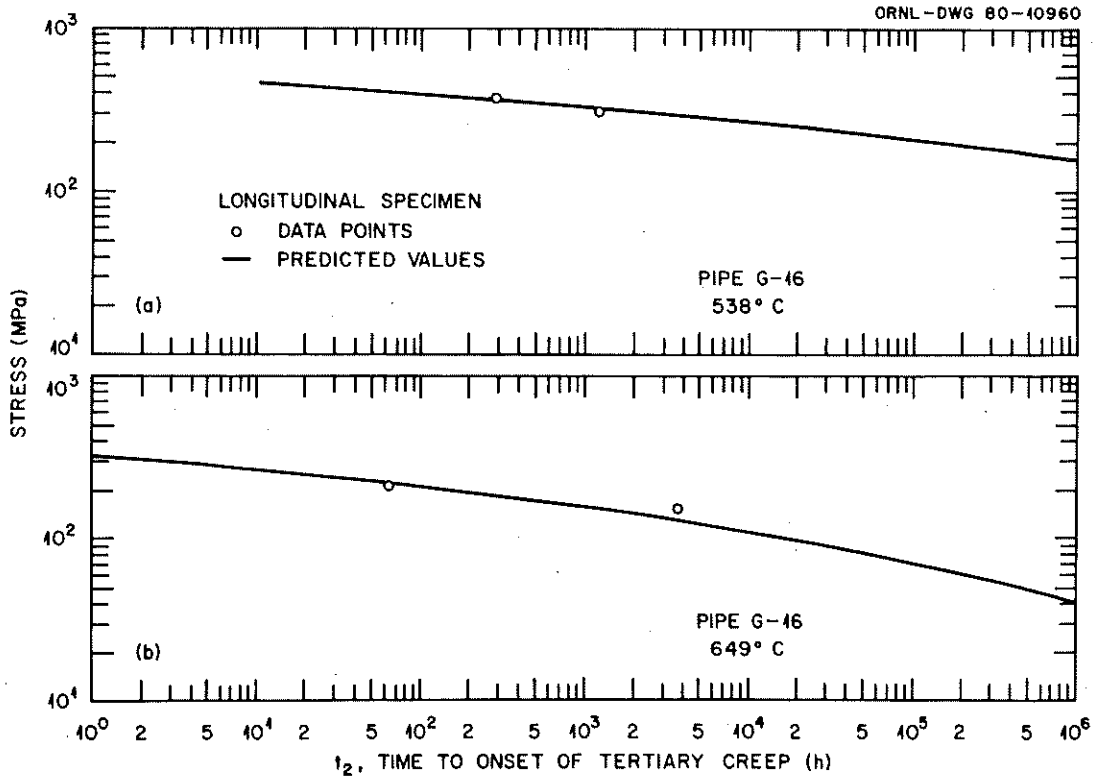


Fig. 27. Comparison of Predicted Time to Onset of Tertiary Creep with Experimental Data for the Welds in Pipe G-16. (a) 538°C. (b) 649°C.

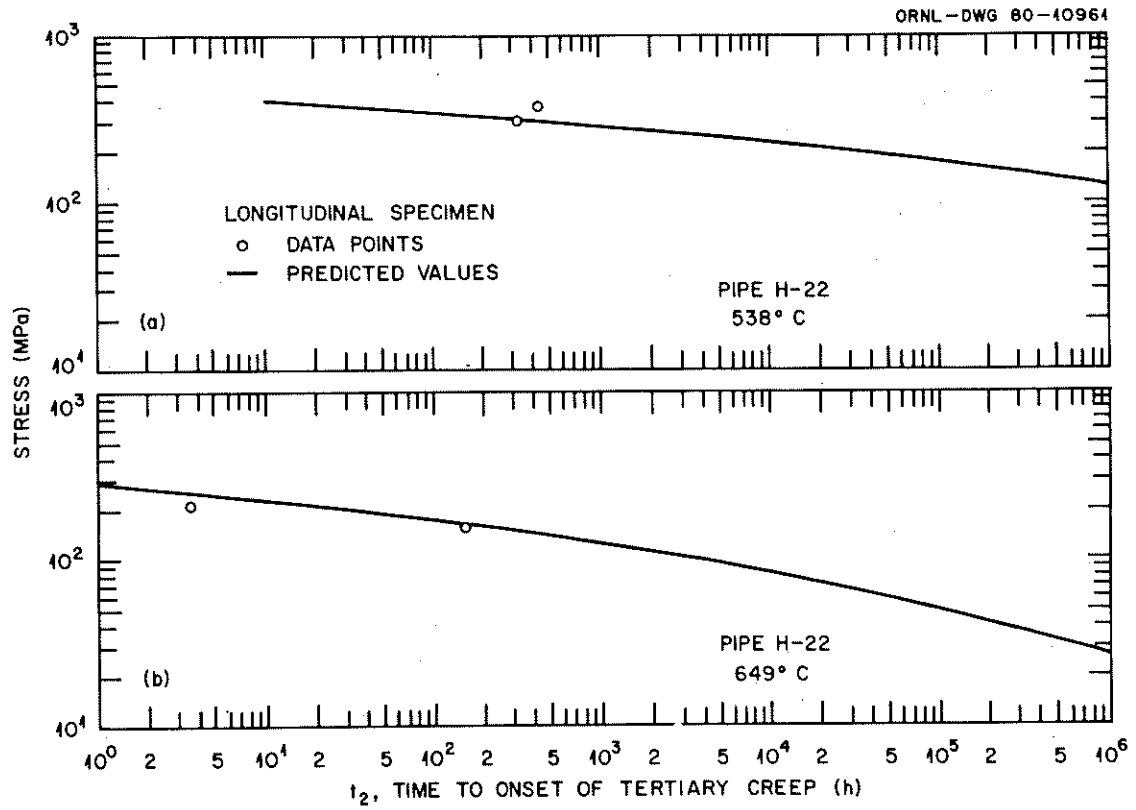


Fig. 28. Comparison of Predicted Time to Onset of Tertiary Creep with Experimental Data for the Welds in Pipe H-22. (a) 538°C. (b) 649°C.

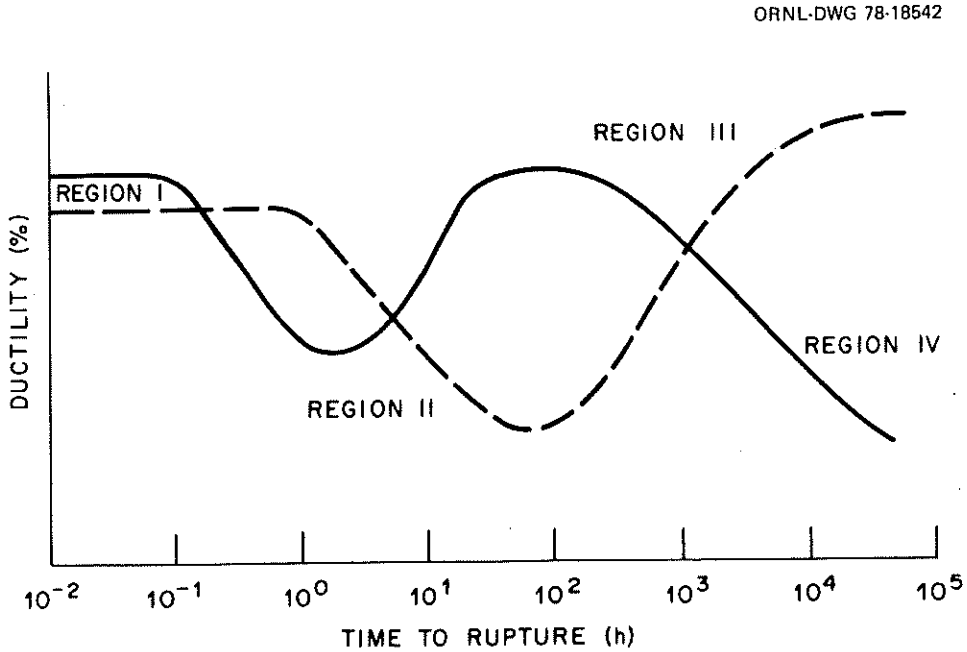


Fig. 29. Schematic Showing Possible Reasons for Large Ductility Variations Observed for Heats of Types 304 and 316 Stainless Steel.

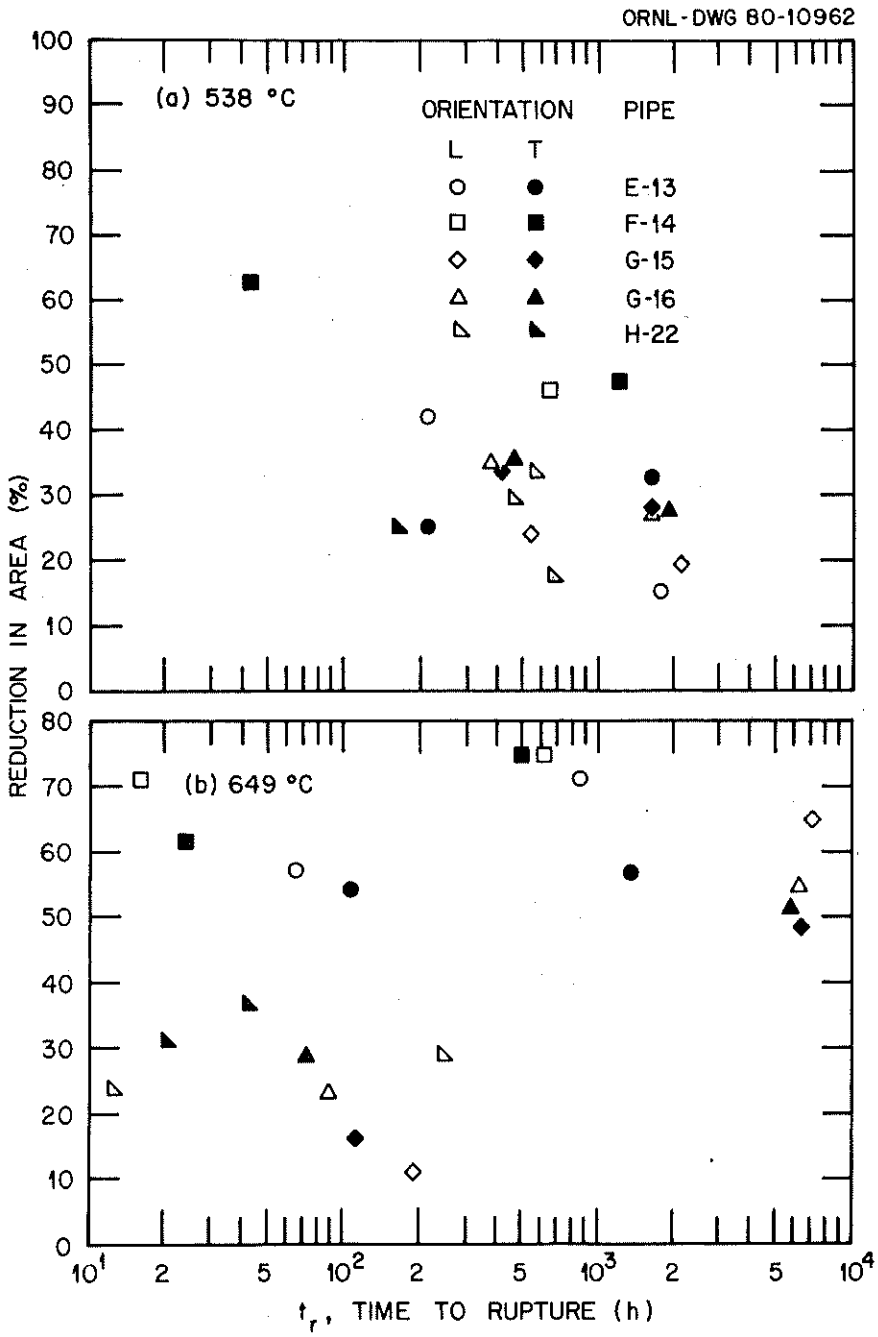


Fig. 30. Comparison of Reduction in Area vs Time to Rupture for All Pipe Welds. (a) 538°C. (b) 649°C.

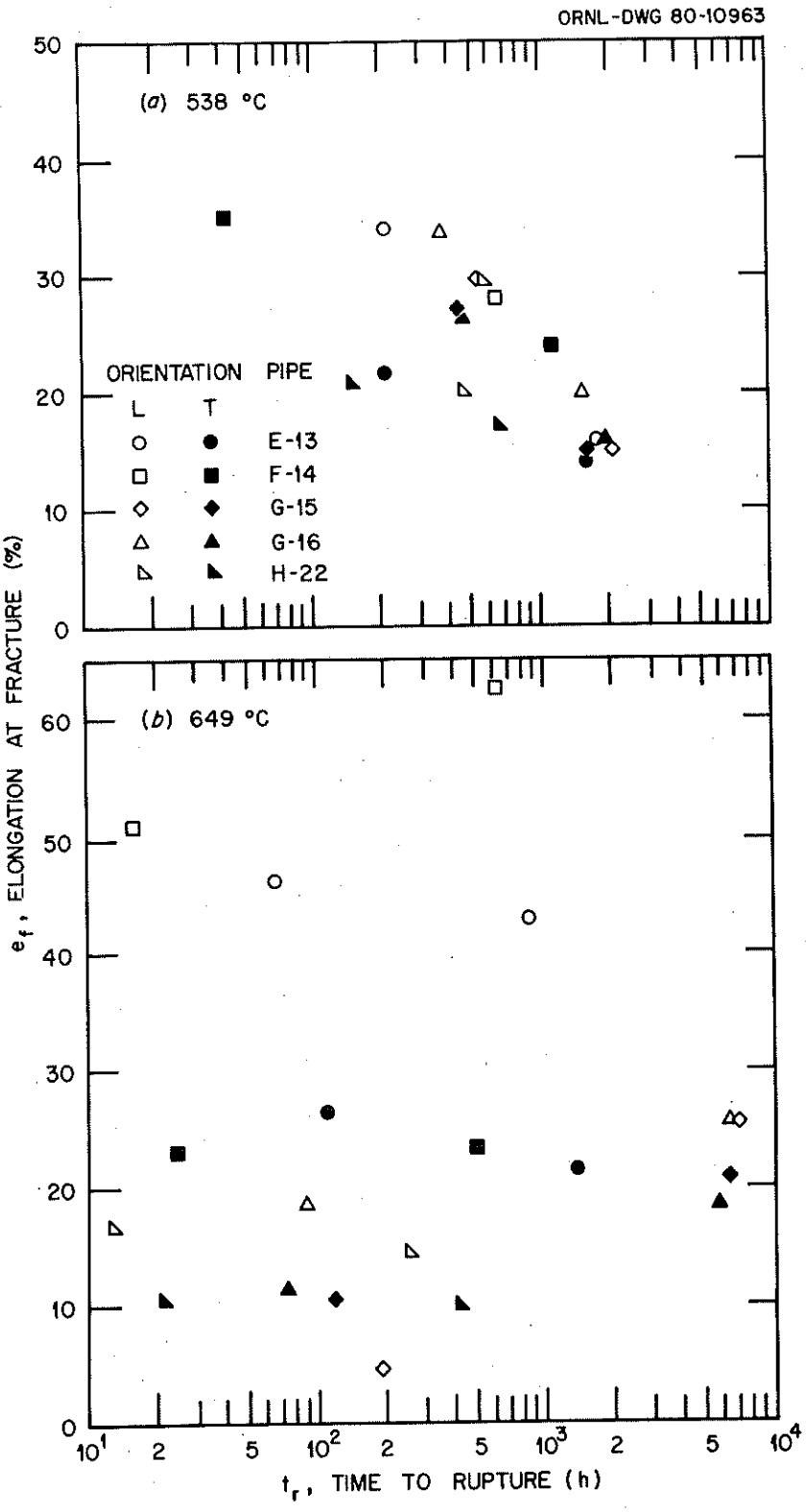


Fig. 31. Comparison of Elongation Fracture vs Time to Rupture. (a) 538°C. (b) 649°C.

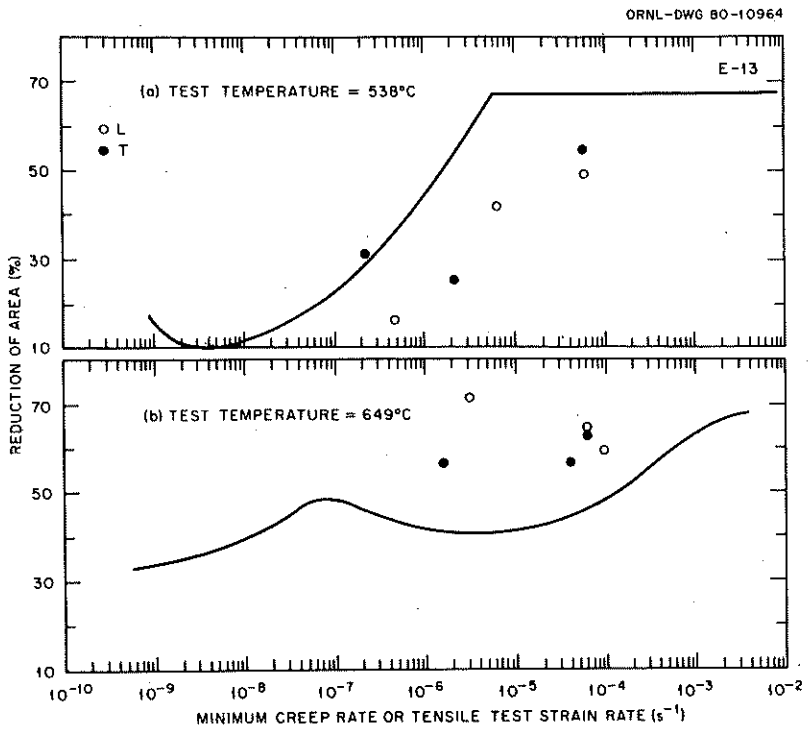


Fig. 32. Comparison of Reduction of Area for the Welds in Pipe E-13 with the Trend Curve for the ORNL Reference Heat of Wrought Type 316 Stainless Steel. (a) 538°C. (b) 649°C.

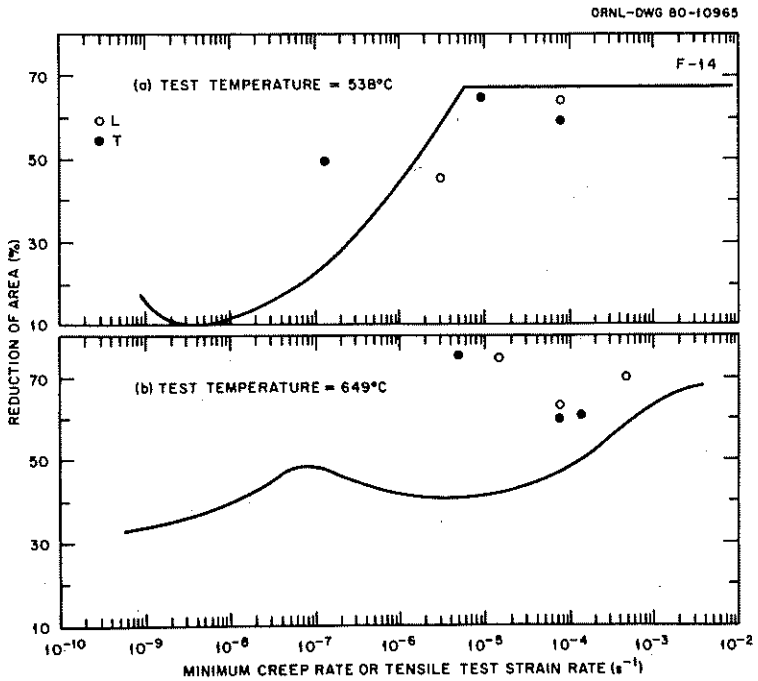


Fig. 33. Comparison of Reduction of Area for the Welds in Pipe F-14 with the Trend Curve for the ORNL Reference Heat of Wrought Type 316 Stainless Steel. (a) 538°C. (b) 649°C.

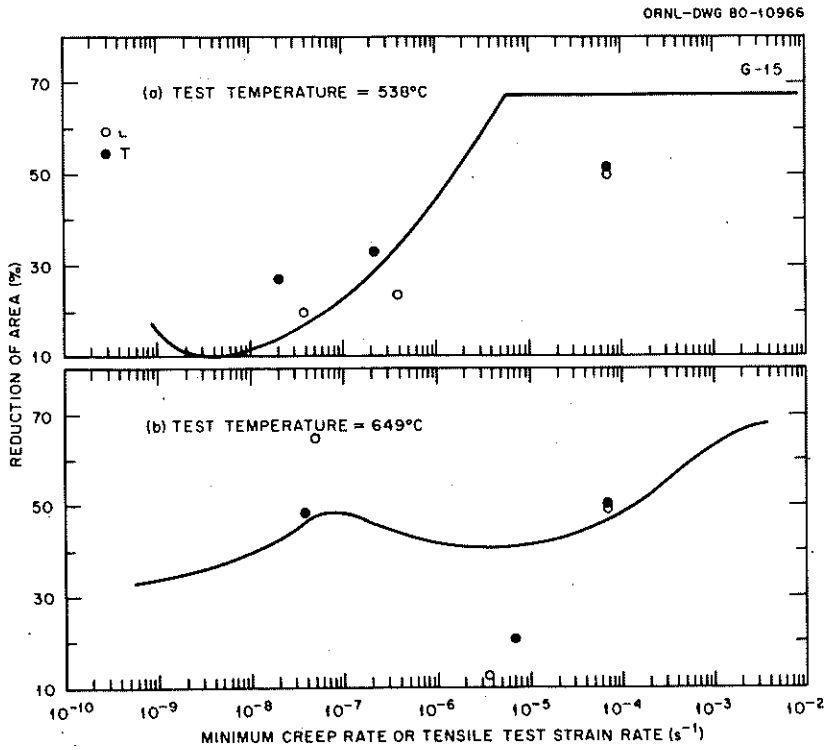


Fig. 34. Comparison of Reduction of Area for the Welds in Pipe G-15 with the Trend Curve for the ORNL Reference Heat of Wrought Type 316 Stainless Steel. (a) 538°C. (b) 649°C.

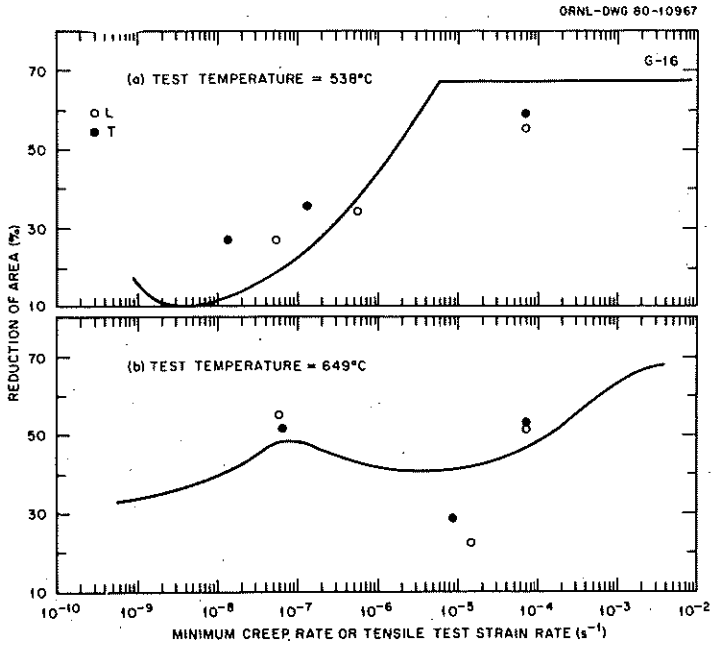


Fig. 35. Comparison of Reduction of Area for the Welds in Pipe G-16 with the Trend Curve for the ORNL Reference Heat of Wrought Type 316 Stainless Steel. (a) 538°C. (b) 649°C.

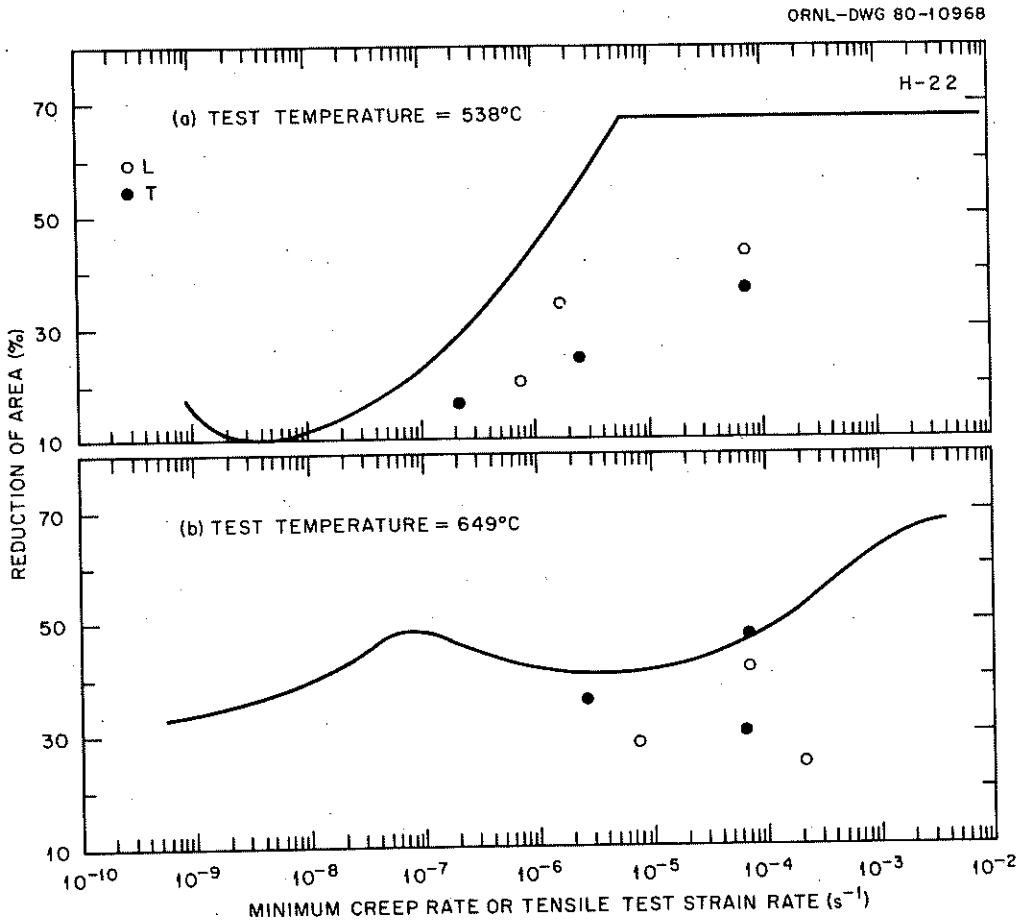


Fig. 36. Comparison of Reduction of Area for the Welds in Pipe H-22 with the Trend Curve for the ORNL Reference Heat of Wrought Type 316 Stainless Steel. (a) 538°C. (b) 649°C.

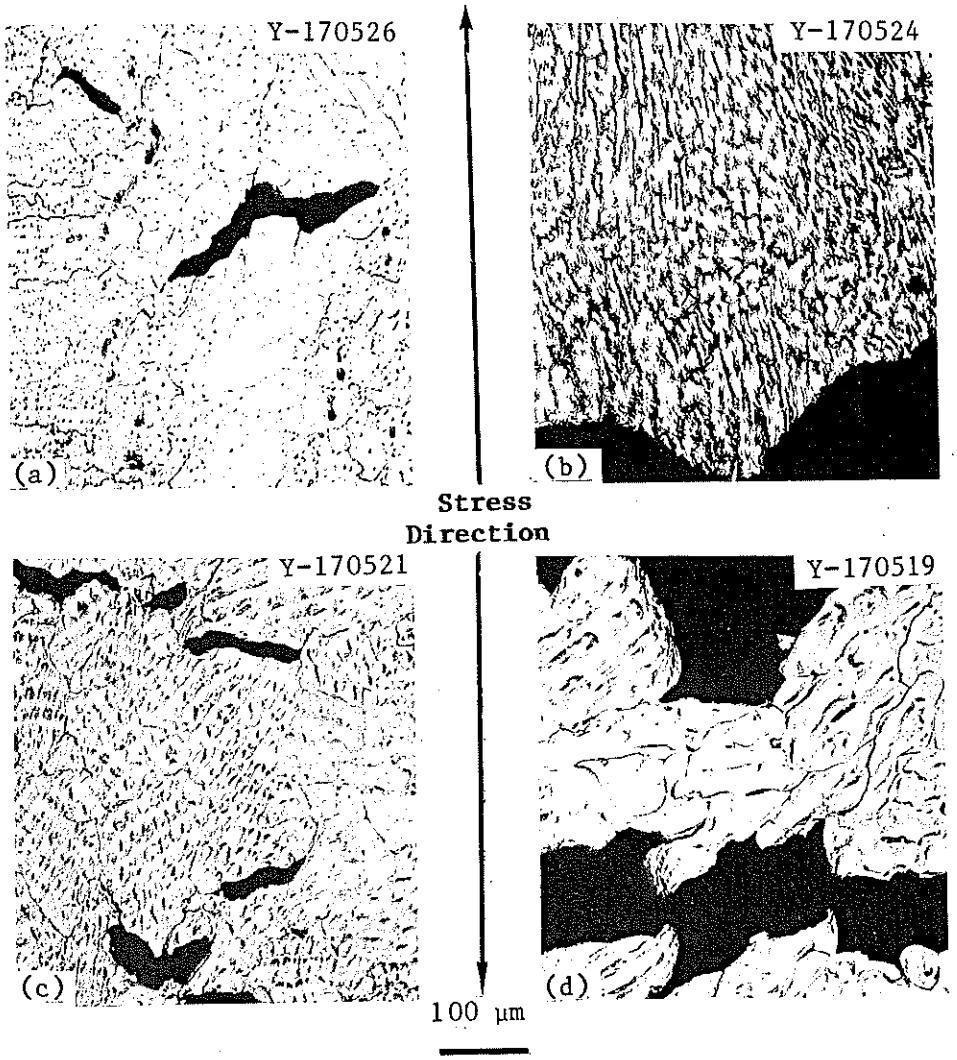


Fig. 37. Longitudinal Creep-Rupture Specimens Tested at 538°C and 310 MPa. Locations are at or near the rupture in weld metal. Etchant: 50 $HNO_3$—50 $H_2O$ applied electrolytically. (a) E-13. (b) F-14. (c) G-15. (d) G-16. (e) H-22.

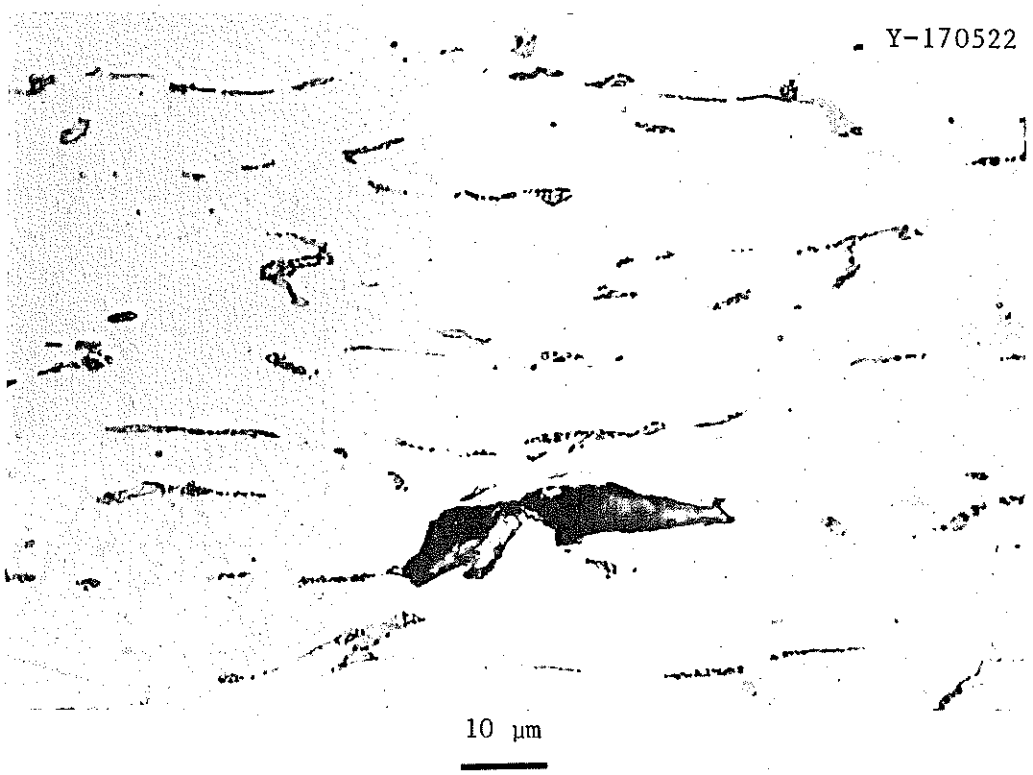


Fig. 38. Longitudinal Creep-Rupture Specimen from F-14 Tested at 538°C and 310 MPa. Etchant: 50 $HNO_3$–50 $H_2O$ applied electrolytically.

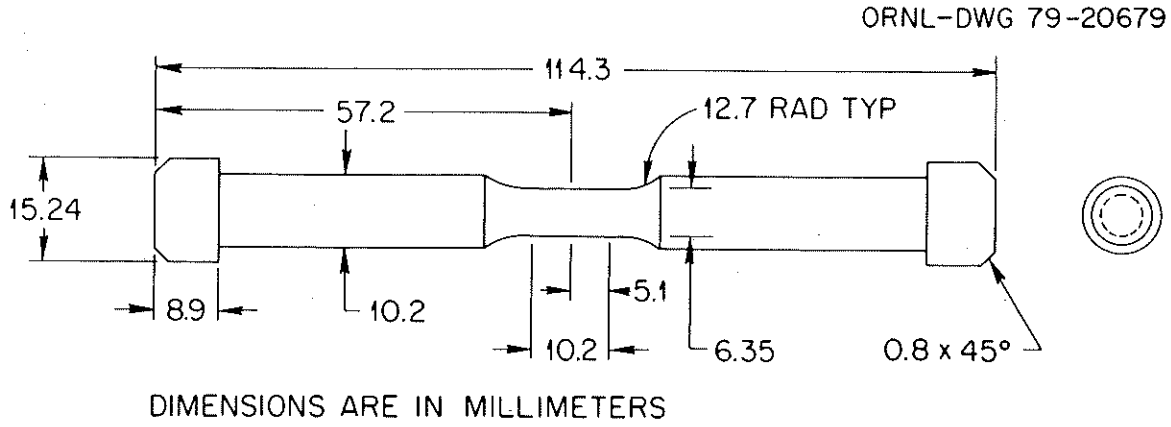


Fig. 39. Uniform Gage Length Fatigue Specimen.

ORNL-DWG 79-20673

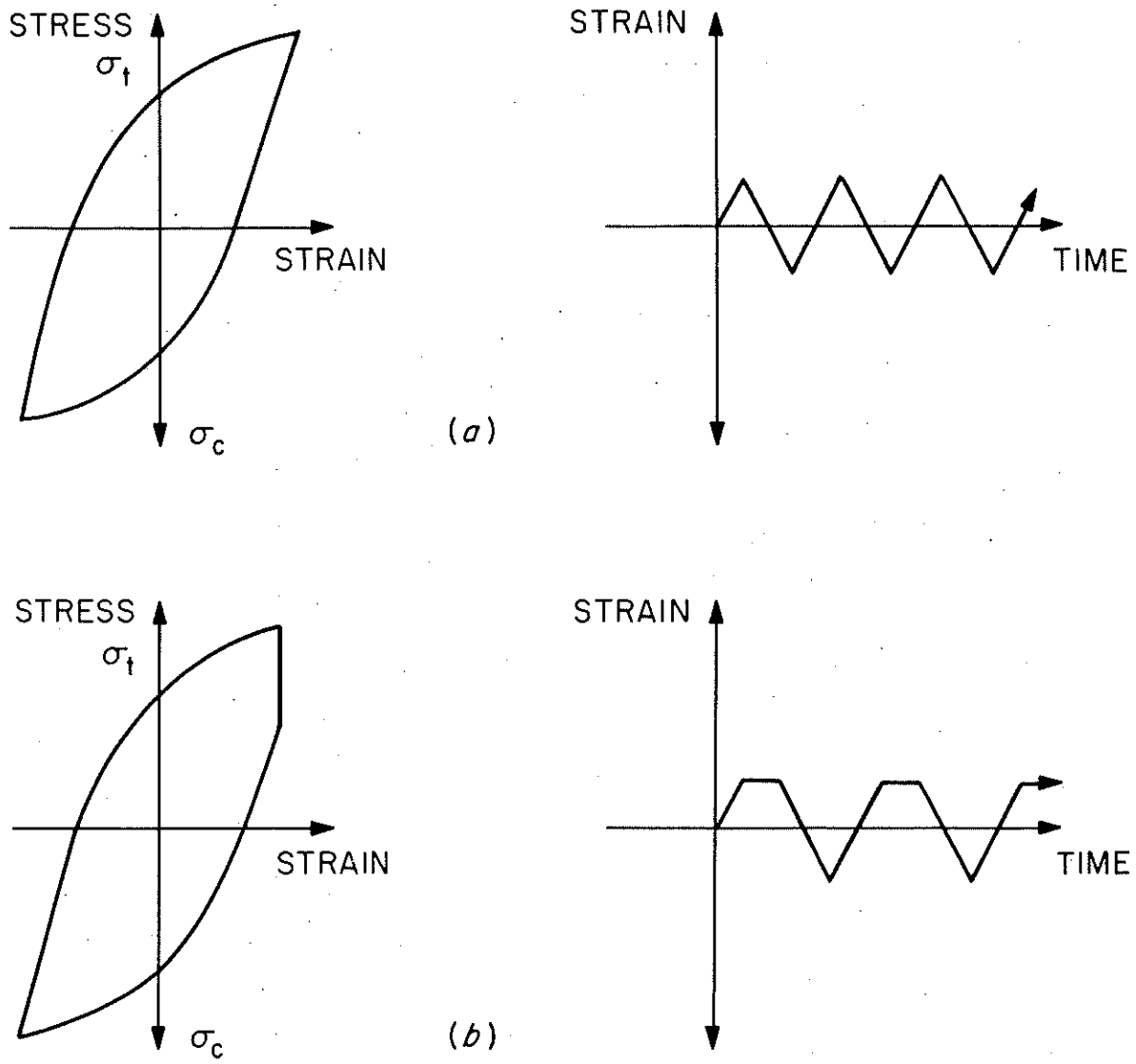


Fig. 40. Fatigue Cycling Waveforms and Resultant Hysteresis Loops. (a) Continuous cycling. (b) Cycling with a tensile hold period.

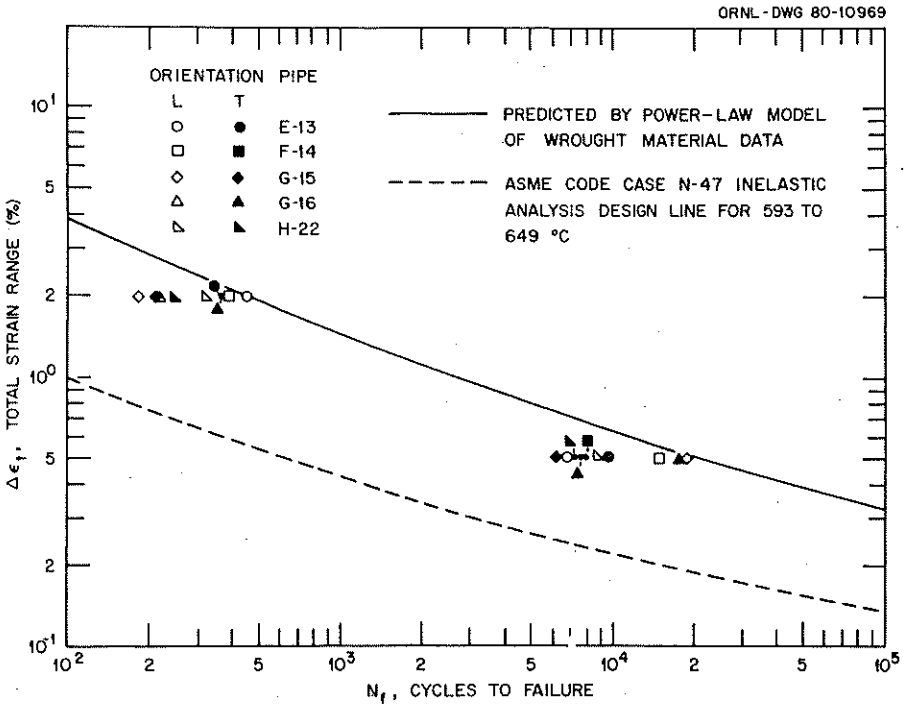


Fig. 41. Comparison of Total Strain Range vs Cycles to Failure for Continuous Cycle Fatigue Tests Performed at 593°C.

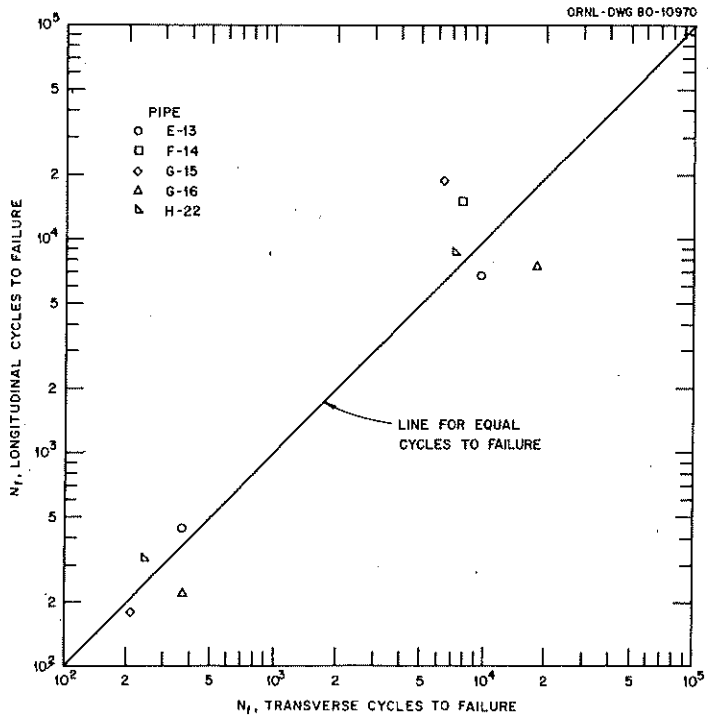


Fig. 42. Comparison of Longitudinal vs Transverse Cycles to Failure for Fatigue Tests at 593°C.

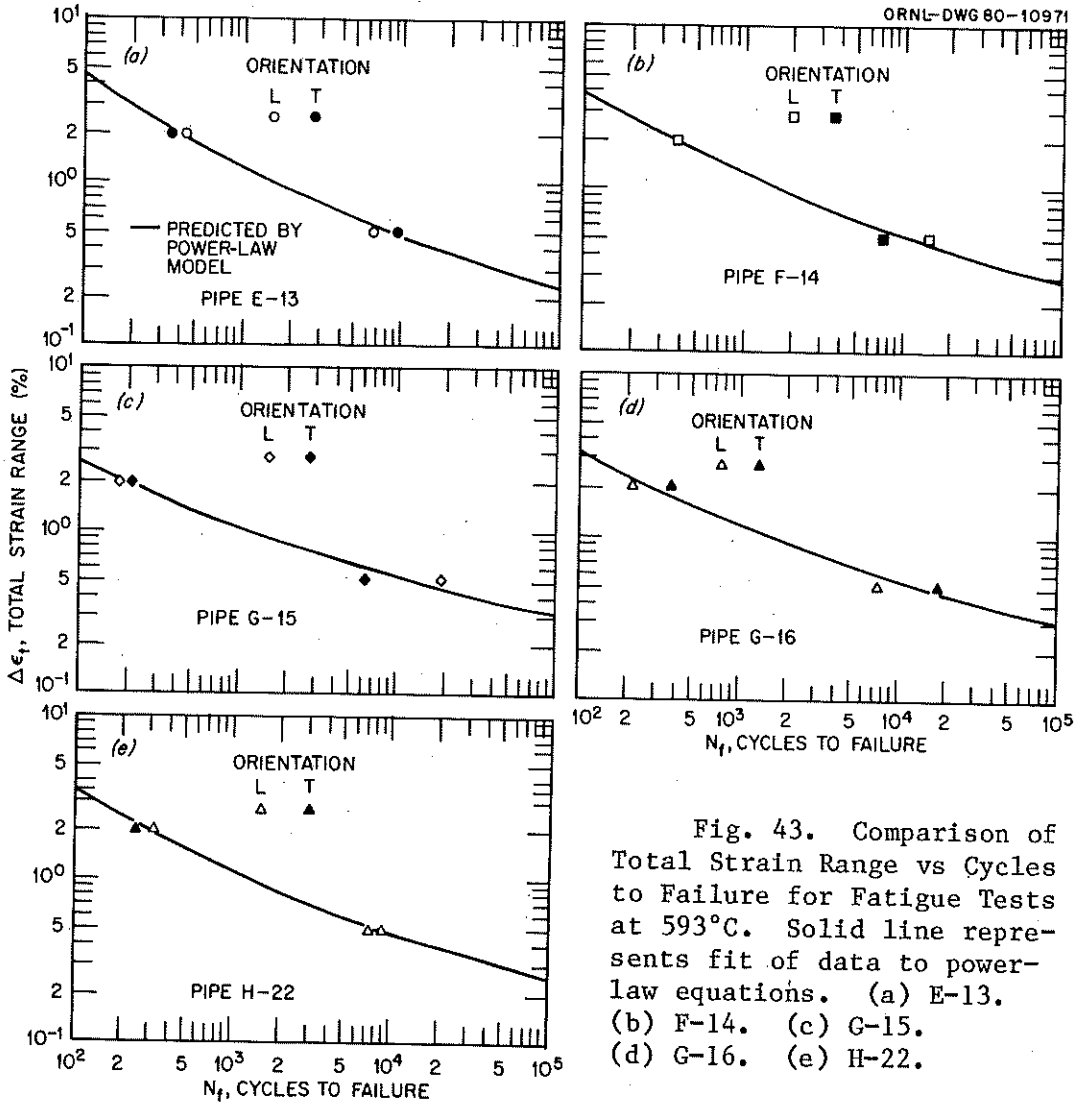


Fig. 43. Comparison of Total Strain Range vs Cycles to Failure for Fatigue Tests at 593°C. Solid line represents fit of data to power-law equations. (a) E-13. (b) F-14. (c) G-15. (d) G-16. (e) H-22.

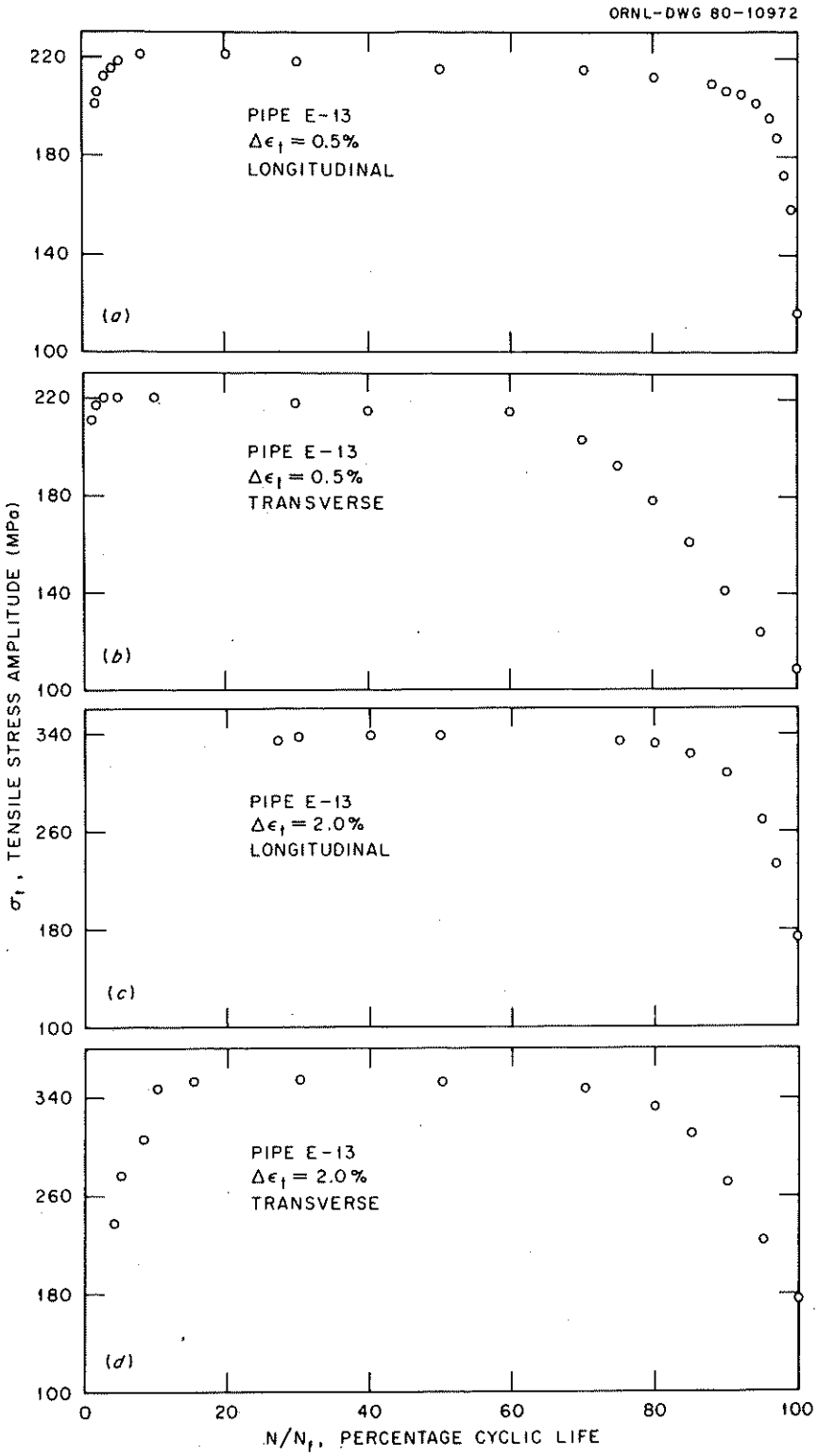


Fig. 44. Comparison of Tensile Stress Amplitude vs Percentage Cyclic Life for Fatigue Tests at 593°C and at Various Total Strains on Welds from Pipe E-13 Oriented in Both Longitudinal (L) and Transverse (T) Directions with Respect to the Weld Seams. (a) 0.5%, L. (b) 0.5%, T. (c) 2.0%, L. (d) 2.0%, T.

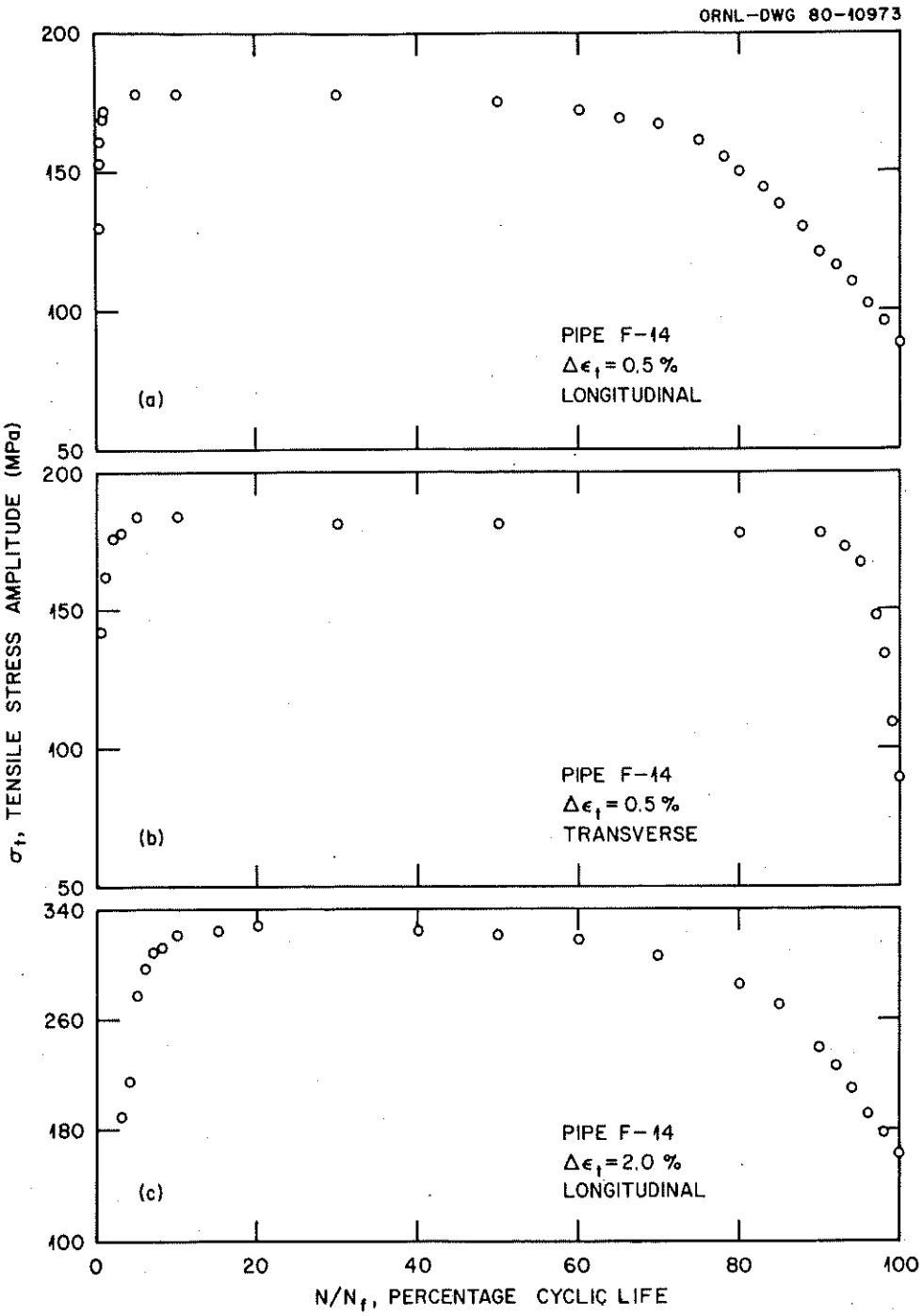


Fig. 45. Comparison of Tensile Stress Amplitude vs Percentage Cyclic Life for Fatigue Tests at 593°C and at Various Total Strains on Welds from Pipe F-14 Oriented in Both Longitudinal (L) and Transverse (T) Directions with Respect to the Weld Seams. (a) 0.5%, L. (b) 0.5%, T. (c) 2.0%, L.

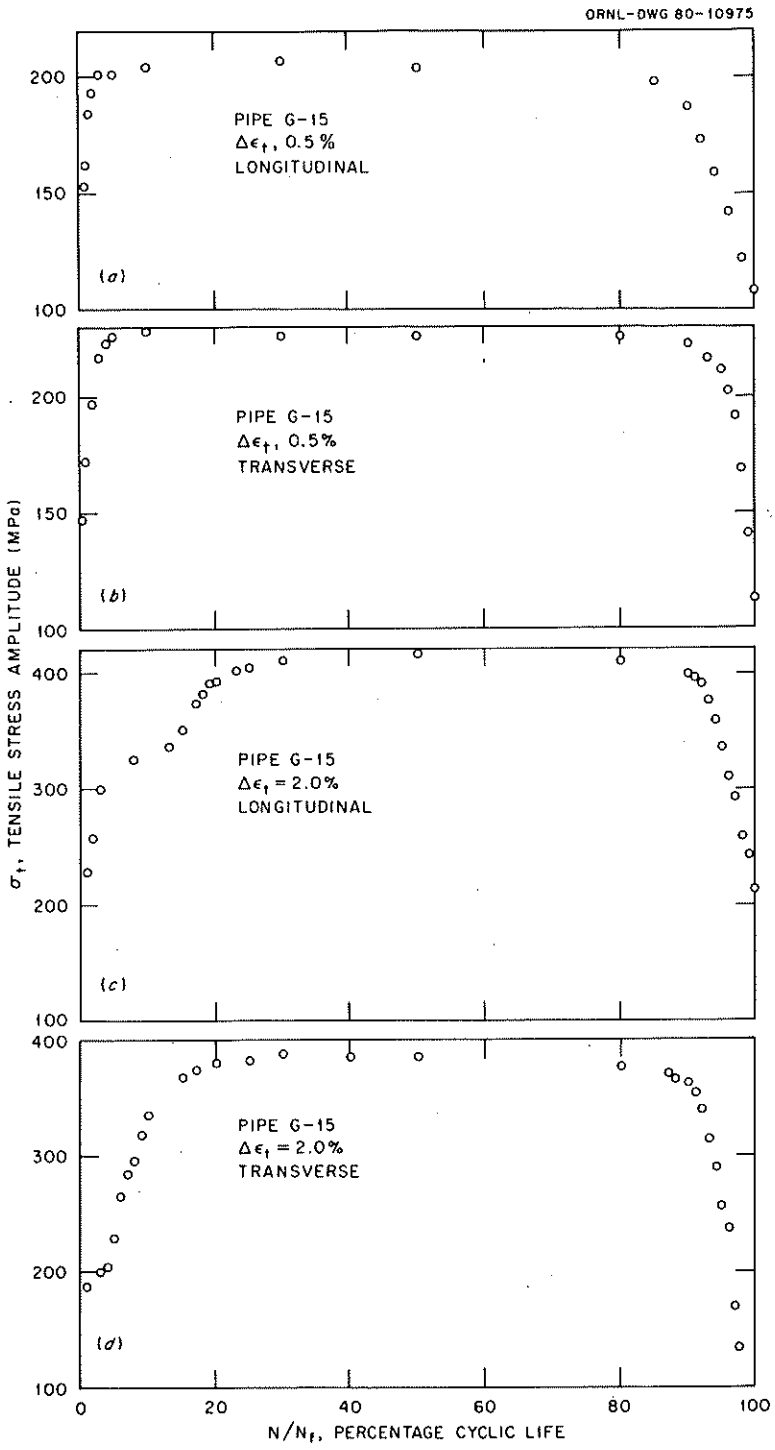


Fig. 46. Comparison of Tensile Stress Amplitude vs Percentage Cyclic Life for Fatigue Tests at 593°C and at Various Total Strains on Welds from Pipe G-16 Oriented in Both Longitudinal (L) and Transverse (T) Directions with Respect to the Weld Seams. (a) 0.5%, L. (b) 0.5%, T. (c) 2.0%, L. (d) 2.0%, T.

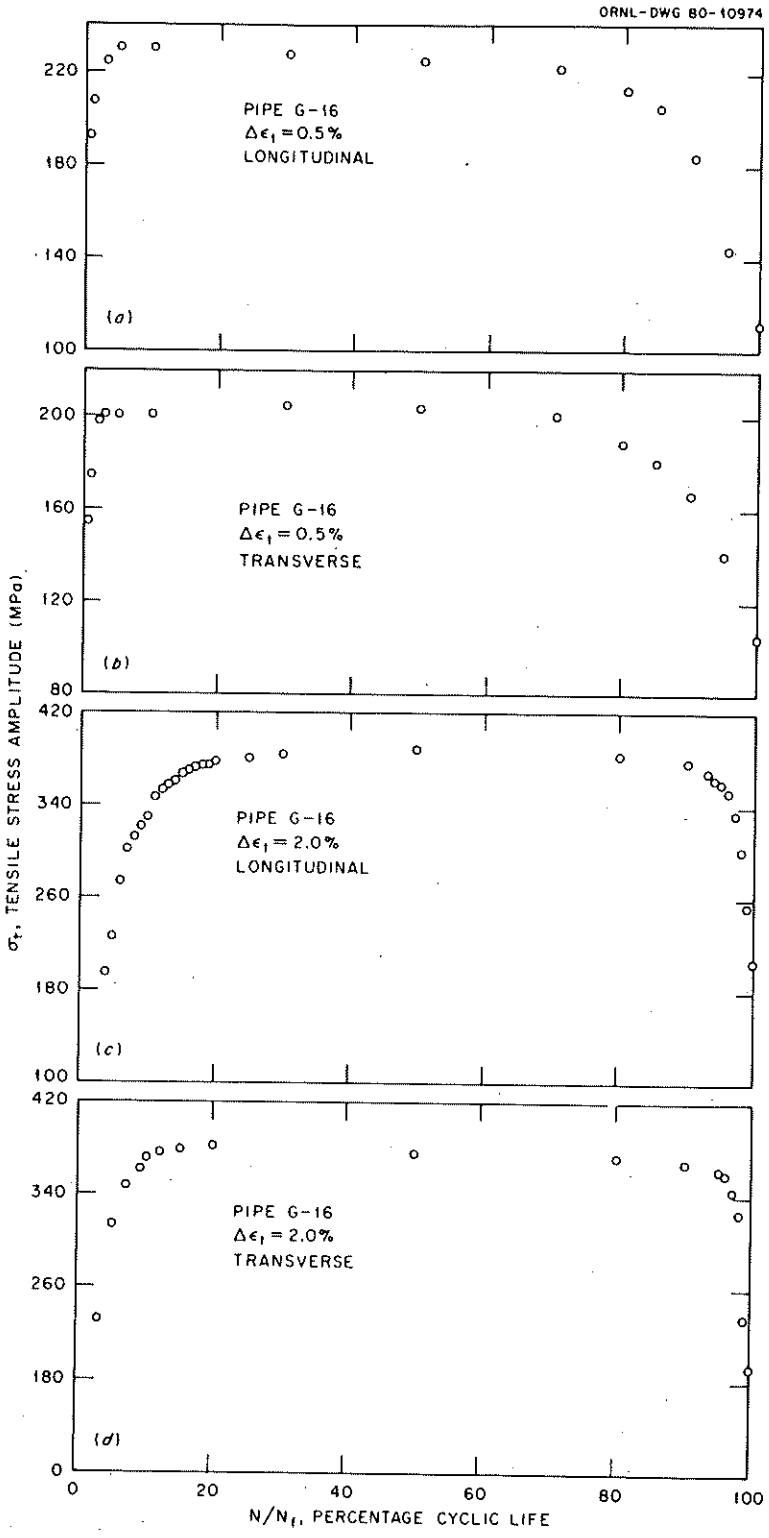


Fig. 47. Comparison of Tensile Stress Amplitude vs Percentage Cyclic Life for Fatigue Tests at 593°C and at Various Total Strains on Welds from Pipe G-15 Oriented in Both Longitudinal (L) and Transverse (T) Directions with Respect to the Weld Seams. (a) 0.5%, L. (b) 0.5%, T. (c) 2.0%, L. (d) 2.0%, T.

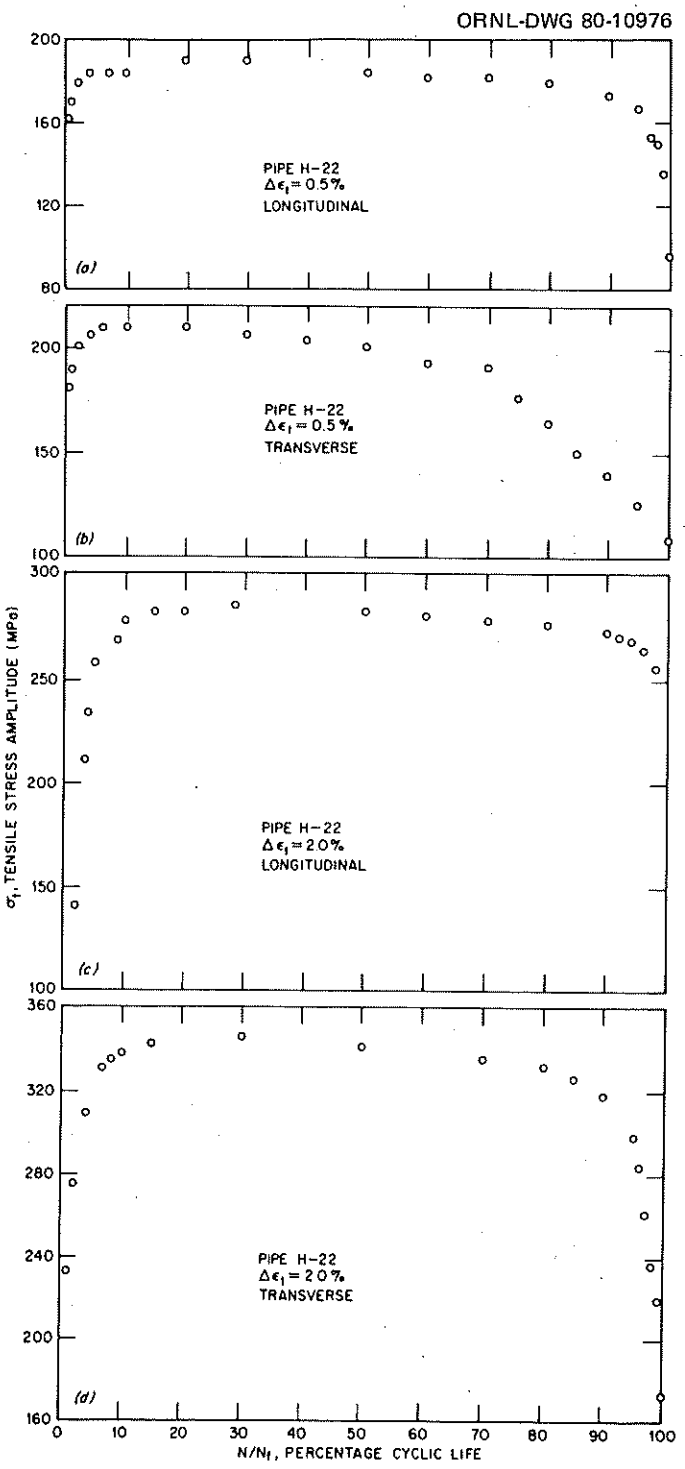


Fig. 48. Comparison of Tensile Stress Amplitude vs Percentage Cyclic Life for Fatigue Tests at 593°C and at Various Total Strains on Welds from Pipe H-22 Oriented in Both Longitudinal (L) and Transverse (T) Directions with Respect to the Weld Seams. (a) 0.5%, L. (b) 0.5%, T. (c) 2.0%, L. (d) 2.0%, T.

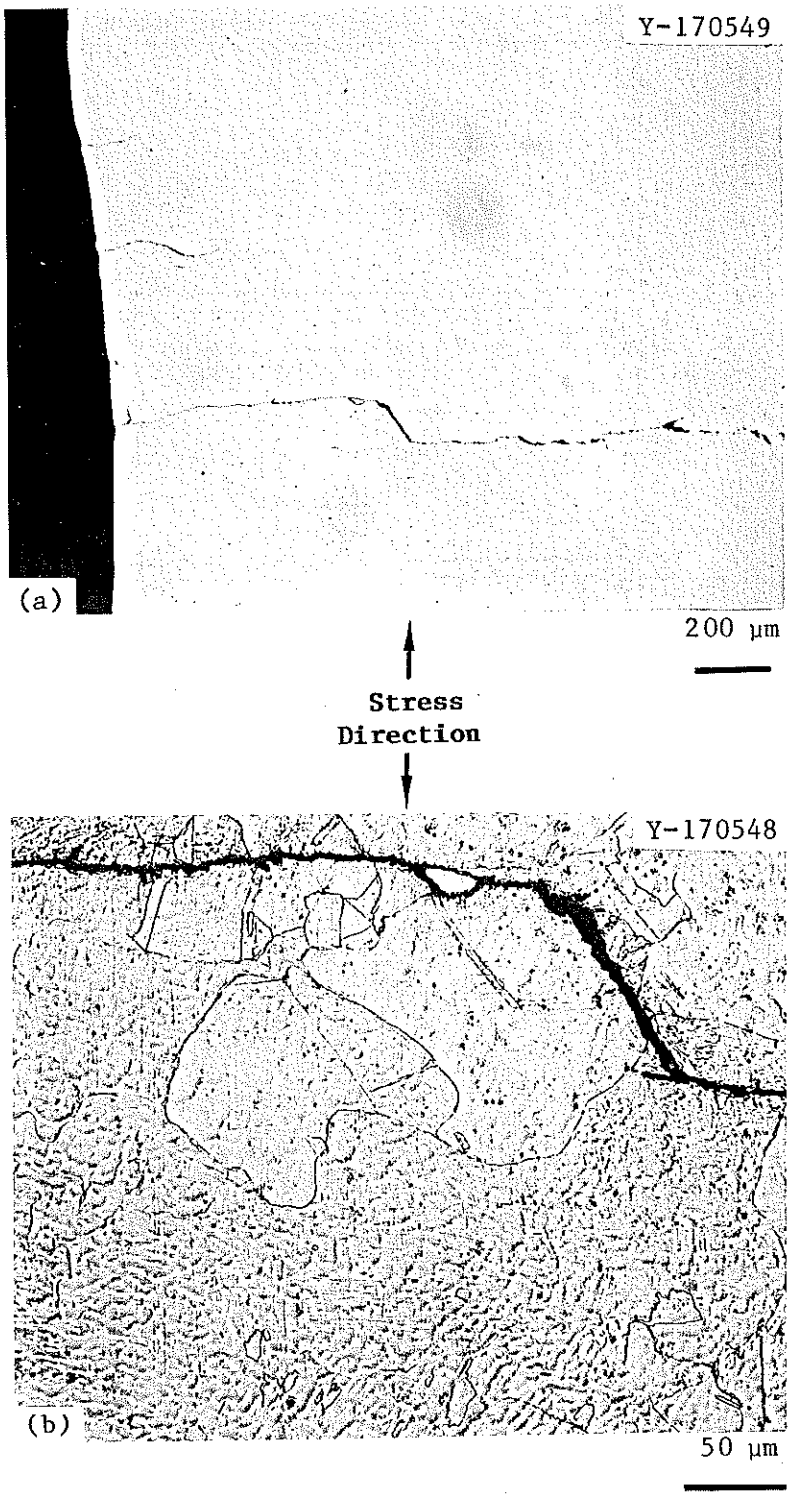


Fig. 49. Secondary Cracks in Longitudinally Oriented Continuous Cycle Fatigue Specimen from Pipe E-13 Tested at 593°C and 2.0% Total Strain Range. Locations are at or near the specimen edge in weld metal. (a) Unetched. (b) Etchant: 50 $HNO_3$–50 $H_2O$ applied electrolytically.

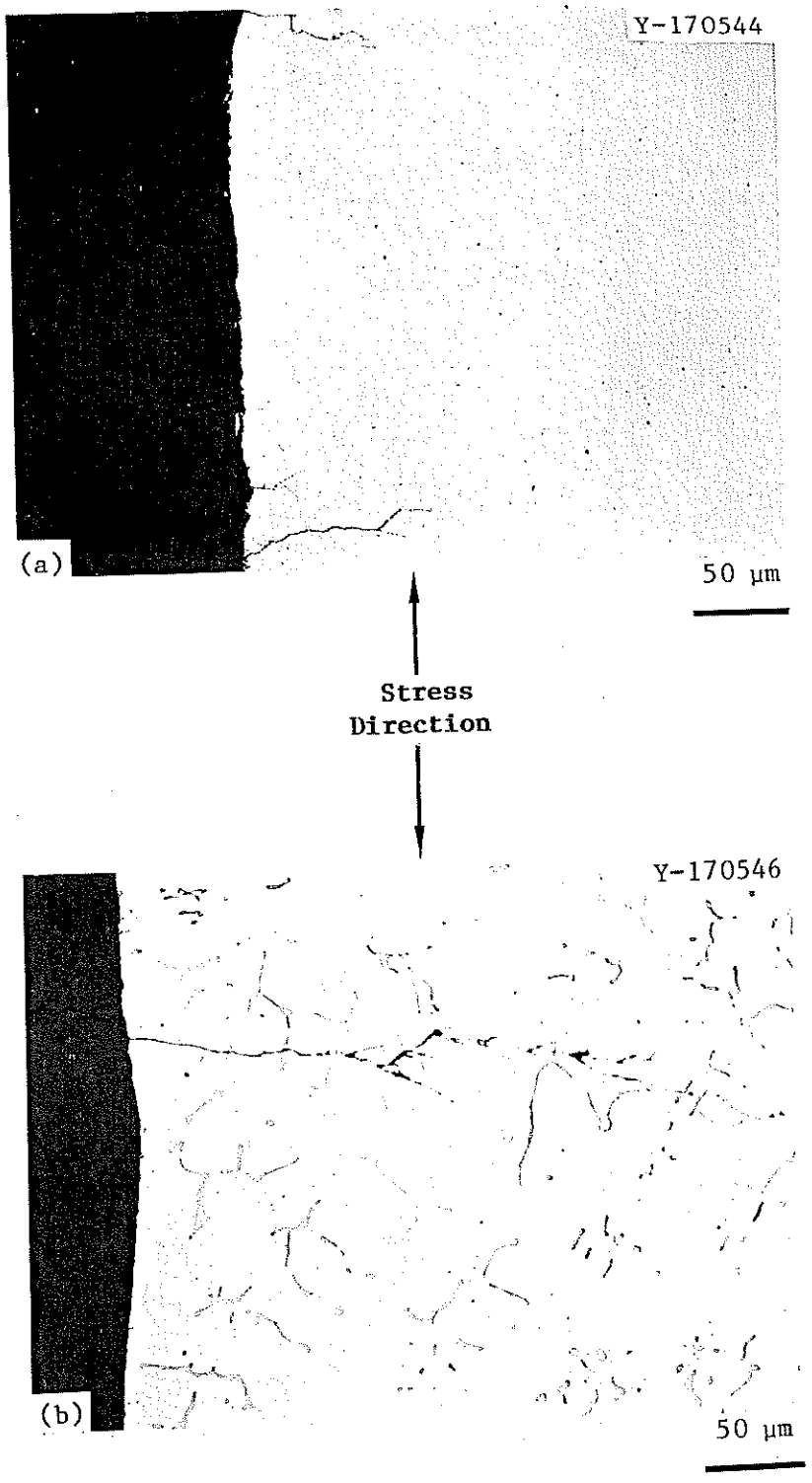


Fig. 50. Secondary Cracks in Longitudinally Oriented Continuous Cycle Fatigue Specimen from Pipe F-14 Tested at 593°C and 2.0% Total Strain Range. Locations are at or near the specimen edge in weld metal. (a) Unetched. (b) Etchant: 15 g $K_3Fe(CN)_6$, 15 g KOH, 100 mL $H_2O$ at 98°C.

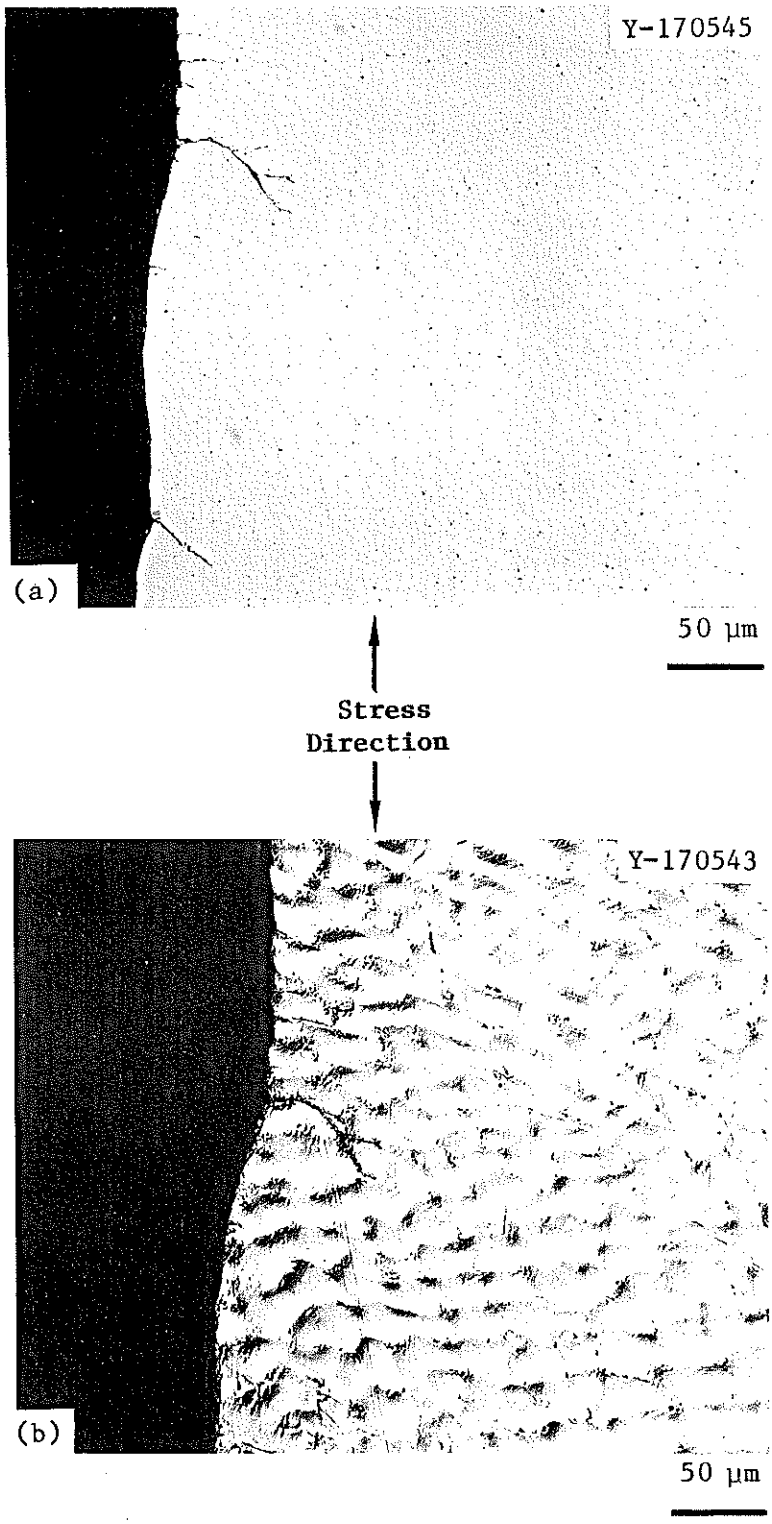


Fig. 51. Secondary Cracks in Longitudinally Oriented Continuous Cycle Fatigue Specimen from Pipe G-15 Tested at 593°C and 2.0% Total Strain Range. Locations are at or near the specimen edge in weld metal. (a) Unetched. (b) Etchant: 50 $HNO_3$—50 $H_2O$ applied electrolytically.

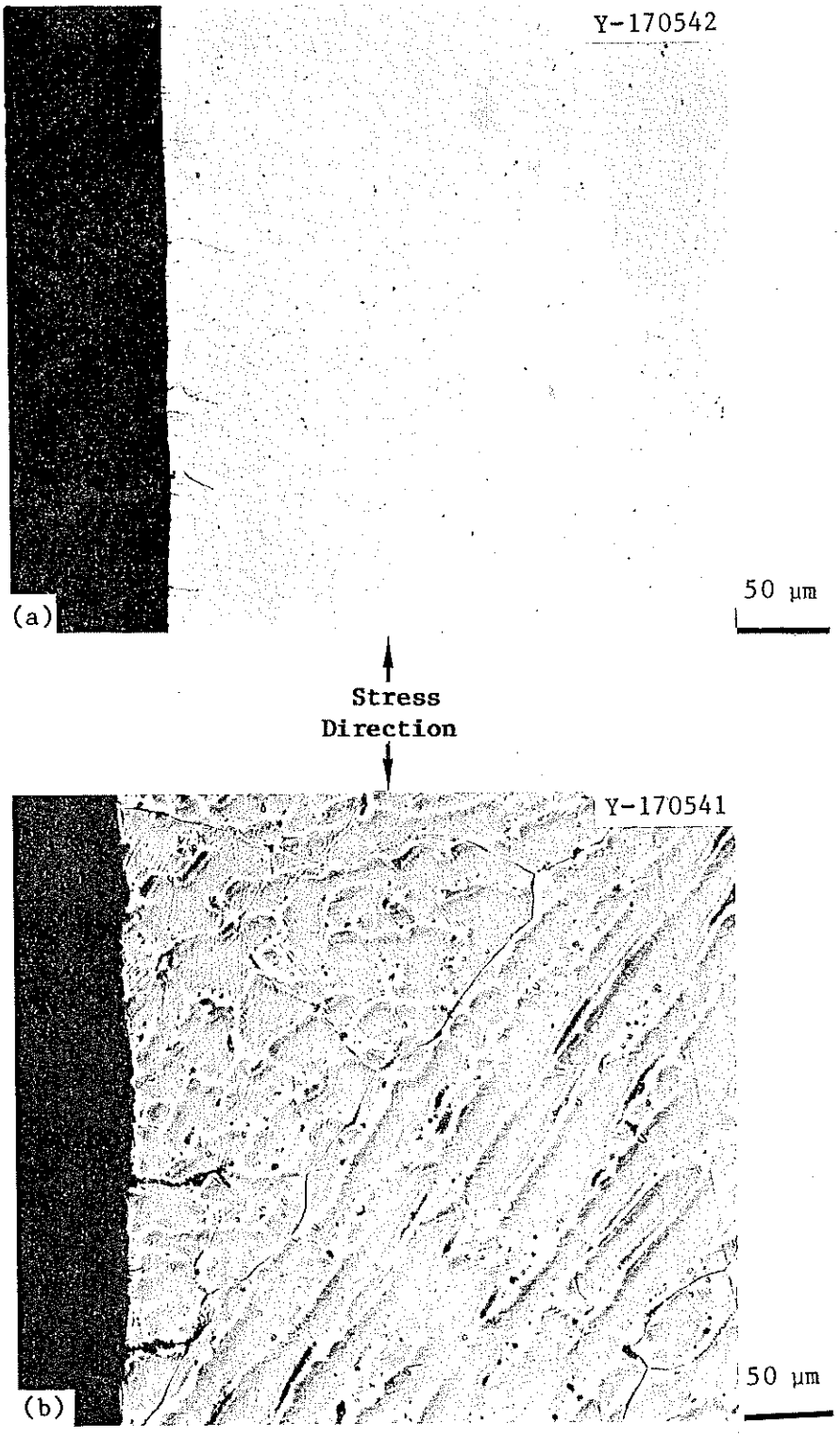


Fig. 52. Secondary Cracks in Longitudinally Oriented Continuous Cycle Fatigue Specimen from Pipe G-16 Tested at 593°C and at 2.0% Total Strain Range. Locations are at or near the specimen edge in weld metal (a) Unetched. (b) Etchant: 50 $HNO_3$–50 $H_2O$ applied electrolytically.

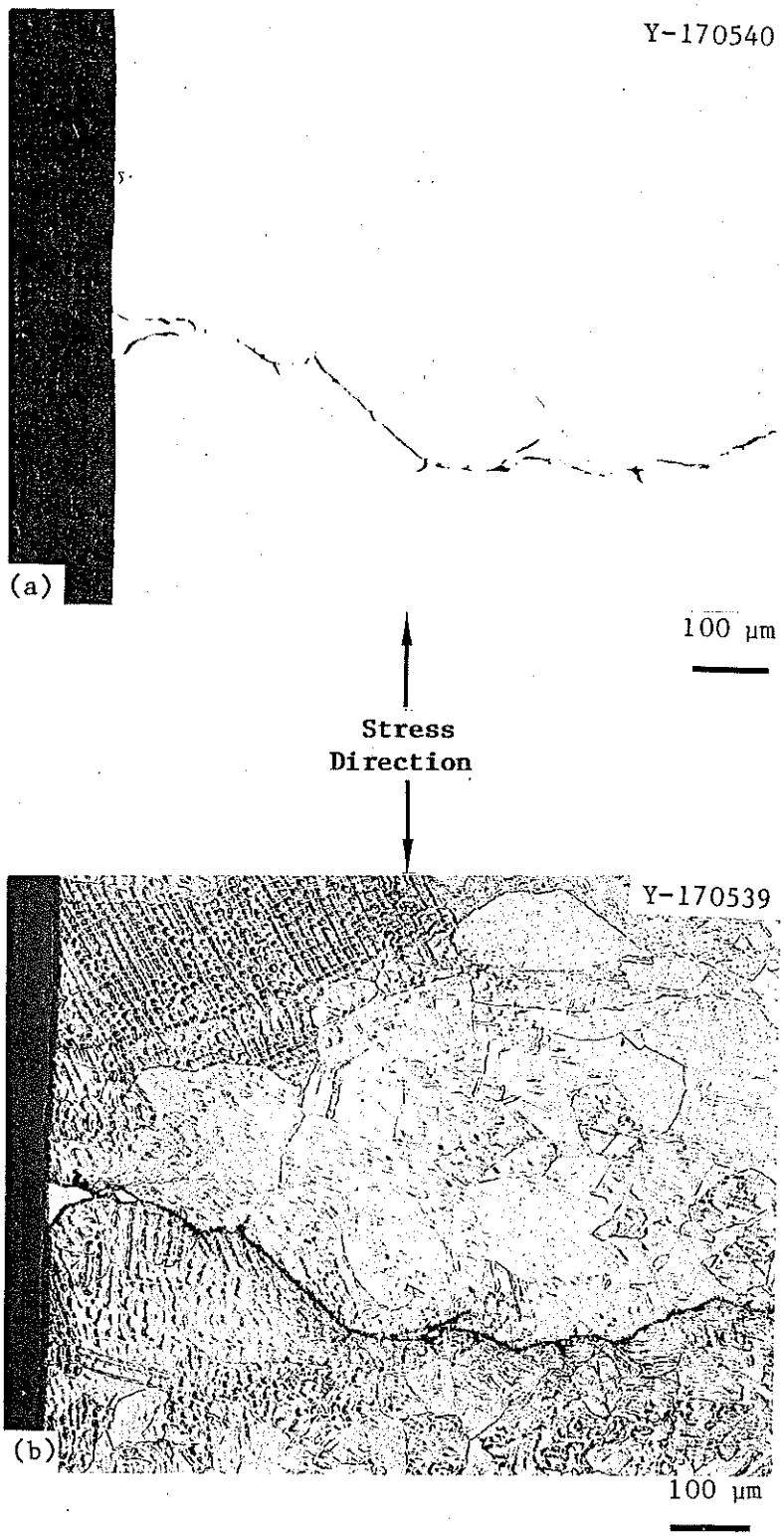


Fig. 53. Secondary Cracks in Longitudinally Oriented Continuous Cycle Fatigue Specimen from Pipe H-22 Tested at 593°C and at 2.0% Total Strain Range. Locations are at or near the specimen edge in weld metal. (a) Unetched. (b) Etchant: 50 $HNO_3$–50 $H_2O$ applied electrolytically.

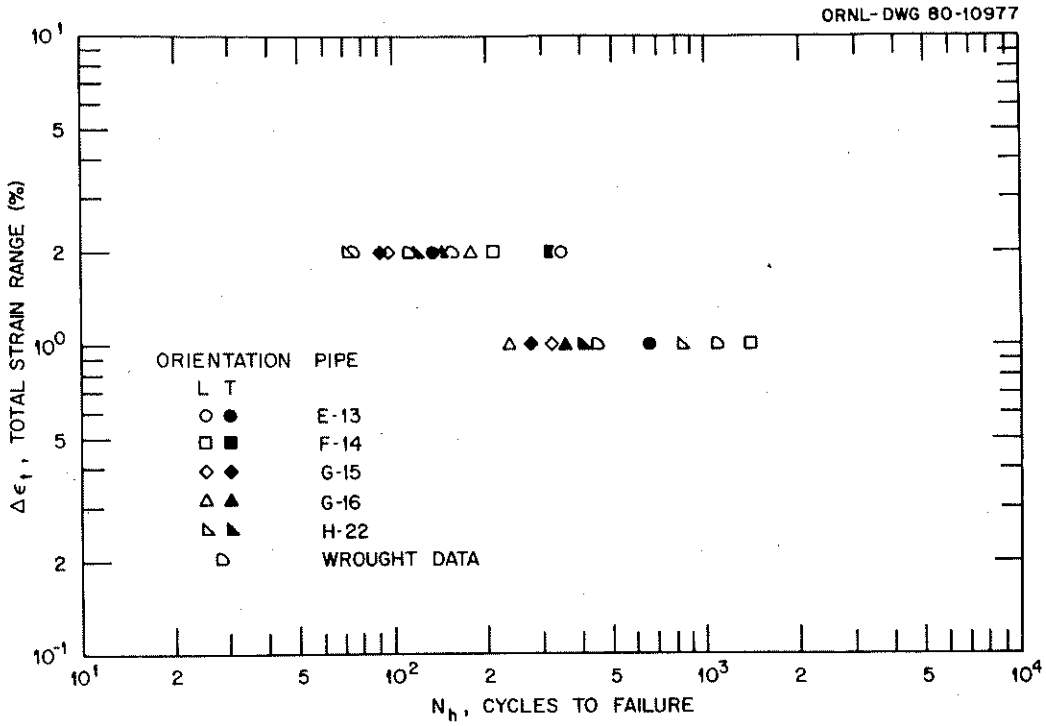


Fig. 54. Comparison of Total Strain Range vs Cycles to Failure for Fatigue Tests at 593°C with a Tensile Hold Period of 0.1 h.

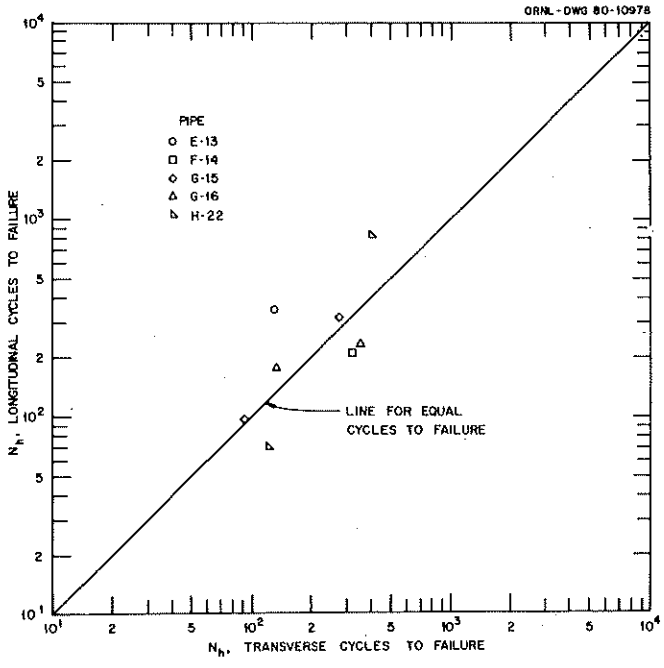


Fig. 55. Comparison of Longitudinal vs Transverse Cycles to Failure for Fatigue Tests at 593°C with a Tensile Hold Period of 0.1 h.

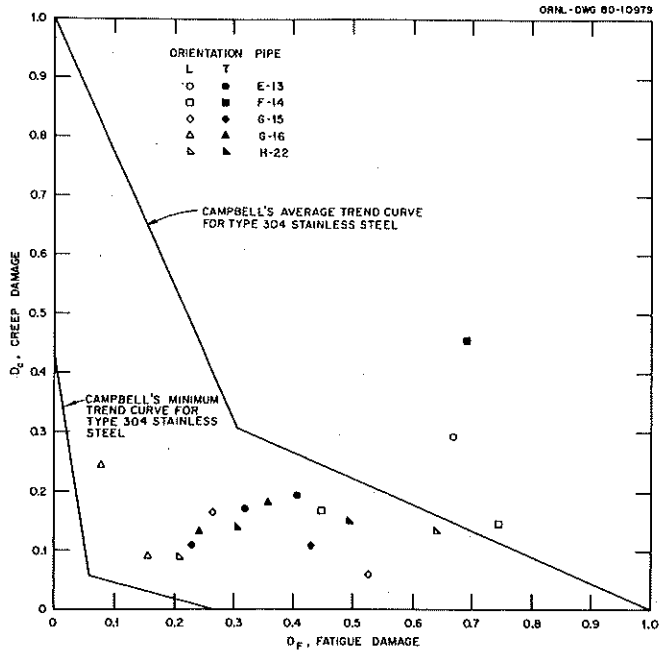


Fig. 56. Comparison of Linear Damage Summation Data (Using $t_r$, Time to Rupture, and $N_f$, Continuous Cycles to Failure) with Campbell's Trend Curves for Type 304 Stainless Steel Creep-Fatigue Tests. [Source of Campbell's data: R. D. Campbell, "Creep/Fatigue Interaction Correlation for 304 Stainless Steel Subjected to Strain-Controlled Cycling with Hold Times at Peak Strain," *J. Eng. Ind.* 93: 887–92 (November 1971).]

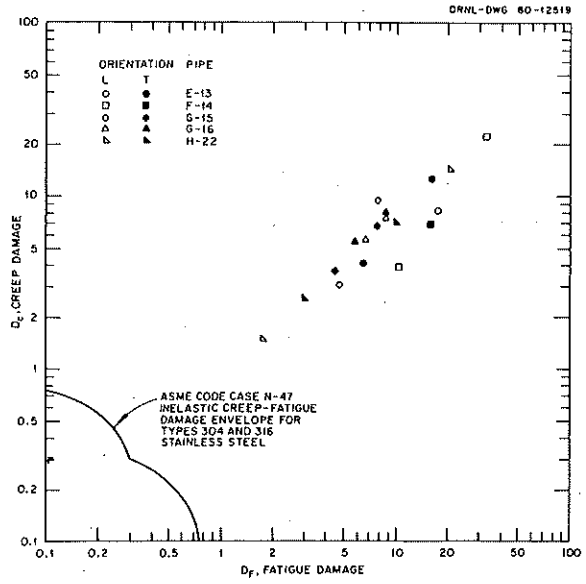


Fig. 57. Comparison of Linear Damage Summation Data (Using $T_d$ and $N_d$) with the ASME Code Case N-47 Inelastic Creep-Fatigue Damage Envelope for Types 304 and 316 Stainless Steel. $T_d$ = Code Case N-47 allowable time for stress values in Fig. I-14.6 B that were divided by the reduction factor from Table T-1411-1; $N_d$ = number of Code Case N-47 design allowable cycles from Fig. T-1420-1.

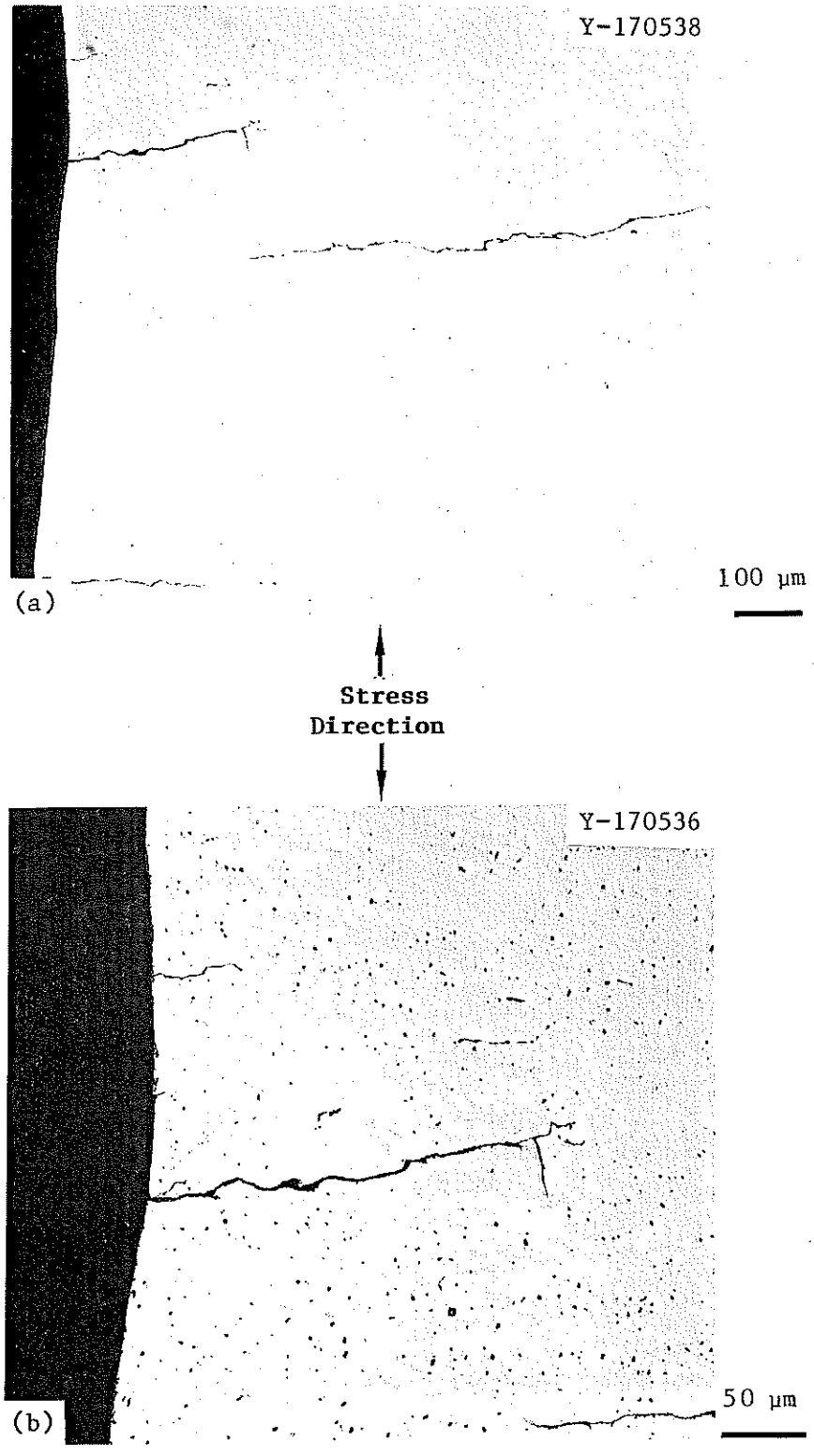


Fig. 58. Secondary Cracks in a Longitudinally Oriented Fatigue Specimen from Pipe E-13 Tested at 593°C with a 2.0% Total Strain Range and a Tensile Hold Period of 0.1 h. Locations are at the specimen edge in weld metal. (a) Unetched. (b) Etchant: 15 g $K_3Fe(CN)_6$, 15 g KOH, 100 mL $H_2O$ at 98°C.

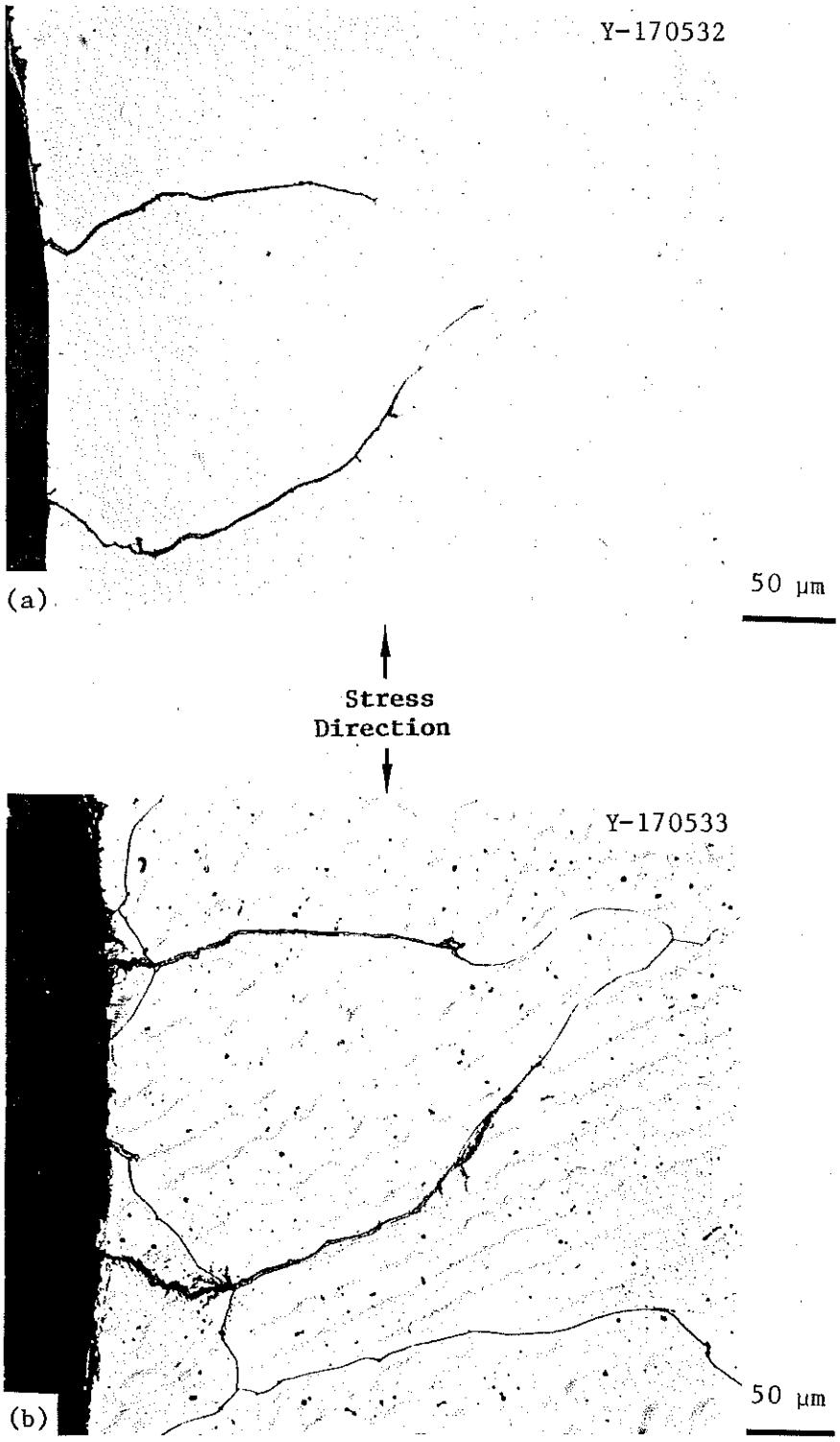


Fig. 59. Secondary Cracksd in a Longitudinally Oriented Fatigue Specimen from Pipe G-15 Tested at 593°C with a 2.0% Total Strain Range and a Tensile Hold Period of 0.1 h. Located at the specimen edge in weld metal. (a) Unetched. (b) Etchant: 50 $HNO_3$—50 $H_2O$ applied electrolytically.

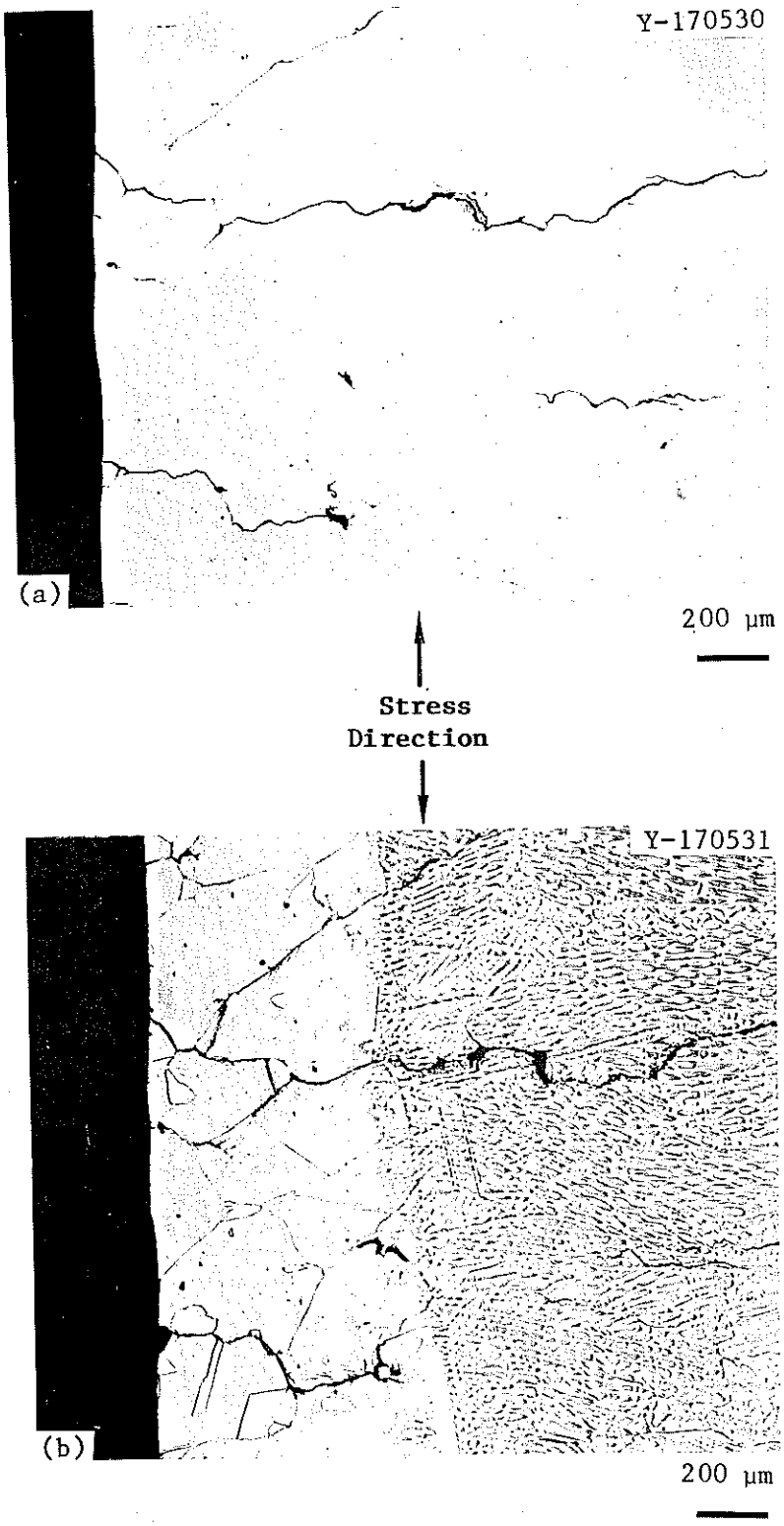


Fig. 60. Secondary Cracks in a Longitudinally Oriented Fatigue Specimen from Pipe G-16 Tested at 593°C with a 2.0% Total Strain Range and a Tensile Hold Period of 0.1 h. Located at the specimen edge in both base metal and weld metal. (a) Unetched. (b) Etchant: 50 $HNO_3$–50 $H_2O$ applied electrolytically.

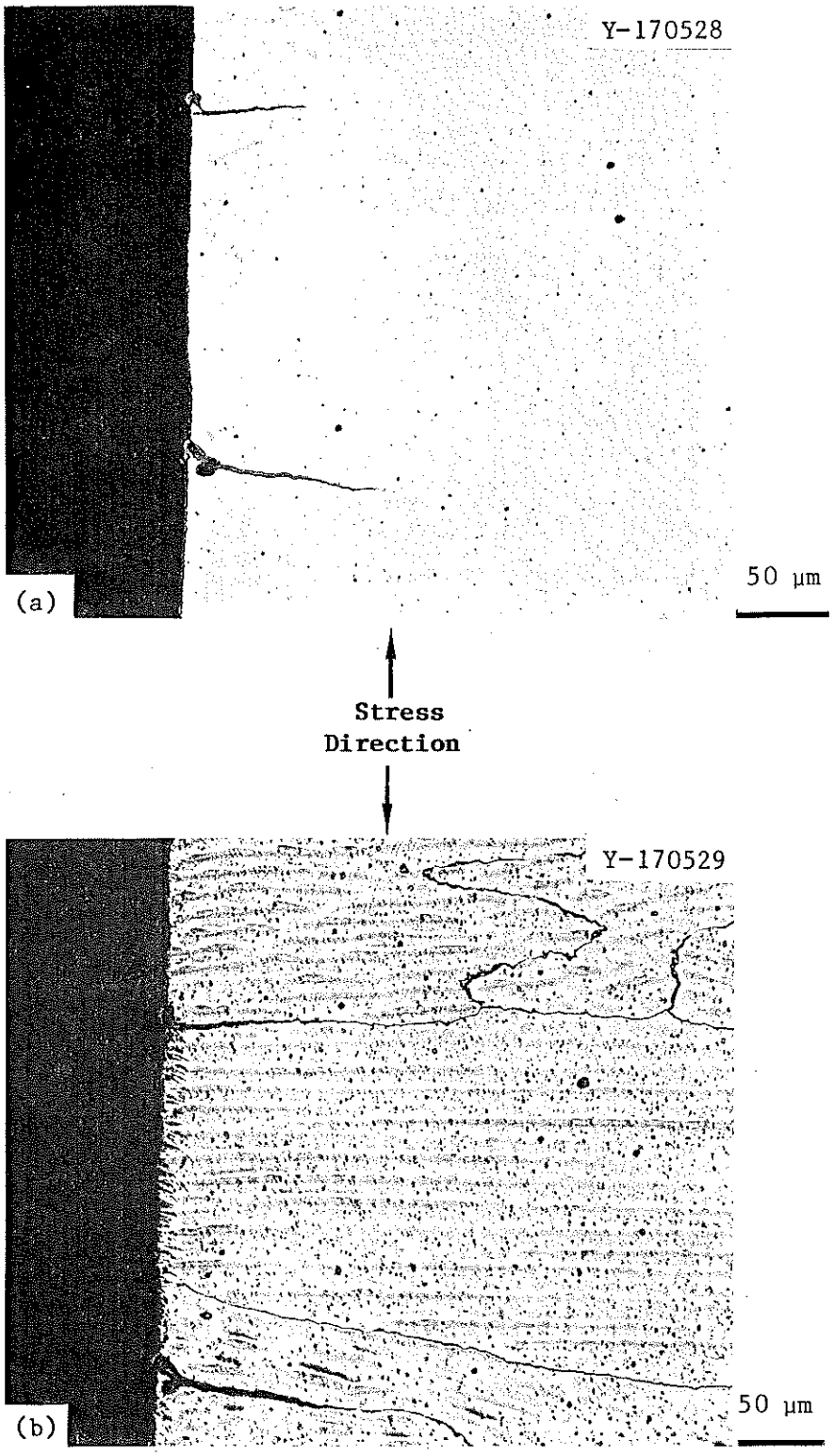


Fig. 61. Secondary Cracks in a Longitudinally Oriented Fatigue Specimen from Pipe H-22 Tested at 593°C with a 2.0% Total Strain Range and a Tensile Hold Period of 0.1 h. Located at the specimen edge in weld metal. (a) Unetched. (b) Etchant: 50 $HNO_3$—50 $H_2O$ applied electrolytically.

ORNL/TM-7394
Distribution
Categories
UC-79h, -k, -r

## INTERNAL DISTRIBUTION

| | | | |
|---|---|---|---|
| 1–2. | Central Research Library | 24. | P. Patriarca |
| 3. | Document Reference Section | 25. | C. E. Pugh |
| 4–5. | Laboratory Records Department | 26–30. | V. K. Sikka |
| 6. | Laboratory Records, ORNL RC | 31. | G. M. Slaughter |
| 7. | ORNL Patent Section | 32. | J. H. Smith |
| 8. | J. J. Blass | 33. | J. O. Stiegler |
| 9. | M. K. Booker | 34. | R. W. Swindman |
| 10. | J. M. Corum | 35. | G. T. Yahr |
| 11. | D. P. Edmonds | 36. | A. L. Bement, Jr. (Consultant) |
| 12. | G. F. Flanagan | 37. | E. H. Kottcamp, Jr. Consultant) |
| 13. | G. M. Goodwin | 38. | Alan Lawley (Consultant) |
| 14–16. | M. R. Hill | 39. | T. B. Massalski (Consultant) |
| 17. | R. L. Huddleston | 40. | M. J. Mayfield (Consultant) |
| 18. | W. J. McAfee | 41. | R. H. Redwine (Consultant) |
| 19–23. | J. W. McEnerney | 42. | J. T. Stringer (Consultant) |

## EXTERNAL DISTRIBUTION

42–43. DOE, DIVISION OF REACTOR RESEARCH AND TECHNOLOGY, Washington, DC 20545

Director

44. DOE, OAK RIDGE OPERATIONS OFFICE, P.O. Box E, Oak Ridge, TN 37830

Office of Assistant Manager for Energy Research and Development

45-246. DOE, TECHNICAL INFORMATION CENTER, P.O. Box 62, Oak Ridge, TN 37830

For distribution as shown in TID-4500 Distribution Category, UC-79h (Structural Materials and Design Engineering); UC-79k (Components); and 79-r (Structural and Component Materials Development)

☆U.S. GOVERNMENT PRINTING OFFICE: 1980-640-245/237